



BNXXXX-v0.0
December 23, 2022

Measurement of inclusive $B \rightarrow \Lambda_c$ branching fractions using Belle data and hadronic Full Event Interpretation

Leonardo Benjamin Rizzato¹.

¹*Institute Jožef Stefan, Ljubljana, Slovenia*

Abstract

Inclusive $B \rightarrow \Lambda_c$ branching fractions were measured most recently by BaBar collaboration. However, the measurement still presented a poor accuracy. A more precise measurement of inclusive $B \rightarrow \Lambda_c$ branching fraction could be useful to gain a better confidence on B meson weak decays treatment. With help of the Full Event Interpretation algorithm, it is possible to perform a more precise measurement of inclusive $B \rightarrow \Lambda_c$ branching fractions using Belle data set.

Changelog

Version 1.0

Version for first review

- introduced the argumentation about the crossfeed ratio parametrization in Sec.4.2
- updated Fig. 34 in Sec.4.2, Table 1, Fig. 36 and Fig. 37 (adjusting the comments)
- changed the linearity tests plots for charged correlated decays (Fig. 38 - Fig. 39 and Fig. 82 and Fig. 83 for anticorrelated decays)
- updated the systematics for chargeed correlated decays: summary Table 2, Sec. 4.8 updated with the results from the 2D fit (having the crossfeed ratio param.), same for Sec. 4.9. And for charged anticorrelated decays: summary Table 15 and Sections 6.8 -6.9.
- added the section about the systematics deriving from the parametrization of crossfeed normalization in the 2D fit (Sec. 4.10 and in charged anticorrelated decays Sec. 6.10), which takes into account the statistical uncertainties of the parameters.
- added the sections about the crossfeed peaking fraction in the 2D fit for anticorrelated decays (Sec. 4.11 and Sec. 6.11)
- Updated Table 14 for anticorrelated decays and also the corresponding plots.
- updated Table 19 for BR values of charged anticorrelated decays
- in the control sample chapter, updated Section 5.6 for the 2D fit on data, just adding the 2D fit performed on data using the parametrized normalization of crossfeed background, with results. And in the last section Sec. 5.13 added the new BR measured value for data.
- added Tracking efficiency to the systematics (see Sections 4.15 - 6.14)
- updated Sec. 5.13 for systematics on the control decay
- added Figures 98 , 99 and 100 in Appendix .2 relative to the optimized cuts discussed in Sec. 5.3
- corrected Fig. 16

Contents

1	Introduction	1
1.1	Analysis Setup	1
1.2	Datasets	1
2	Event selection and reconstruction	2
2.1	B_{tag} reconstruction	2
2.2	Λ_c reconstruction	2
2.3	Wrongly reconstructed B_{tag} candidates	3
3	Signal selection optimization	4
4	$B^- \rightarrow \Lambda_c^+$ decays	6
4.1	Probability Density Functions (PDFs) for the two dimensional fit	11
4.2	Two dimensional fit	27
4.3	Probability Density Functions (PDFs) for the B_{tag}	33
4.4	B_{tag} fit	35
4.5	Λ_c and FEI efficiency	36
4.6	Studies of Systematic Effects	38
4.7	Continuum background modeling	38
4.8	Crossfeed background modeling	40
4.9	Crossfeed ratio	40
4.10	Parametrization of crossfeed normalization in the 2D fit	41
4.11	Crossfeed peaking fraction in the 2D fit	42
4.12	Efficiencies	42
4.13	Fit biases	43
4.14	PID efficiency correction	43
4.15	Tracking efficiency	44
4.16	Sideband fit on data	44
4.17	Measured $B^+ \rightarrow \bar{\Lambda}_c^- X$ inclusive Branching Fraction	45
5	$B^- \rightarrow D^0$ control decay	47
5.1	Dataset used	47
5.2	Event selection and reconstruction	47
5.3	Signal selection optimization	47
5.4	Probability Density Functions (PDFs) for two dimensional fit	48
5.5	2D Fit on Monte Carlo simulated data	52
5.6	2D Fit on data	53
5.7	Probability Density Functions (PDFs) for the B_{tag}	56
5.8	B_{tag} Fit on Monte Carlo simulated data	57
5.9	B_{tag} Fit on data	59
5.10	PID efficiency correction	60
5.11	D^0 and FEI efficiency	60

5.12	Studies of Systematic Effects	61
5.13	Measured $B^+ \rightarrow \bar{D}^0 X$ inclusive Branching Fraction	61
6	$B^- \rightarrow \bar{\Lambda}_c^-$ decays	63
6.1	Probability Density Functions (PDFs) for the two dimensional fit	63
6.2	Two dimensional fit	69
6.3	Probability Density Functions (PDFs) for the B_{tag}	74
6.4	B_{tag} fit	76
6.5	Λ_c and FEI efficiency	77
6.6	Studies of Systematic Effects	78
6.7	Continuum background modeling	78
6.8	Crossfeed background modeling	80
6.9	Crossfeed ratio	80
6.10	Parametrization of crossfeed normalization in the 2D fit	81
6.11	Crossfeed peaking fraction in the 2D fit	81
6.12	Efficiencies	81
6.13	Fit biases	81
6.14	Tracking efficiency	81
6.15	Measured $B^+ \rightarrow \Lambda_c^+$ inclusive Branching Fraction	82
Appendix		83
.1	$B^- \rightarrow \Lambda_c^+$ decays: additional plots	85
.2	$B^- \rightarrow D^0$ decays: additional plots	91
.3	$B^- \rightarrow \bar{\Lambda}_c^-$ decays: additional plots	96
References		100

¹ 1 Introduction

² Inclusive B meson baryonic decays with a Λ_c baryon in the final state are the most
³ abundant, due to a relatively large V_{cb} element of the CKM matrix. The *BaBar* experiment
⁴ measured their branching fractions to be around the percent level (see ref. [1]). However, the
⁵ branching fractions were determined with big uncertainties: nearly 50% on the measured
⁶ values or, in the case of the $B^0 \rightarrow \Lambda_c^+$ decay, only an upper limit could be established.
⁷ A more precise measurement of inclusive $B \rightarrow \Lambda_c$ branching fractions may shed light on
⁸ the appropriateness of B meson weak decays treatment, particularly of strong interaction
⁹ effects modelling. Predictions for inclusive branching fractions are given, for example, in
¹⁰ ref. [2] or in [3] for $B \rightarrow \Lambda_c p$ decays.

¹¹ Exploiting the Full Evenet Interpretation (FEI) algorithm, developed for the Belle
¹² II experiment, it may be possible to perform a more precise measurement of inclusive
¹³ $B \rightarrow \Lambda_c$ branching fractions, using the full Belle data set. A more precise measurement
¹⁴ may also trigger further research on currently scarce theory predictions for B meson decays
¹⁵ to charm baryons.

¹⁶ 1.1 Analysis Setup

¹⁷ The reconstruction is performed with BASF2 release 05-02-03 together with the `b2bii`
¹⁸ package in order to convert the *Belle* MDST files (BASF data format) to *Belle II* MDST files
¹⁹ (`BASF2` data format). The FEI version used is `FEI_B2BII_light-2012-minos`.

²⁰ 1.2 Datasets

²¹ The Belle detector acquired a dataset of about $L_0 \approx 710 fb^{-1}$ of integrated luminosity in
²² its lifetime at the $\Upsilon(4S)$ energy of 10.58 GeV, which corresponds to about $771 \times 10^6 B\bar{B}$
²³ meson pairs. Additionally, several streams of Monte-Carlo (MC) samples were produced,
²⁴ where each stream of MC corresponds to the same amount of data that was taken with
²⁵ the detector. No specific signal MC was used: instead of producing dedicated signal MC
²⁶ samples, the samples were obtained by filtering the decays of interest from the generic
²⁷ on-resonance MC samples. The following samples were used in this analysis:

- ²⁸ • data
- ²⁹ • MC - 10 streams of B^+B^- and $B^0\bar{B}^0$ (denoted as `charged` and `mixed`) for signal
³⁰ decays and backgrounds.
 - ³¹ - 6 streams of $q\bar{q}$ produced at $\Upsilon(4S)$ resonance energy
 - ³² - 6 streams of $q\bar{q}$ produced at 60 MeV below $\Upsilon(4S)$ resonance energy, where each
³³ stream corresponds to $1/10 \times L_0$.

35 2 Event selection and reconstruction

36 In this chapter the procedure for reconstruction of the events where one B meson decays
37 inclusively to a Λ_c baryon and the accompanying B meson decays hadronically.

38 2.1 B_{tag} reconstruction

39 The FEI is an exclusive tagging algorithm that uses machine learning to reconstruct
40 B meson decay chains and calculates the probability that these decay chains correctly
41 describe the true process. In this analysis only hadronically reconstructed decay chains
42 are considered. The training called `FEI_B2BII_light-2012-minos` is used. Tag-side B
43 meson candidates are required to have a beam-constrained mass greater than $5.22 \text{ GeV}/c^2$
44 and $-0.15 < \Delta E < 0.07 \text{ GeV}$.

45 In the case of multiple candidates in the same event, the candidate with the highest
46 SignalProbability (the signal probability calculated by FEI using FastBDT) is chosen. To
47 suppress the background consisting of B^0 events misreconstructed as B^+ (and vice-versa)
48 from neutral (charged) decays also a B^0 (B^+) candidate is reconstructed with FEI and if
49 its SignalProbability is higher than the charged (neutral) reconstructed B meson, the event
50 is discarded. This constitutes a sort of crossfeed-veto, rejecting part of events belonging
51 to the other typology of decays of interest: for example in the case one is interested
52 in reconstructing $B^{+/-}$ decays and the event actually contains B^0/\bar{B}^0 decays, the FEI
53 reconstructed neutral B meson candidate most likely presents a higher SignalProbability
54 than the charged FEI reconstructed candidate.

55 2.2 Λ_c reconstruction

56 In the *rest of event* (ROE) of the reconstructed B_{tag} meson, to select $\Lambda_c \rightarrow pK\pi$ signal
57 candidates, the following event selection criteria are applied (same PID cuts were used for
58 example in the Belle Note 1521 https://belle.kek.jp/secured/belle_note/gn1521/BN_v1.pdf). Charged tracks with the impact parameters perpendicular to and along the
60 nominal interaction point (IP) are required to be less than 2 cm and 4 cm respectively
61 ($dr < 2 \text{ cm}$ and $|dz| < 4 \text{ cm}$).

62 The pion tracks are required to be identified with $\frac{\mathcal{L}_\pi}{\mathcal{L}_K + \mathcal{L}_\pi} > 0.6$. The kaon tracks are
63 required to be identified with $\frac{\mathcal{L}_K}{\mathcal{L}_K + \mathcal{L}_\pi} > 0.6$, and the proton/anti-proton tracks are
64 required to be identified with $\frac{\mathcal{L}_{p/\bar{p}}}{\mathcal{L}_K + \mathcal{L}_{p/\bar{p}}} > 0.6$ and $\frac{\mathcal{L}_{p/\bar{p}}}{\mathcal{L}_\pi + \mathcal{L}_{p/\bar{p}}} > 0.6$, where the $\mathcal{L}_{\pi,K,p/\bar{p}}$ are the
65 likelihoods for pion, kaon, proton/anti-proton, respectively, determined using the ratio of
66 the energy deposit in the ECL to the momentum measured in the SVD and CDC, the
67 shower shape in the ECL, the matching between the position of charged track trajectory
68 and the cluster position in the ECL, the hit information from the ACC and the dE/dx
69 information in the CDC.

70 For the Λ_c candidates a vertex fit is performed with `TreeFitter`, requiring it to converge.
71 If there are more than one Λ_c combination, then the best candidate based on the χ^2
72 probability is chosen. The Λ_c signal region is defined to be $|M_{\Lambda_c} - m_{\Lambda_c}| < 20 \text{ MeV}/c^2$ (\sim

⁷³ 3σ), here m_{Λ_c} is the nominal mass of m_{Λ_c} .

⁷⁴

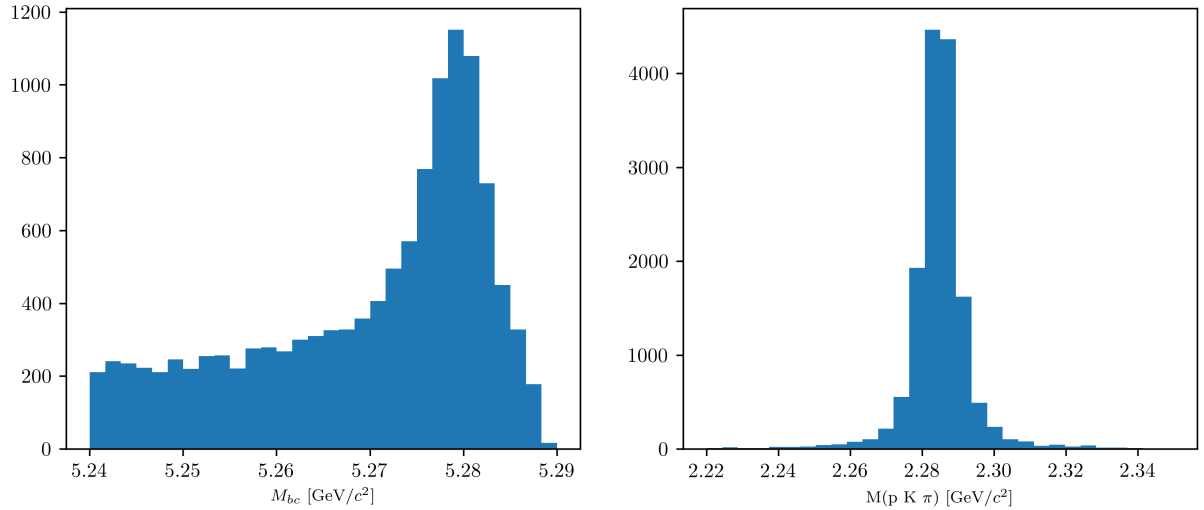


Figure (1) M_{bc} and $M(pK\pi)$ distributions of B_{tag} and Λ_c candidates reconstructed in the signal sample.

⁷⁵ 2.3 Wrongly reconstructed B_{tag} candidates

⁷⁶ In the case of the signal sample the distributions for the beam-constrained mass M_{bc} and
⁷⁷ for the correctly reconstructed Λ_c candidates, look like in Fig. 1. If one then investigates
⁷⁸ the M_{bc} distribution of the B_{tag} candidates reconstructed with FEI, it can be seen that
⁷⁹ there is a peaking structure for wrongly reconstructed B mesons (as in Fig. 2), according
⁸⁰ to the BASF2 internal truth matching variable **isSignal**. It is obvious from this that the
⁸¹ BASF2 internal truth matching variable cannot be used to separate properly the signal
⁸² events in correctly and wrongly reconstructed B mesons. In the study BELLE2-NOTE-TE-
⁸³ 2021-026 <https://docs.belle2.org/record/2711/files/BELLE2-NOTE-TE-2021-026.pdf> a possible solution was found developing new variables that can be used for an
⁸⁵ improved truth matching for the FEI (those variables were added to a newer BASF2
⁸⁶ release than the one used for this study). In the present study instead a more "traditional"
⁸⁷ approach was adopted: fitting the M_{bc} distribution with a sum of PDFs that account for the
⁸⁸ flat (background) component and the peaking (signal) component. The first component
⁸⁹ represents the combinatorial background, i.e. B mesons that were mis-reconstructed,
⁹⁰ and therefore those events are denoted from now on as "**misreconstructed signal**".
⁹¹ The peaking component represents the correctly reconstructed signal events in M_{bc} and
⁹² therefore denoted from now on as "**reconstructed signal**". Only the second one is then
⁹³ considered for the signal yield, while the first is counted as a background. To validate this
⁹⁴ method a control decay study was performed on the flavor correlated $B^+ \rightarrow \bar{D}^0$ channel.

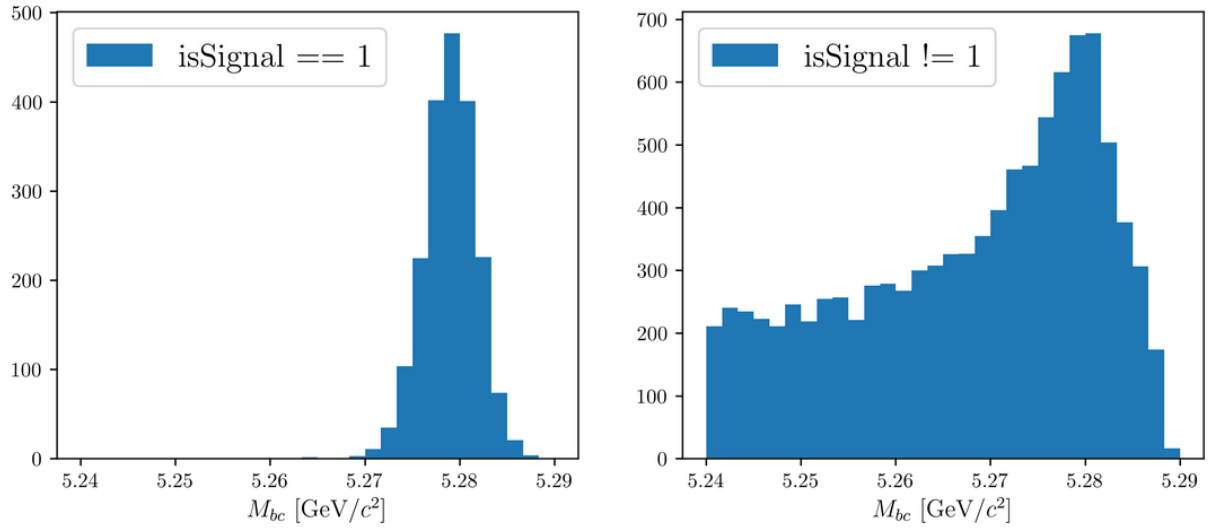


Figure (2) M_{bc} distribution of B_{tag} candidates reconstructed in the signal sample, truth-matched (on the left) and not (on the right).

95 3 Signal selection optimization

96 To further enhance the purity of the signal decays, an optimization procedure is adopted
 97 to determine optimal cuts for a set of variables for each decay mode under investigation
 98 by this study. The cuts on the following variables are optimized:

- 99 • *foxWolframR2*: the event based ratio of the 2-nd to the 0-th order Fox-Wolfram
 100 moments
- 101 • *SignalProbability*: the already mentioned signal probability calculated by FEI using
 102 FastBDT
- 103 • $p_{CMS}^{\Lambda_c}$: momentum of the Λ_c candidates in the center of mass system

104 The optimization is based on the Figure Of Merit (FOM): $FOM = \frac{S}{\sqrt{S+B}}$
 105 Where S and B are respectively signal and background events in the signal region:
 106 $M_{bc} > 5.27 \text{ GeV}/c^2$, $2.2665 < M(pK\pi) < 2.3065 \text{ GeV}/c^2$.

107 Due to the issue reported in Sec. 2.3, to separate signal events that peak in M_{bc} from
 108 the ones that are not (which are then categorized as background events), the events
 109 reconstructed in the signal sample are fitted with a sum of Crystal Ball function and
 110 Argus for each cut value on the corresponding variable to optimize (as in Fig. 3).

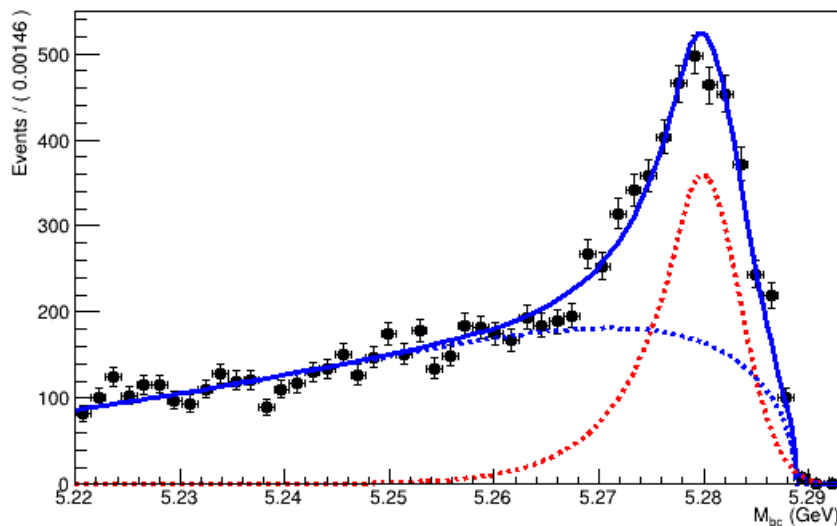


Figure (3) Example of a fit used to separate the correctly reconstructed B mesons (described by the red dotted Crystal Ball function) from the wrongly reconstructed ones (described by the blue dotted Argus function).

¹¹¹ **4 $B^- \rightarrow \Lambda_c^+ \text{ decays}$**

¹¹² First, in order to suppress the continuum background the cut on *foxWolframR2* is
¹¹³ optimized. Fig. 4 shows the *foxWolframR2* distributions for signal and continuum events.

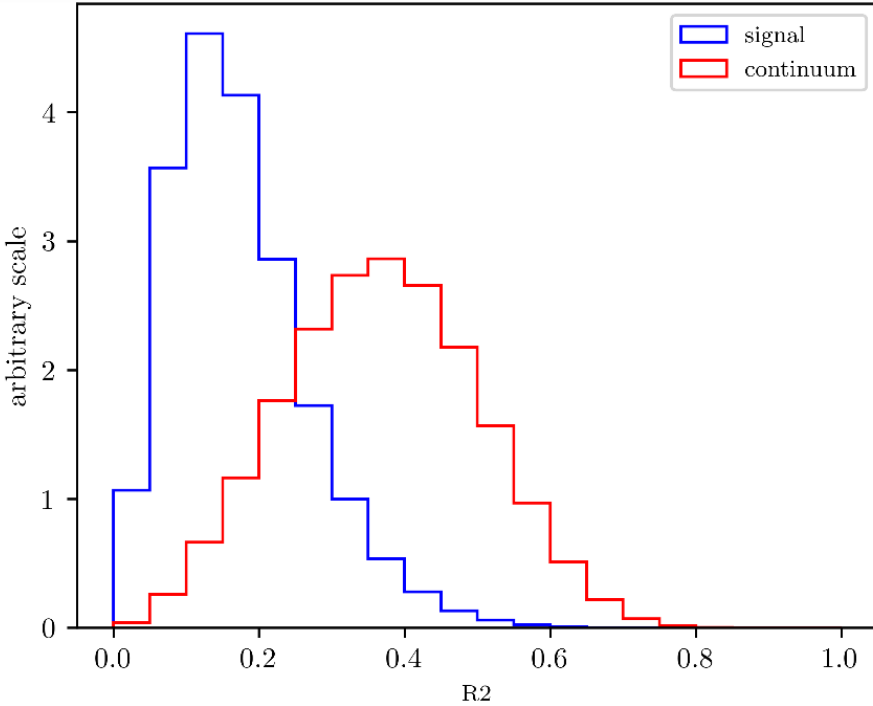


Figure (4) Distribution of the *foxWolframR2* variable for signal and continuum background events.

¹¹⁴
¹¹⁵ With the optimized cut $\text{foxWolframR2} < 0.27$, the cut on SignalProbability is
¹¹⁶ optimized in the same way (see Fig. 7).

¹¹⁷ With the optimized cut SignalProbability > 0.01 , the cut on *foxWolframR2* variable is
¹¹⁸ rechecked (Fig. 8). Being the maximum values fluctuating around $\text{foxWolframR2} < 0.3$,
¹¹⁹ this cut is the one finally chosen for this variable.

¹²⁰ With the optimized cuts on SignalProbability and *foxWolframR2* variable, the cut
¹²¹ on $p_{CMS}^{\Lambda_c}$ is optimized

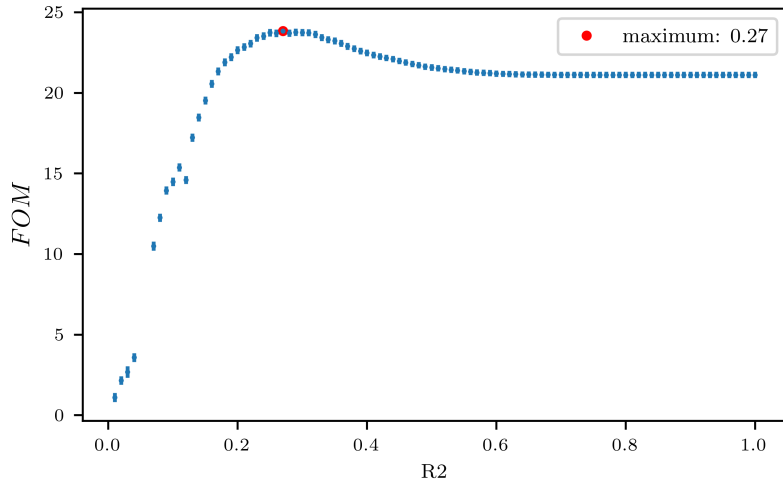


Figure (5) Figure of Merit values calculated at several cuts on the *foxWolframR2* variable

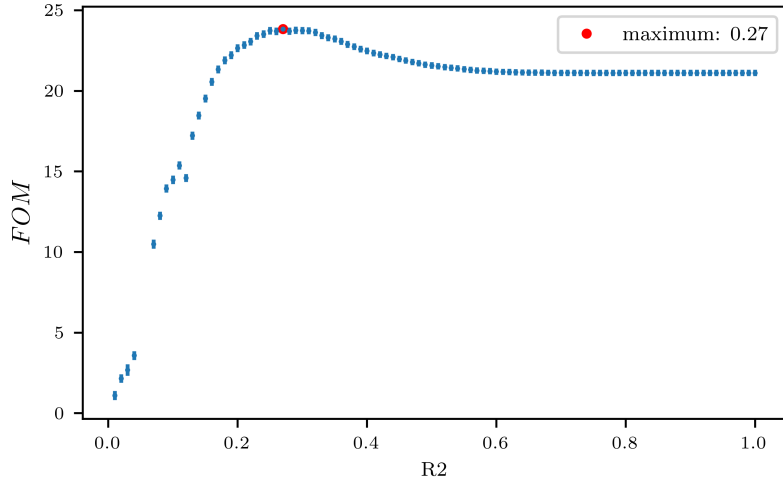


Figure (6) Figure of Merit values calculated at several cuts on the *foxWolframR2* variable

123 From Fig. 9 one can see that with values of the cut above $p_{CMS}^{\Lambda_c} < 1.8 \text{ GeV}/c^2$ a
 124 plateau of maximum FOM values is reached. But such a cut would still be useful to reject
 125 some background events as one can see from Fig. 10.

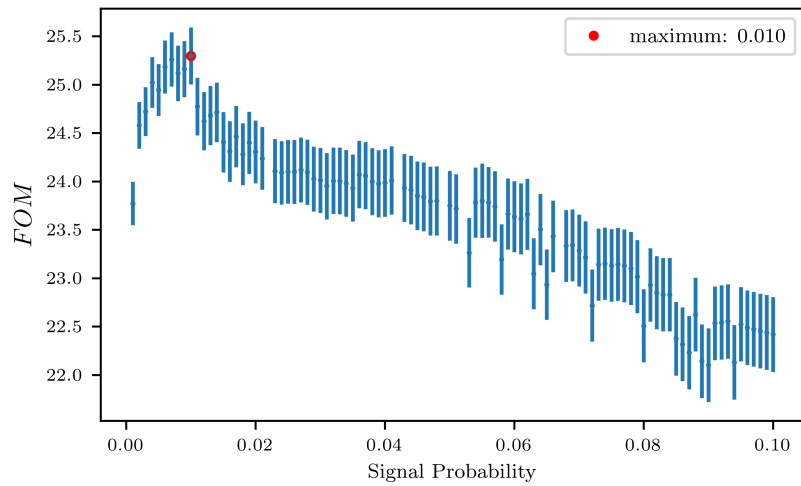


Figure (7) Figure of Merit values calculated at several cuts on the SignalProbability variable

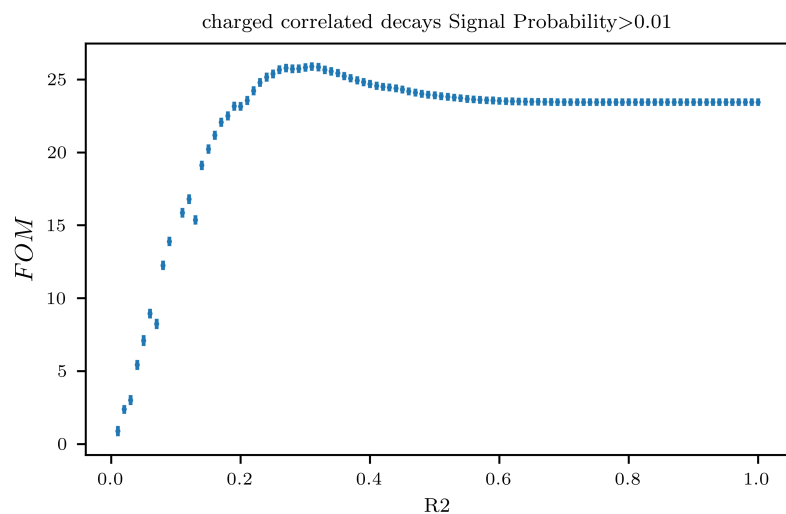


Figure (8) Figure of Merit values calculated at several cuts on the *foxWolframR2* variable

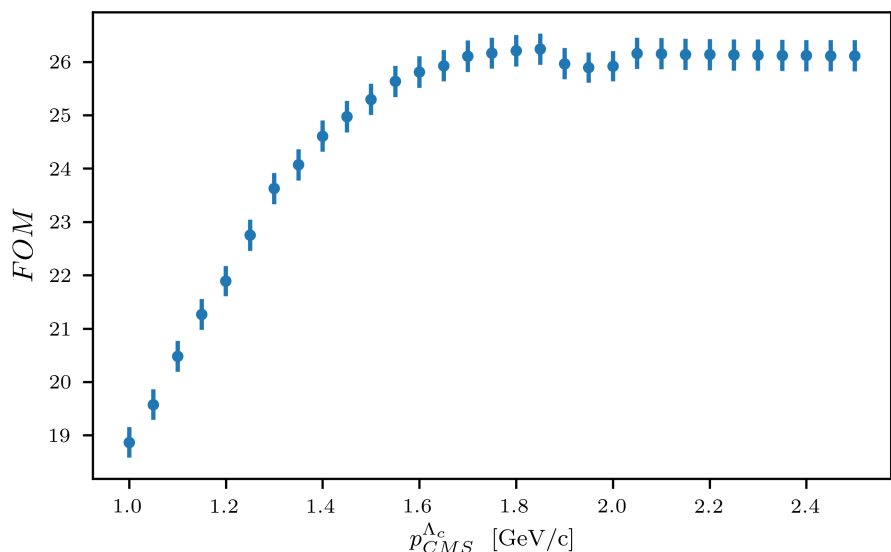


Figure (9) Figure of Merit values calculated at several cuts on the momentum of the Λ_c candidates in the center of mass system

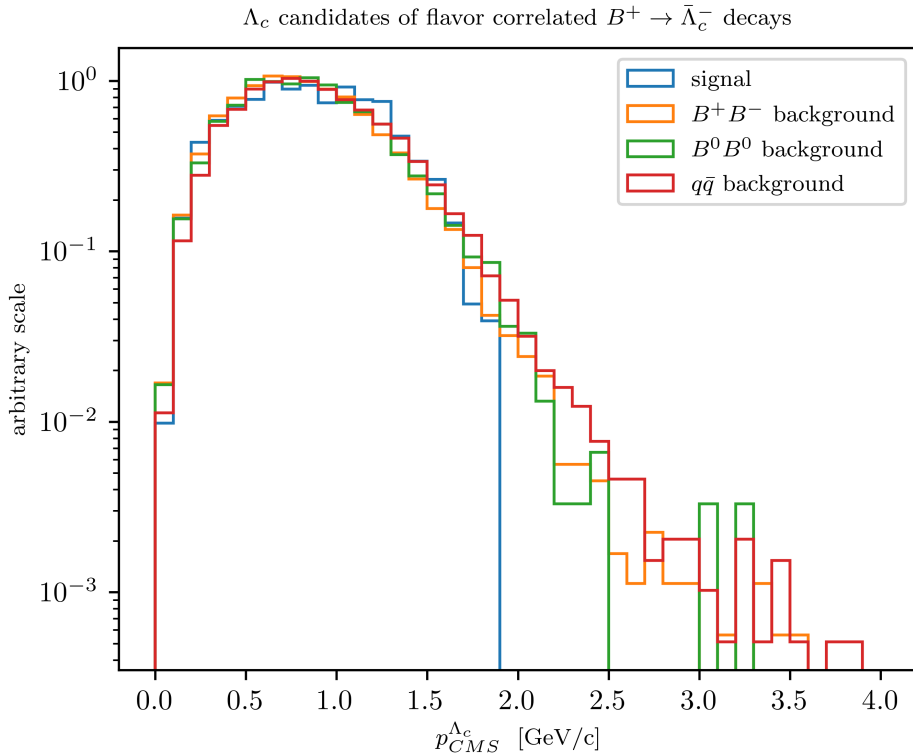


Figure (10) Distribution of Λ_c candidates momenta in the center of mass system

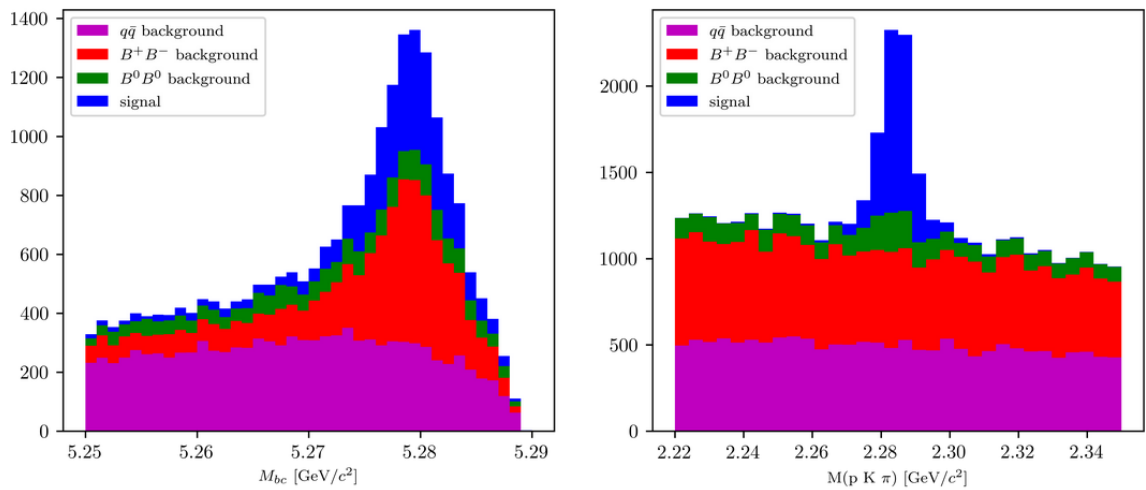


Figure (11) Distribution of M_{bc} (left) and invariant mass of charged correlated Λ_c candidates (right), in the signal region after the above mentioned selection cuts.

130 To measure the inclusive branching fraction of $B^- \rightarrow \Lambda_c^+ X$ the following quantities
 131 need to be known:

$$Br(B^- \rightarrow \Lambda_c^+ X) = \frac{N_{tag,\Lambda_c} \cdot \epsilon_{FEI}^+}{N_{tag} \cdot Br(\Lambda_c^+ \rightarrow pK^-\pi^+) \epsilon_{\Lambda_c} \epsilon_{FEI,sig}^+} \quad (1)$$

132
 133 Where

- 134 • N_{tag,Λ_c} is the reconstructed signal yield obtained from a two dimensional fit of M_{bc}
 135 and $M(pK\pi)$ in the final sample.
- 136 • N_{tag} is the reconstructed signal yield obtained from the M_{bc} fit of all the tagged B
 137 mesons in the final sample.
- 138 • ϵ_{Λ_c} is the Λ_c reconstruction efficiency.
- 139 • ϵ_{FEI}^+ represents the hadronic tag-side efficiency for generic B^+B^- events.
- 140 • $\epsilon_{FEI,sig}^+$ represents the hadronic tag-side efficiency for B^+B^- events where the tagged
 141 B meson decays hadronically and the accompanying meson decays inclusively into
 142 the studied signal channel.
- 143 • $Br(\Lambda_c^+ \rightarrow pK^-\pi^+)$: the branching fraction of the decay mode used to reconstruct
 144 the Λ_c baryon.

145 Here a decision was made not to rely on the estimated number of B meson pair, as it is
 146 usually done, and the absolute FEI efficiency, since the latter shows large discrepancy
 147 between MC and data (see i.e. the results reported in the PhD Thesis by M. Gelb [4] and
 148 also by J. Schwab [5]) and also it depends strongly on the signal-side (i.e. $\epsilon_{FEI}^+ \neq \epsilon_{FEI,sig}^+$).
 149 Instead, to limit the systematics, the branching ratio normalization is obtained using the
 150 fitted tagged B mesons and the ratio $\epsilon_{FEI,sig}^+/\epsilon_{FEI}^+$ measured on MC, which is expected to
 151 be described much better rather than the absolute FEI efficiency.

152 The final samples contain both signal and background candidates from various sources
 153 and in order to extract N_{tag,Λ_c} and N_{tag} unbinned extended maximum-likelihood fits are
 154 performed.

155 In the next sections the methods used to determine the above mentioned quantities are
 156 described. First the fit model that accurately describes the distributions in the $B_{tag} + \Lambda_c$
 157 final sample will be described.

158 4.1 Probability Density Functions (PDFs) for the two dimensional 159 fit

160 The PDFs used to describe the signal distributions are discussed first. The final sample of
 161 total signal events presents a peak around the expected B meson mass and a tail at low
 162 M_{bc} values.

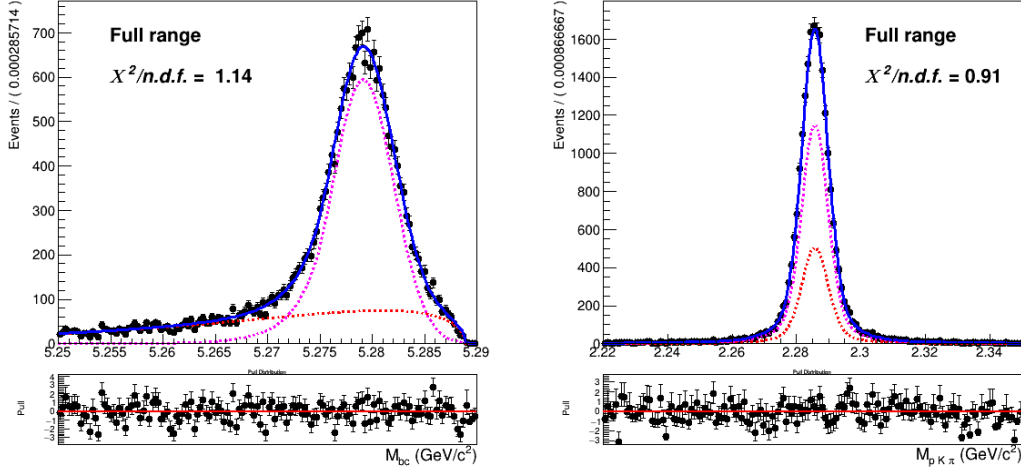


Figure (12) Two dimensional fit of total signal events in M_{bc} and $M(pK\pi)$

163 The 2D fit shown in Fig. 12 is performed on five streams of signal MC with a sum of
 164 the following probability density functions:

$$P_{B,\Lambda_c}^{recSig}(M_{bc}, M(pK\pi)) = \Gamma_{CB}(M_{bc}) \times \rho_G(M(pK\pi)) \quad (2)$$

165 $P_{B,\Lambda_c}^{misSig}(M_{bc}, M(pK\pi)) = \Gamma_{ARG}(M_{bc}) \times \rho_G(M(pK\pi)) \quad (3)$

166 The first is used to fit the reconstructed signal and $\Gamma_{CB}(M_{bc})$ is a Crystal Ball function.
 167 The second is used to model the misreconstructed signal and $\Gamma_{ARG}(M_{bc})$ is an Argus
 168 function. In both cases a sum of three Gaussian functions $\rho_G(M(pK\pi))$ describes the
 169 mass of the Λ_c baryon.

171 As already said in Sec. 2.3, only the reconstructed signal considered for the signal
 172 yield, while the misreconstructed signal is considered as background. Other background
 173 components that will be discussed in the next pages are:

- 174 • **generic** (charged B) background
- 175 • **crossfeed** (neutral B) background
- 176 • **continuum** background

¹⁷⁷ **Generic background**

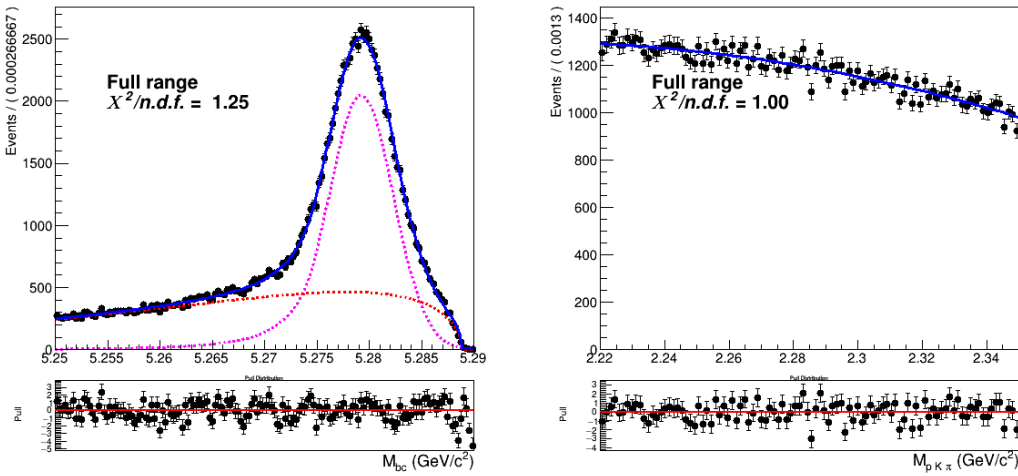


Figure (13) Two dimensional fit of generic (B^+B^-) events in M_{bc} and $M(pK\pi)$.

¹⁷⁸ The generic background deriving from other B^+B^- events presents a similar shape of the
¹⁷⁹ distribution in M_{bc} (see Fig. 13): the probability density functions used for it are again a
¹⁸⁰ Crystal Ball and an Argus. For both functions the parameters differ from the ones used in
¹⁸¹ Eq. 2-4.1. Instead, the flat background in $M(pK\pi)$ can be described with a second order
¹⁸² Chebychev polynomial function. The two dimensional PDF in this case is given by:

$$P_{B,\Lambda_c}^{GenBkg}(M_{bc}, M(pK\pi)) = [\Gamma_{CB}(M_{bc}) + \Gamma_{ARG}(M_{bc})] \times \rho_{Cheb2}(M(pK\pi)) \quad (4)$$

183 **Crossfeed background**

184 The contamination of misreconstructed B^0 events in the B^+ signal (and vice-versa) induces
 185 a background which peaks near the B meson mass, as one can see in Fig. 14, independently
 186 from the category of events in the Λ_c mass (see Figures 15- 16). Since among the
 187 misreconstructed B^0 events there are also $B^0 \rightarrow \Lambda_c$ decays (peaking at the Λ_c mass, see
 188 e.g. Fig. 15), this background contribution is also named "crossfeed background".

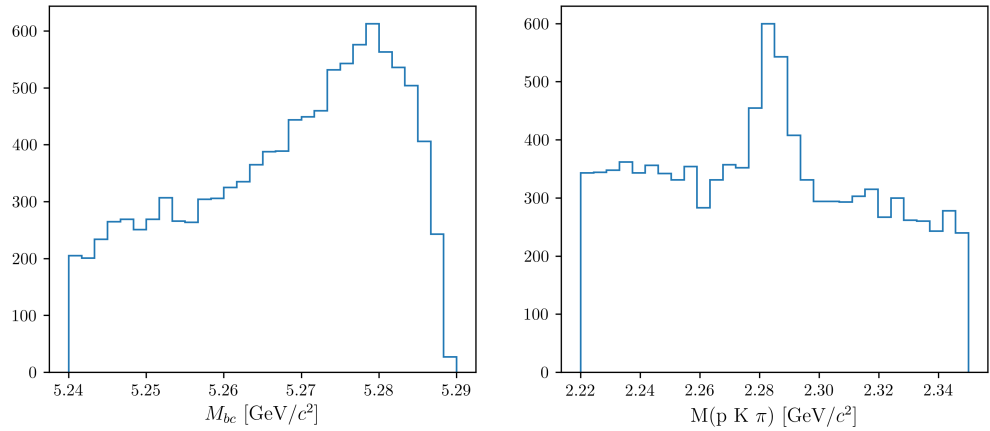


Figure (14) M_{bc} and $M(pK\pi)$ distributions of crossfeed background events.

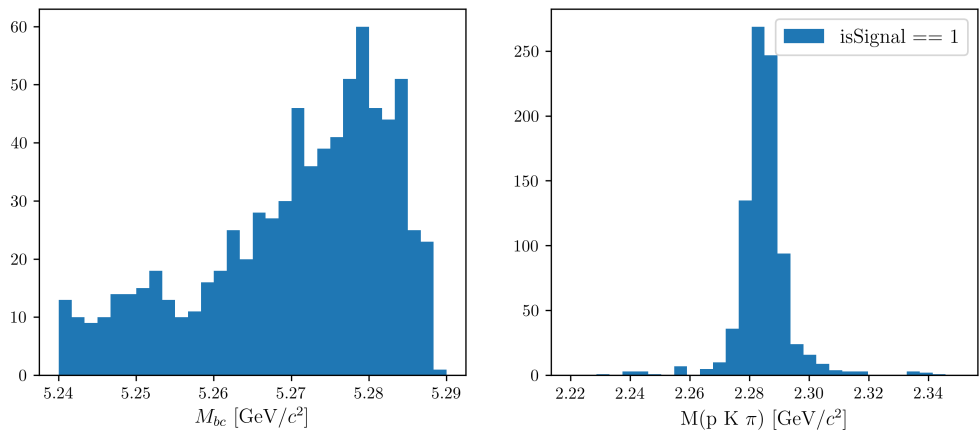


Figure (15) M_{bc} and $M(pK\pi)$ of crossfeed events peaking at the Λ_c mass, i.e.: where true Λ_c baryons were correctly reconstructed.

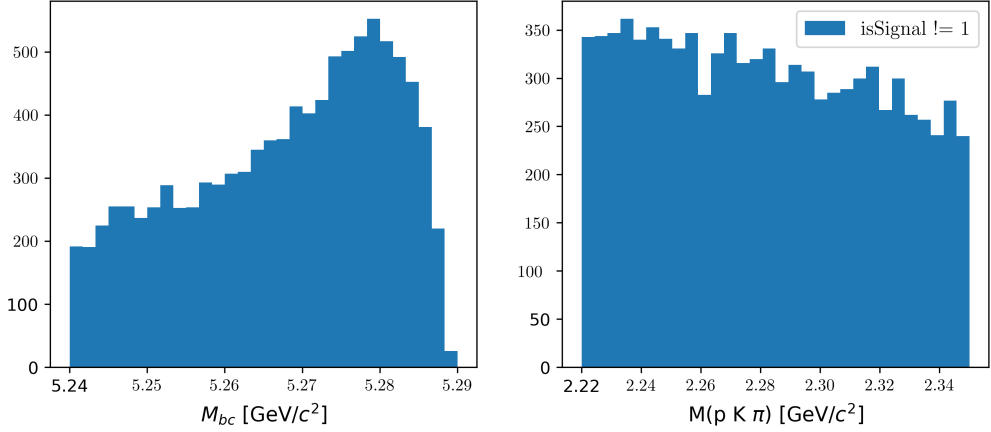


Figure (16) M_{bc} and $M(pK\pi)$ of crossfeed events without Λ_c peak, i.e.: where Λ_c baryons were not present or not correctly reconstructed.

Fig. 17 shows the projections in M_{bc} and $M(pK\pi)$ of the two dimensional fit of this type of background. The M_{bc} is modelled with a sum of Novosibirsk (colored in magenta) and Argus function (colored in red). Whereas the $M(pK\pi)$ distribution is described by the sum of a first order Chebychev polynomial and the peak by the same sum of three Gaussian functions used to describe the signal peak. In fact the latter is the result of the reconstruction of crossfeed events $B^0 \rightarrow \Lambda_c$. Therefore the 2D PDF can be written as:

195

$$P_{B,\Lambda_c}^{CrossBkg}(M_{bc}, M(pK\pi)) = [\Gamma_{Nov}(M_{bc}) + \Gamma_{ARG}(M_{bc})] \times [\rho_{Cheb1}(M(pK\pi)) + \rho_G(M(pK\pi))] \quad (5)$$

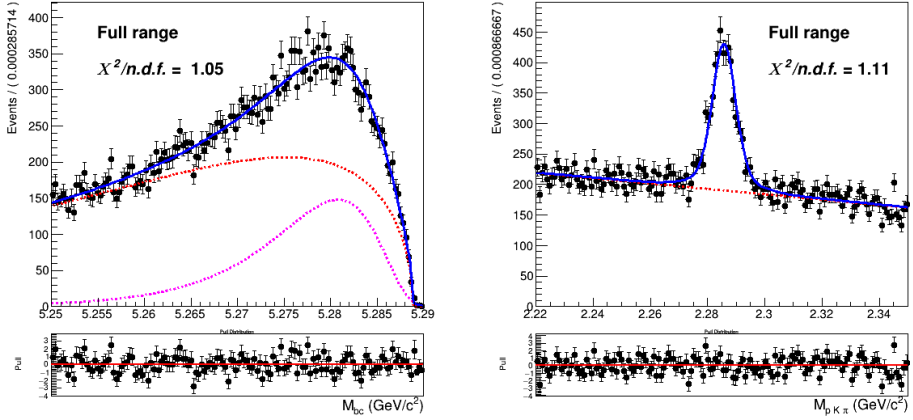


Figure (17) Two dimensional fit of crossfeed ($B^0\bar{B}^0$) events in M_{bc} and $M(pK\pi)$.

From the projections plotted in Fig. 17 the distributions appear to be well described by the PDF discussed above. Though the agreement in the Λ_c invariant mass is not fully

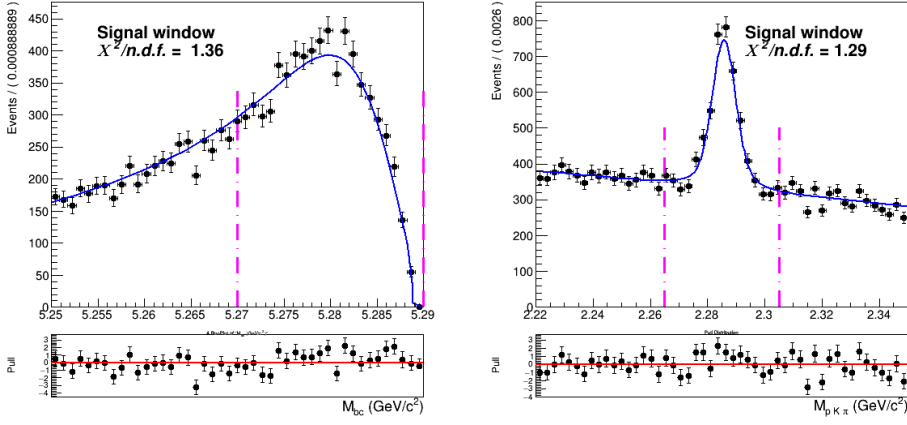


Figure (18) Signal region projections in M_{bc} and $M(pK\pi)$.

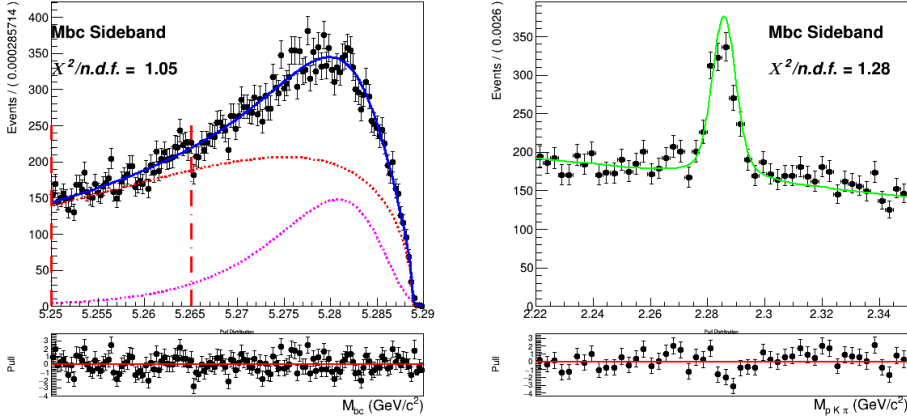


Figure (19) M_{bc} sideband region projection.

198 respected when different regions of M_{bc} are considered, as one can see from Fig. 18 and
 199 Fig. 19. The fraction of the amount of peaking events is not uniform among different M_{bc}
 200 regions. Since this background typology is peaking in both the observables of the fit, the
 201 potential correlation between them could have an impact on the signal yield extraction in
 202 the total fit.

203 To minimize this effect, and to avoid possible biases deriving from this feature, a
 204 correction is attempted. The M_{bc} is divided in 5 different regions. As shown in Figures
 205 21a-21e, for each of these regions a fit on the projected Λ_c invariant mass is performed to
 206 extract 5 values of the fraction of peaking events in those regions (all other parameters are
 207 fixed). Those values are then used for a parametrization of this parameter as a function of
 208 M_{bc} .

209 From the plot shown in Fig. 20 one can see that it is possible to describe the trend with a
 210 linear dependence with a good approximation.

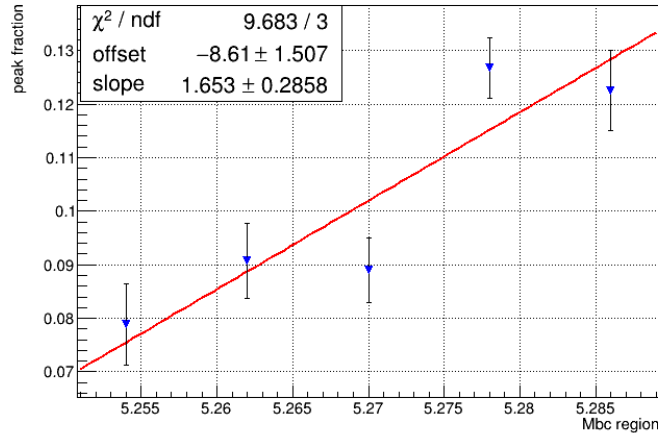


Figure (20) Invariant mass peak fraction as a function of M_{bc} .

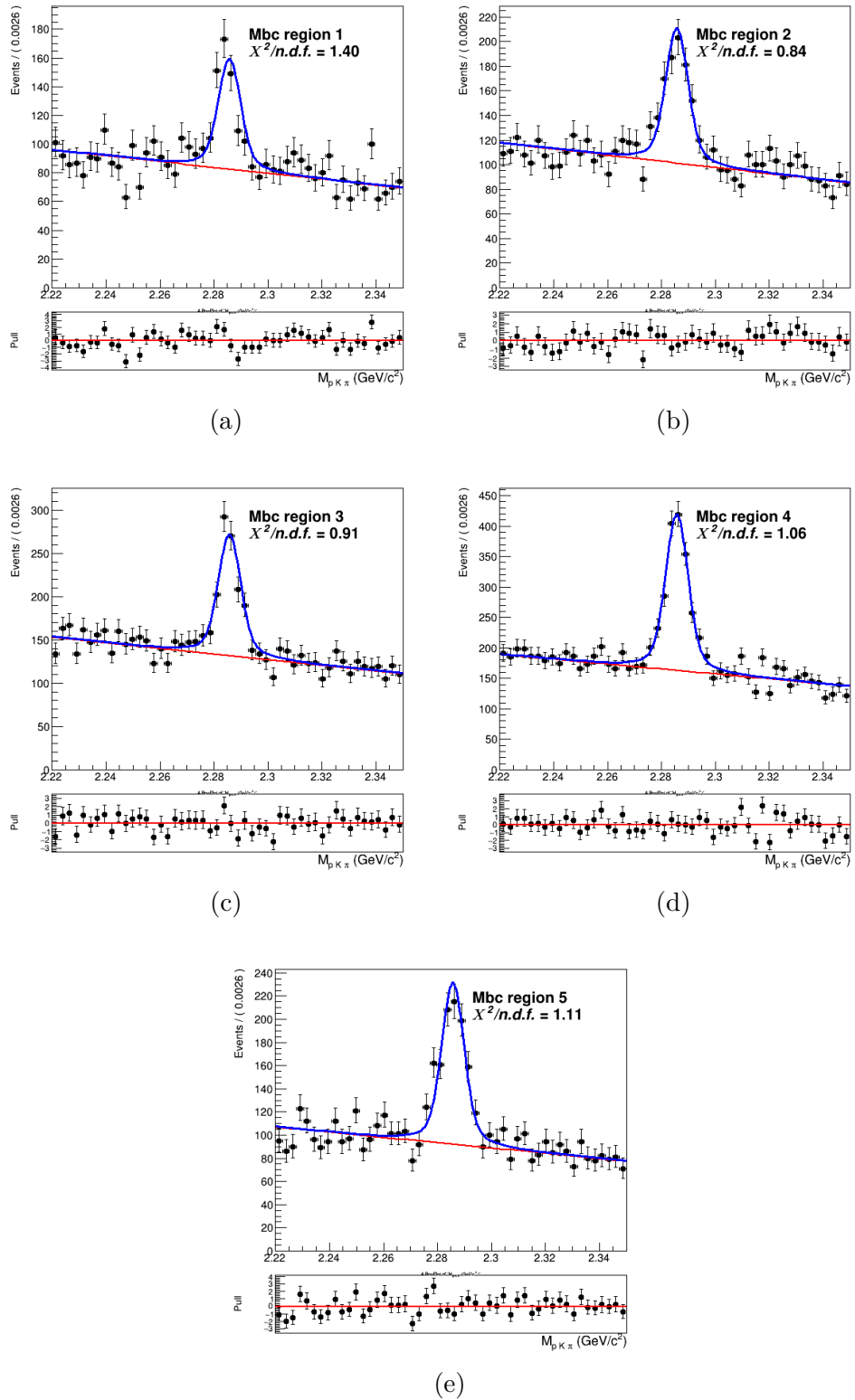


Figure (21) Fits of $M(pK\pi)$ in 5 different regions of M_{bc} : $5.25 < M_{bc} < 5.258 \text{ GeV}/c^2$, $5.258 < M_{bc} < 5.266 \text{ GeV}/c^2$, $5.266 < M_{bc} < 5.274 \text{ GeV}/c^2$, $5.274 < M_{bc} < 5.282 \text{ GeV}/c^2$, $5.282 < M_{bc} < 5.29 \text{ GeV}/c^2$.

211 The 2D PDF describing the crossfeed background is consequently modified:

212

$$P_{B,\Lambda_c}^{CrossBkg}(M_{bc}, M(pK\pi)) = [\Gamma_{Nov}(M_{bc}) + \Gamma_{ARG}(M_{bc})] \times [F(M(pK\pi)|M_{bc})] \quad (6)$$

213 where the conditional PDF $F(M(pK\pi)|M_{bc})$ describing the invariant mass is still a sum of
 214 $\rho_{Cheb1}(M(pK\pi))$ and $\rho_G(M(pK\pi))$, but their fraction is now parametrized as a function
 215 of M_{bc} .

216 In Figures 22- 23 one can appreciate the improvement obtained with this correction.

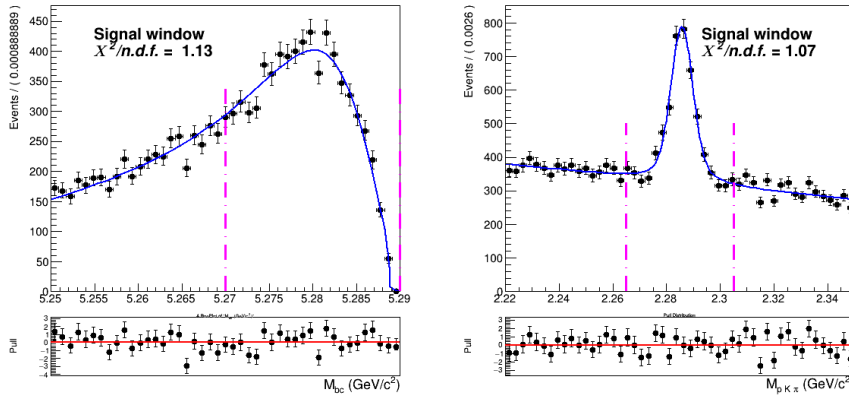


Figure (22) Signal region projections in M_{bc} and $M(pK\pi)$ after the parametrization.

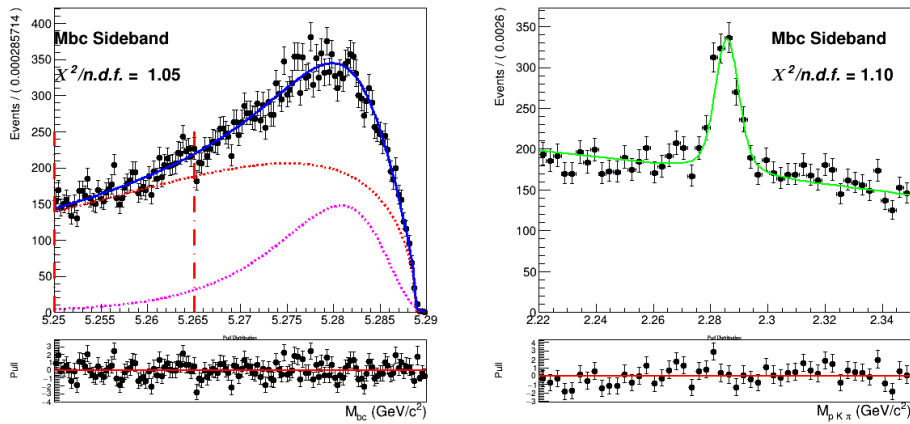


Figure (23) M_{bc} sideband region projection after the parametrization.

217 **Continuum background**

218 Besides the dataset recorded at the energy of the $\Upsilon(4S)$ resonance ($E_{CMS}^{on-res} = 10.58$ GeV),
 219 the *Belle* experiment recorded a sample of $89.4 fb^{-1}$ at an energy 60 MeV below the
 220 nominal $\Upsilon(4S)$ resonance ($E_{CMS}^{off-res} = 10.52$ GeV). The dataset allows to check for an
 221 appropriate modeling of the continuum MC simulation. Using the official tables
 222 (<https://belle.kek.jp/secured/nbb/nbb.html>) the off-resonance sample is scaled by

$$\frac{\mathcal{L}^{on-res}}{\mathcal{L}^{off-res}} \left(\frac{E_{CMS}^{off-res}}{E_{CMS}^{on-res}} \right)^2 \quad (7)$$

taking into account the difference in luminosity and in E_{CMS} (Energy in center of mass system).

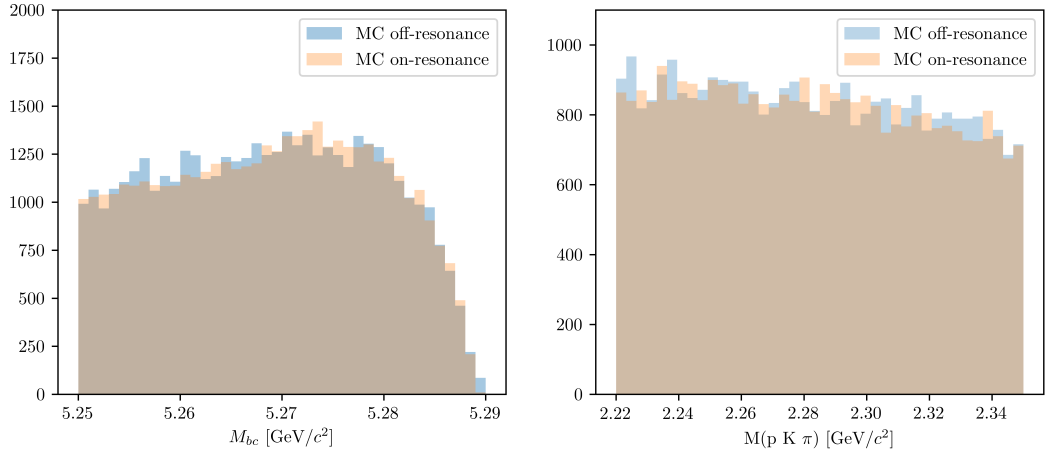


Figure (24) M_{bc} and $M(pK\pi)$ comparison between on-/off-resonance (scaled) Monte Carlo simulated continuum. The scaling is applied according to Eq. (7) and shifting the M_{bc} distribution by $E_{CMS}^{on-res} - E_{CMS}^{off-res}$.

The plot in Fig.24 shows the M_{bc} and $M(pK\pi)$ distributions in the MC on-/off-resonance continuum after the scaling¹.

Ideally, provided that there's a good agreement between MC and data for the off-resonance sample and also between the MC on-/off-resonance continuum after the scaling, one could directly use the scaled off-resonance data to describe the continuum background in the fit on data. There are two reasons that prevent this very straightforward approach:

- First, since the off-resonance MC (and data) present very low statistics (Fig. 26a shows the Λ_c invariant mass in off-resonance data), scaling them with all the applied selection cuts would cause the PDF describing the continuum to be very much affected by statistical fluctuations.
- Secondly, the B meson candidates are reconstructed in both on-resonance and off-resonance events for values of $M_{bc} \geq 5.22 \text{ GeV}/c^2$, but the E_{CMS} differs: there can be effects of correlations between the applied *SignalProbability* cut and the M_{bc} variable that one needs to take into account.

¹it is obtained with the MC off-resonance sample being composed of 6 streams: the total amount is normalized

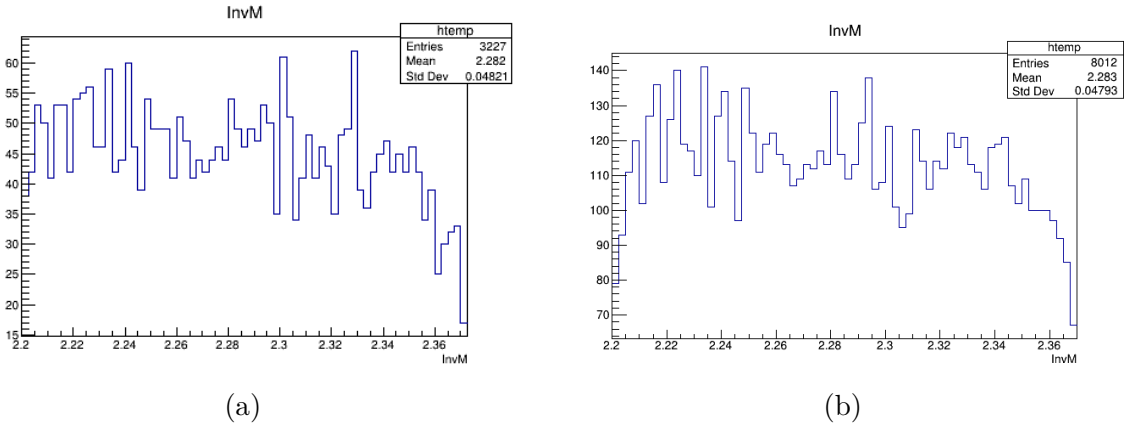


Figure (26) On the left: Λ_c invariant mass in off-resonance data (all nominal cuts applied). On the right: Λ_c invariant mass in off-resonance data after the continuum suppression cut removal.

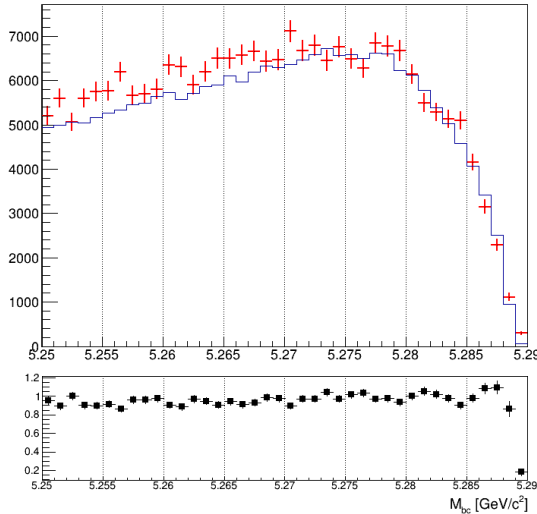


Figure (25) M_{bc} distributions of the MC (scaled) off-resonance sample (in red) and on-resonance (in blue) using 5 streams statistics and all nominal selection cuts applied.

In Fig. 25 one can notice some discrepancy in the shapes, apart from the not negligible statistical fluctuations in the (scaled) off-resonance distribution. In the Λ_c invariant mass one doesn't expect correlation effects, but nevertheless there can be differences due to the limited statistics of the off-resonance sample. In fact, in the case of on-resonance MC some events in which Λ_c candidates survive nominal selection cuts are visible and can be described with a small Gaussian on the top of the flat background (Fig.31a). On the contrary the off-resonance sample doesn't show anything else beside the flat background (the Fig.31b shows a 5 streams statistics).

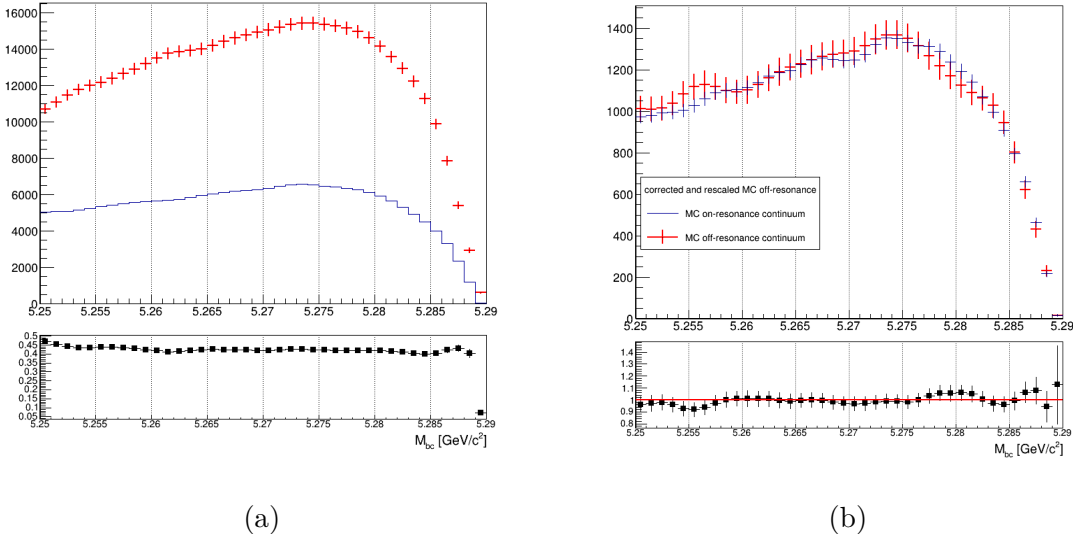


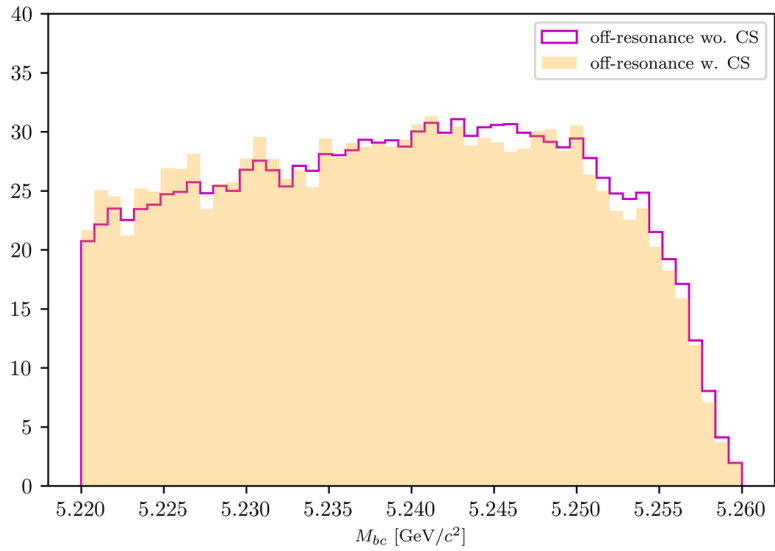
Figure (27) On the left: M_{bc} distributions of the MC off-resonance sample without continuum suppression and the MC continuum sample with applied continuum suppression. On the right: M_{bc} distributions of the corrected scaled MC off-resonance and on-resonance MC continuum.

247 The procedure adopted to obtain the PDF describing the continuum background M_{bc}
248 distribution is the following:

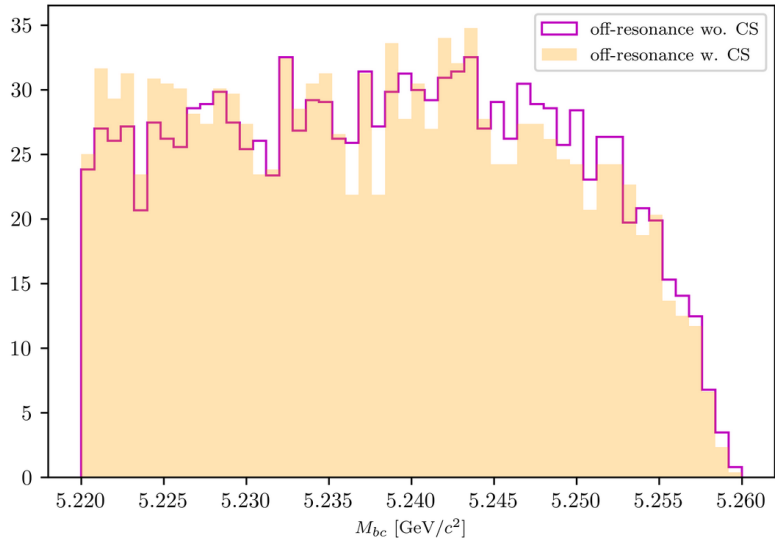
- 249
- 5 streams of off-resonance MC were scaled according to Eq. (7) without continuum
250 suppression being applied and compared to the distribution of 5 streams of on-
251 resonance continuum
 - From a ratio plot, like the one in Fig. 27a, the bin-correction is obtained to correct
252 the off-resonance data in the scaling procedure. To obtain the shape that can describe
253 the continuum background M_{bc} distribution on data the continuum suppression is not
254 applied on the off-resonance continuum sample, in order to acquire more statistics.
255

256 This procedure is first tested on an independent MC sample (see Fig. 27b) to check the
257 result on simulated data before applying it on data.

258 The validity of the method relies on the fact that on-/off-resonance continuum events are
259 well modeled in MC and that the shape of the M_{bc} distribution doesn't change significantly
260 when removing the continuum suppression cut both on MC and data (as one can see
261 from Figures 28a - 28b). Additionally, the continuum suppression cut efficiency should
262 be the same in data and MC in order to have the correct scaling on data with the above
263 mentioned method. Fig. 29 shows the distribution of the *foxWolframR2* variable in
264 off-resonance MC and data. The slight shift visible in data can cause a different impact on
265 data in terms of rejected continuum background when applying the *foxWolframR2* < 0.3
266 cut. It is found to reject about 60% of the continuum background in data, whereas it



(a)



(b)

Figure (28) Above: M_{bc} distributions of the MC off-resonance sample (5 streams) with and without continuum suppression. Below: M_{bc} distributions on data with and without continuum suppression.

rejects 55% of the continuum background in MC (56% in on-resonance MC). Therefore in data one can expect about 2.25% less continuum background events. This discrepancy is not statistical significant (the statistical uncertainty for the continuum background events is of the level of $\sim 1\%$), a simple correction to the number of events can be applied on data and its possible systematics can be then taken into account.

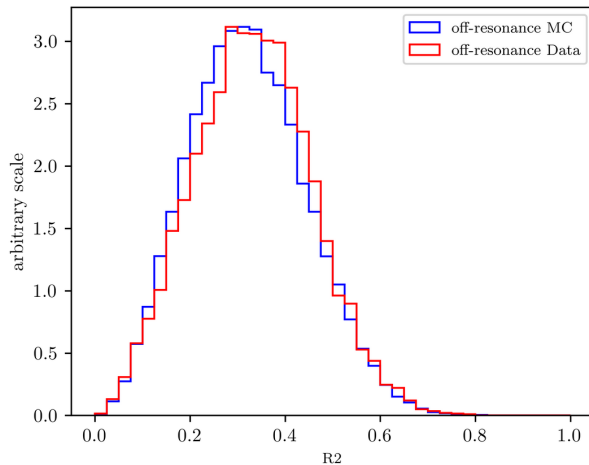


Figure (29) Distributions of variable $foxWolframR2$ in off-resonance MC and data.

²⁷² The obtained distribution can be then fitted (see Fig. 30), i.e. with a Novosibirsk function.
²⁷³ This is the procedure which can be then applied on the off-resonance data to obtain the M_{bc} shape describing the continuum background in data.

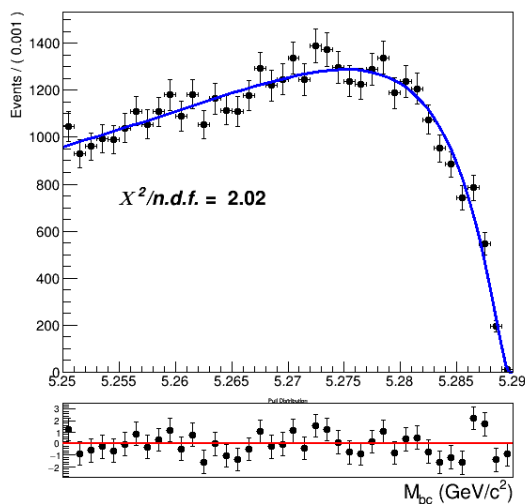


Figure (30) Fit of the M_{bc} distribution MC (scaled) off-resonance continuum (one stream).

²⁷⁴

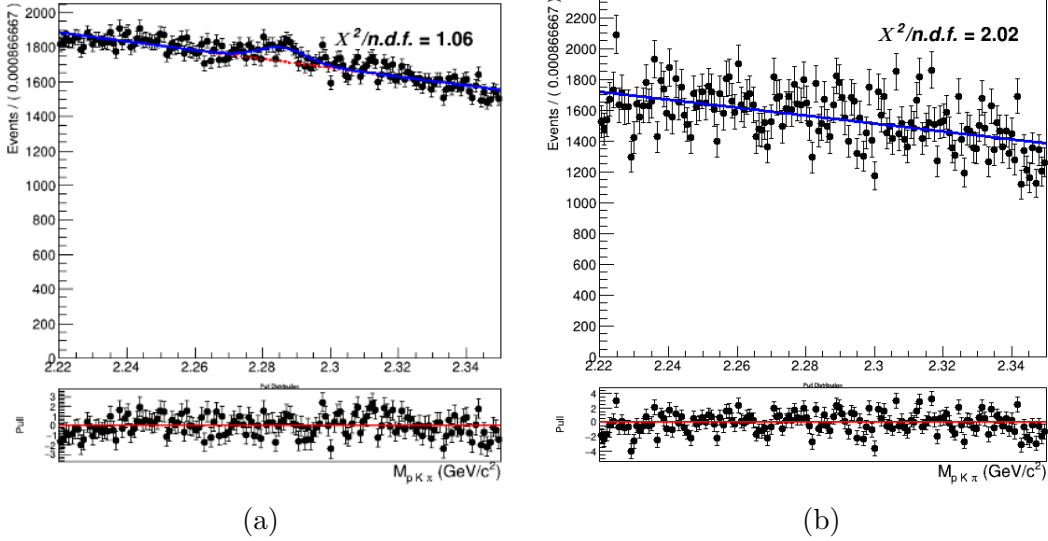


Figure (31) Comparison between 5 streams of MC on-resonance continuum 31a) and off-resonance (scaled) continuum in $M(pK\pi)$ (31b).

275 The shape describing the Λ_c invariant mass is obtained from the simulated on-resonance
 276 continuum, again using 5 streams statistics (see Fig. 31a).

277 Finally, it is possible to examine the validity of the whole procedure on the independent
 278 stream. Fig. 33 shows the M_{bc} , $M(pK\pi)$ projections of the two dimensional fit with the
 279 one-dimesional PDFs obtained with the above described procedure. The 2D PDF used
 280 can be written as:

281

$$282 \quad P_{B,\Lambda_c}^{Continuum}(M_{bc}, M(pK\pi)) = \Gamma_{Nov}(M_{bc}) \times [\rho_{Cheb1}(M(pK\pi)) + \rho_{G1}(M(pK\pi))]$$

283

284 where, as already anticipated, the invariant mass is described by a sum of a first order
 285 Chebychev polynomial and the peak by a single Gaussian function.

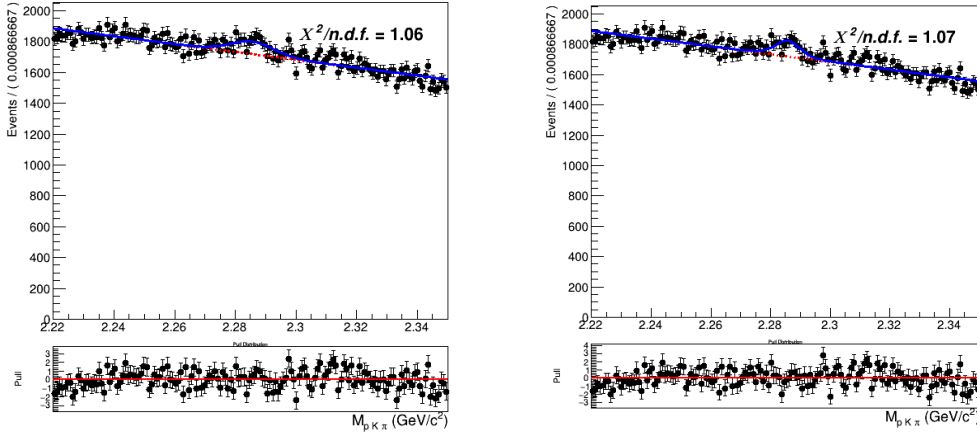


Figure (32) Λ_c invariant mass fits using five streams. On the left: fit of the Λ_c invariant mass of on-resonance continuum using the one Gaussian description (all nominal cuts applied). On the right: fit of the Λ_c invariant mass of on-resonance continuum using the same three gaussian PDF to describe the peak in the signal invariant mass (all nominal cuts applied).

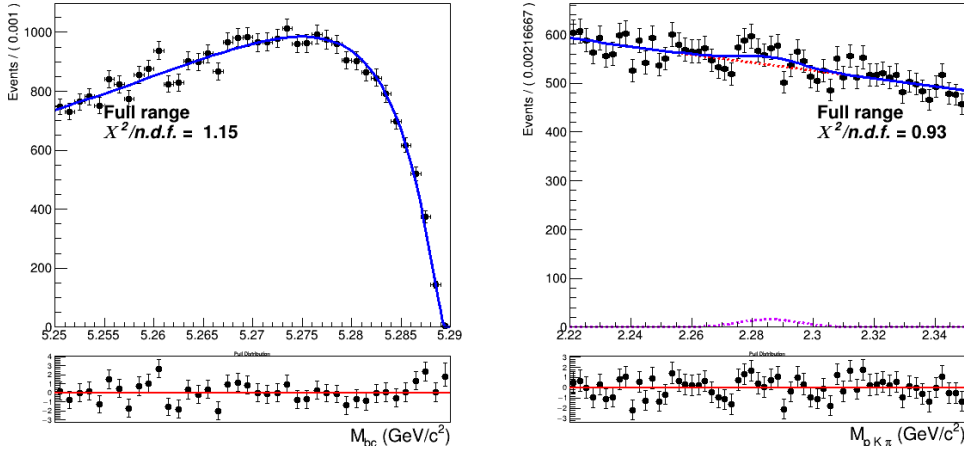


Figure (33) Two dimensional fit of continuum events (one stream).

286 It was then also investigated to alternatively use the same triple Gaussian PDF (used
 287 in Eq. 2 for the signal peak) to describe the peak, as it is shown in Fig. 32 . The two
 288 descriptions seem to be equivalent. The final fits described in Sec. 4.2 were performed
 289 with the one Gaussian description (keeping all parameters fixed), but it was also tried
 290 with the alternative three Gaussian description (with main Gaussian having the width as
 291 free parameter): no significant difference was noticed and the signal yields differ by only
 292 about 10% of the statistical uncertainties. Though, for consistency reasons, on data the
 293 second description will be applied.

294 **4.2 Two dimensional fit**

295 All the already discussed PDFs describing the various categories of events were constructed
 296 using five streams. Then an independent stream is used to test if the total PDF enables
 297 to extract the signal yield in an unbiased way. In order to test this a total of six fits are
 298 performed on six different streams of generic MC. Exemplary, the distributions of stream
 299 0 overlaid by the fitted PDF are depicted in Fig. 34 (see Appendix .1 for the projections
 300 in signal and sideband regions). In all six fits all the shaping parameters are kept fixed,
 301 except:

- 302
 - σ_{G1} : the width of the wider of the three Gaussian functions in $\rho_G(M(pK\pi))$
 - 303 • σ_{CB} parameter for the Crystal Ball describing the signal peak in M_{bc}

304 In the M_{bc} distribution the σ_{CB} parameter for the Crystal Ball describing the generic
 305 background is expressed as function of the signal σ_{CB} with a ratio fixed from the MC. As
 306 for the normalizations, mis-/reconstructed signal events and generic background events
 307 are floated in the two dimensional unbinned maximum likelihood fits. The continuum
 308 background normalization is kept fixed to the value obtained by the off-resonance scaling
 309 procedure. Instead, the normalization of crossfeed background events deserves a special
 310 treatment, a possible choice would be to express it as a function of the ratio of crossfeed
 311 events with respect to the misreconstructed signal events and keep it fixed to the MC value
 312 (this is done then in the fit on all tagged B mesons, i.e. in Sec. 4.4). This would make
 313 sense according to the fact that the two categories of events are similar: in both cases the
 314 B mesons were not correctly reconstructed, either because of missing or wrongly added
 315 particles (misreconstructed signal events) or, in the case of crossfeed events because it was
 316 a different one (B^0 meson instead of charged one). Since the amount of misreconstructed
 317 signal depends on the branching ratio itself, this method is not viable. Therefore, as for the
 318 crossfeed background the normalization of the PDF described in Eq. (6) is parametrized
 319 in the form:

$$N_{CrossBkg} P^{CrossBkg}(M_{bc}, M(pK\pi)) = k \cdot N_{B^0} \cdot N_{misRecSig}/N_{sig} \cdot P^{CrossBkg}(M_{bc}, M(pK\pi)) \quad (8)$$

- 320
 - 321 • defining a sort of "probability ratio": $k = \frac{N_{crossfeed}/N_{B^0}}{N_{misRecSig}/N_{sig}}$, where the numerator
 represents the probability of misreconstructing B^0 as B^+ events and the denominator
 the probability of misreconstructing signal events. This ratio is calculated from MC
 and will be kept fixed also while fitting data.

- 324
- 325
 - 326 • N_{B^0} is the total number of B^0 events in the dataset (MC or data).
 - 327 • $N_{misRecSig}$ is the floated normalization of misreconstructed signal events
 - 328 • $N_{sig} = N_{recSig}/\epsilon$ is the total number of signal events expressed as function of the
 floated normalization of reconstructed signal events and the signal reconstruction
 efficiency.

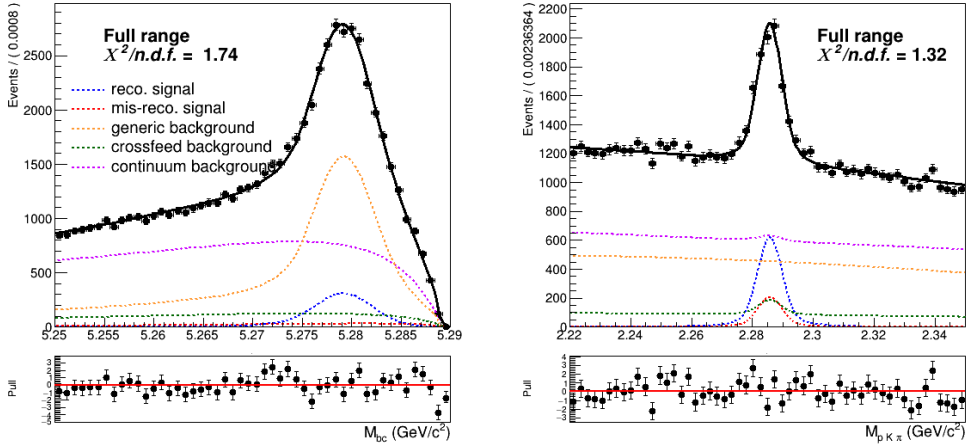


Figure (34) Two dimensional fit on stream 0 Monte Carlo simulated data.

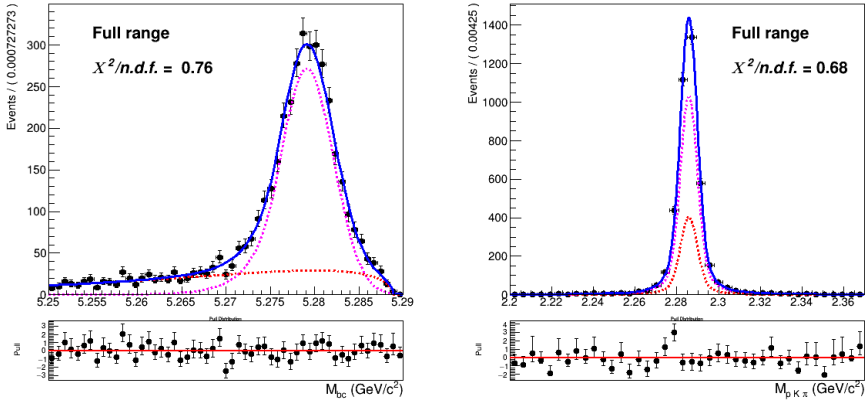


Figure (35) Two dimensional fit of Total Signal of stream 0 used to extract the expected reconstructed (corresponding to the PDF colored in magenta) and expected misreconstructed yields (corresponding to the PDF colored in red).

330 In Table 1 the signal yields of the fits (**Reconstructed Signal**) to the two dimensional
 331 distributions for the six streams of $B^- \rightarrow \Lambda_c^+$ flavor-correlated decays are listed and
 332 compared to the yields obtained from fits of signal distributions of each individual stream.
 333 The latter are the "expected" yields of reconstructed signal from a fit to the total signal
 334 events in the individual stream as the one plotted on Fig. 35 where all the parameters of
 335 the PDFs described in Eq. (2) are kept fixed and the corresponding yields are extracted
 336 from the fit.

	Reconstructed Signal		Total Signal			
	fit	expected	fit	MC truth	fit - MC truth	
stream 0	3072 ± 113	2928 ± 66	4037 ± 121	4061	-24	-0.6%
stream 1	2919 ± 115	2956 ± 66	4098 ± 126	4084	14	0.3%
stream 2	2627 ± 119	2940 ± 66	4031 ± 126	4138	-107	-2.6%
stream 3	2865 ± 111	2850 ± 66	4140 ± 123	4105	35	0.9%
stream 4	3328 ± 119	3046 ± 67	4076 ± 126	4176	-100	-2.2%
stream 5	2959 ± 114	2816 ± 65	4080 ± 129	4001	79	2.0%
sum	17770	17538	24462	24565	-103	-0.4%

Table (1) Comparison of fitted and expected signal yields, fitted and truth-matched total signal for six streams of Belle generic MC when fitting the two dimensional distributions of M_{bc} and $M(pK\pi)$.

337 The table also reports the fitted and truth-matched number of total signal (sum of reconstructed
 338 and misreconstructed signal) events. One can notice that, despite the deviations
 339 of total signal events being within statistical uncertainties, the results for reconstructed
 340 signal (first column) show fluctuations which exceed the statistical uncertainties, especially
 341 in case of stream 2 and 4 (see also Fig. 36 and Fig. 37) One can notice also an overall
 342 tendency towards higher values for the signal yields (the sum is about $2\sigma^{stat.}$ away from
 343 the sum computed for the expected yields).

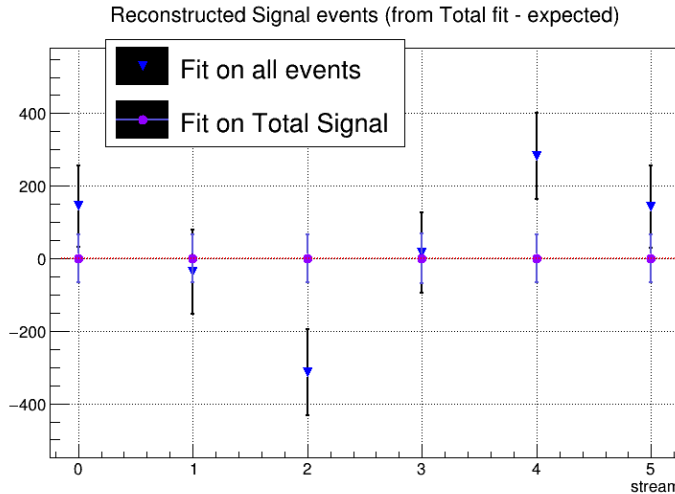


Figure (36) Differences between results from the fits and "expected" values for signal yields as reported in the first columns on Table1 .

344 Additionally, one can investigate the behaviour for different signal-to-background ratio.
 345 Thus, a second test of the fit model is performed. Using the six independent streams
 346 the amount of total signal is varied between 25% and 150% of the nominal values. The
 347 plot in Fig. 38 shows the values of reconstructed signal obtained in the total fits versus
 348 those expected by the fits on total signal events. One can see that the values distribute

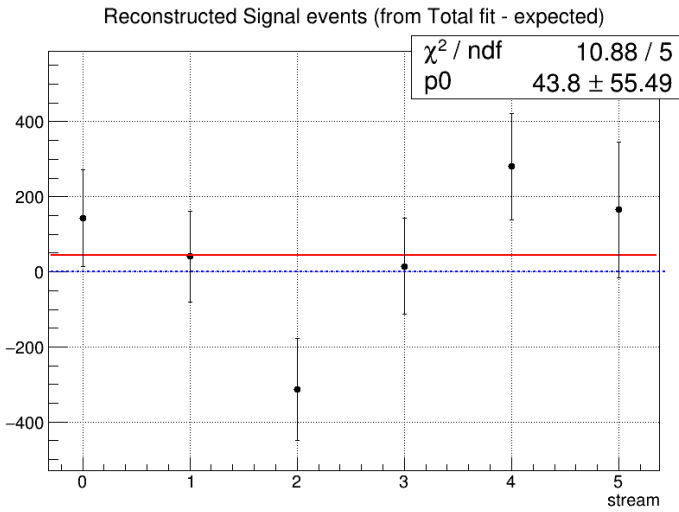


Figure (37) Fitted-expected subtracted values for reconstructed signal yields with associated uncertainties summed in quadrature.

³⁴⁹ according to a linear dependence. In Fig. 39 the linearity test is expressed in terms of
³⁵⁰ $\mathcal{B}(B^+ \rightarrow \bar{\Lambda}_c^- X)$ instead.

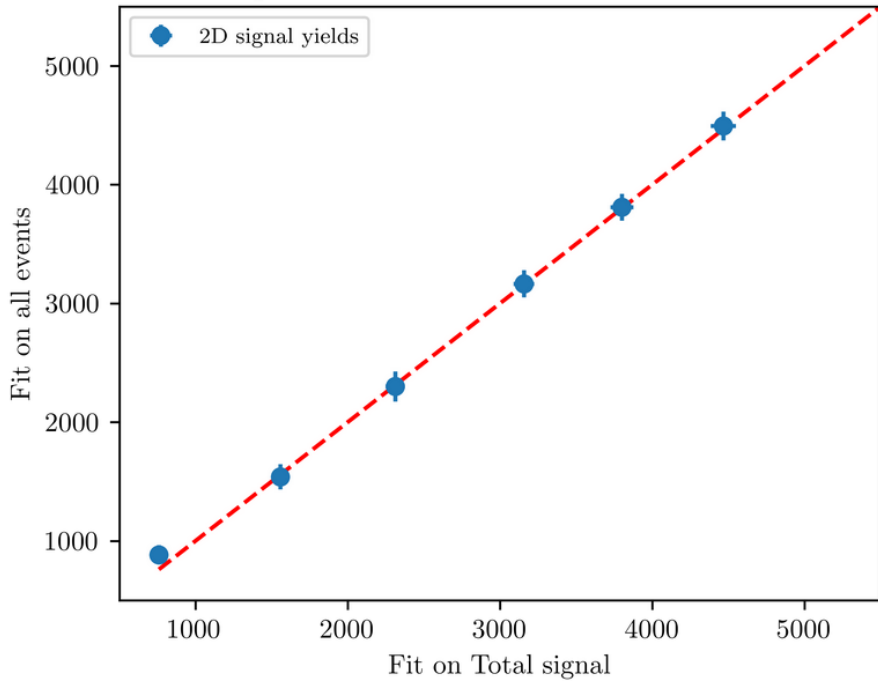


Figure (38) Linearity test: on the x-axis the obtained reconstructed signal yields from fits on different amounts of total signal; on y-axis the yields of reconstructed signal obtained fitting all events (as in Fig. 34). The dashed red line represents the 1:1 linear dependence.

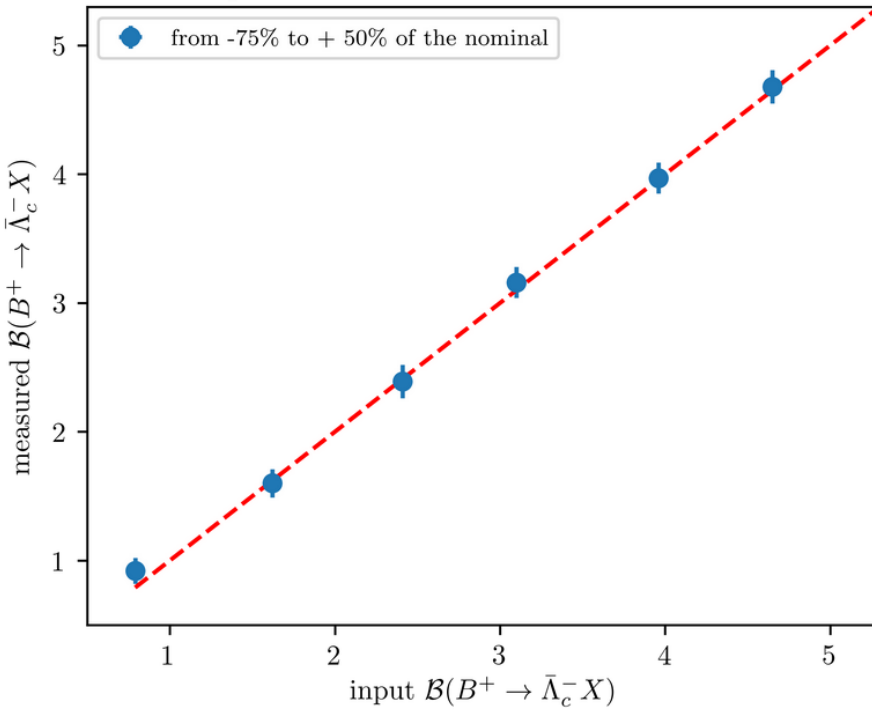


Figure (39) Linearity test: on the x-axis the input branching ratio value corresponding to the signal yields displayed on the x-axis in Fig. 38; on y-axis the measured branching fraction values corresponding to the signal yields of reconstructed signal displayed on the y-axis in Fig. 38.

351 For the fit model also toy MC pseudo-experiments were performed in order to confirm the
 352 behavior of the fit setup. With toy MC experiments the yields, errors and the pulls of the
 353 fit are studied by generating our own pseudo-datasets, according to the MC (see plots in
 354 the next page). 3×10^3 pseudo-datasets are constructed, where each dataset was generated
 355 with the expected amount of events, distributed according to the Poisson distribution.
 356 Then the composition of each toy pseudo-experiment is fitted as if they were data, and
 357 the pull-value distributions of the fit results are calculated. The pulls distributions are
 358 centered at zero, indicating there's no significant bias in the fitted yields/parameters.

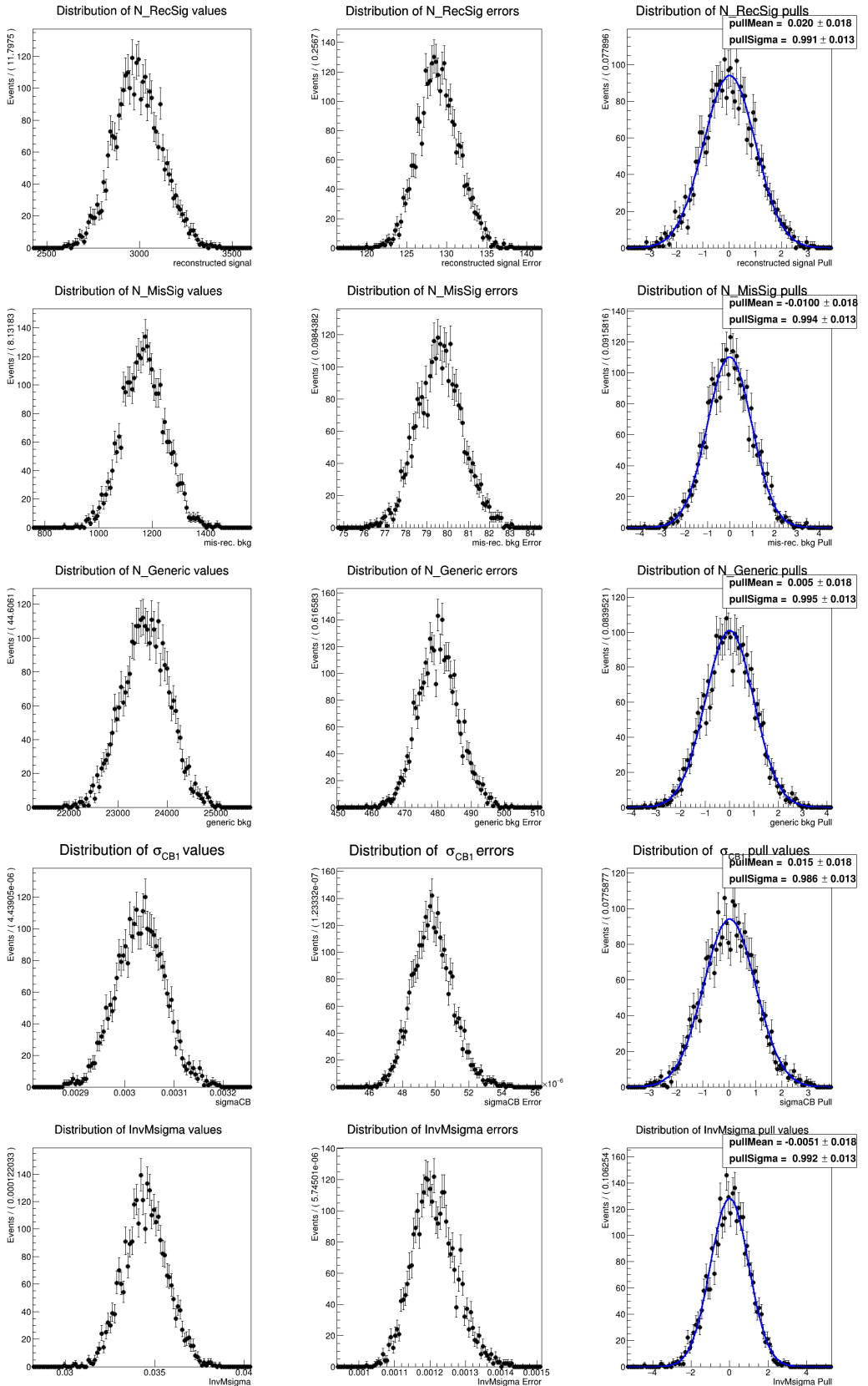


Figure (40) Toy MC study plots for the two dimensional fit model

359 4.3 Probability Density Functions (PDFs) for the B_{tag}

360 The M_{bc} distribution of the tagged B mesons is fitted with a Crystal Ball as for the
 361 "peaking" component and the "flat" component is fitted with a Novosibirsk function (Fig.
 362 41). The crossfeed background, consisting of neutral B mesons tagged as charged B , is
 363 fitted instead with a sum of a Novosibirsk and an asymmetric Gaussian PDF (Fig. 42).
 364 Both fits shows a $\chi^2/n.d.f.$ considerably higher than one and pulls exceeding 3σ deviation
 365 in some regions, but the systematics represented by this is negligible compared to other
 366 sources of systematic uncertainties and statistical uncertainties in the two dimensional fit.

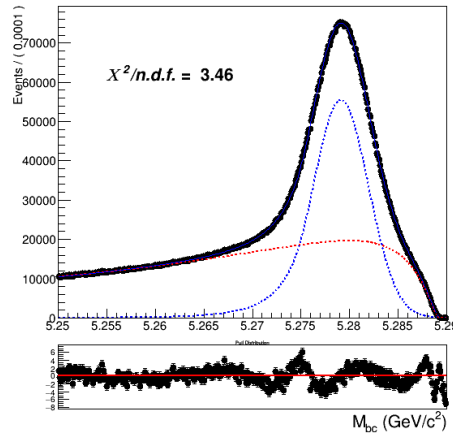


Figure (41) Fitted distribution of tagged charged B mesons: reconstructed signal events are described by the blue dotted PDF, the misreconstructed with a Novosibirsk function (red dotted).

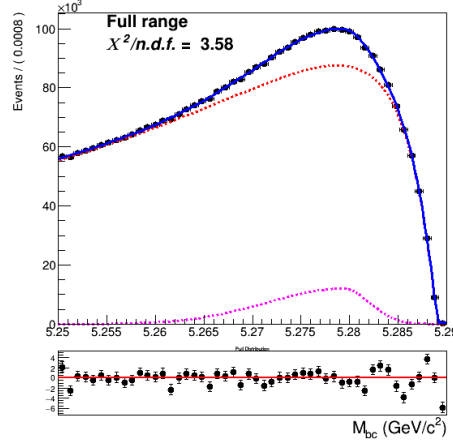


Figure (42) Crossfeed distribution fitted with a sum of Novosibirsk (red) and asymmetric Gaussian PDF (magenta)

367 As for the continuum background, a similar procedure as the one described already for the
 368 two dimensional fit was adopted:

- 369 • first the off-resonance sample is scaled accordingly
 370 • the ratio between the scaled off-resonance and the on-resonance in MC is calculated
 371 in each bin (see Fig.43a)
 372 • the bin-correction is applied on an independent stream and the scaled and bin-
 373 corrected M_{bc} distribution is compared with the on-resonance distribution as shown
 374 in Fig.43b

375 As for the B_{tag} continuum background the statistics is much larger than in the 2D sample,
 376 there's no need to remove the continuum suppression cut on the off-resonance sample.

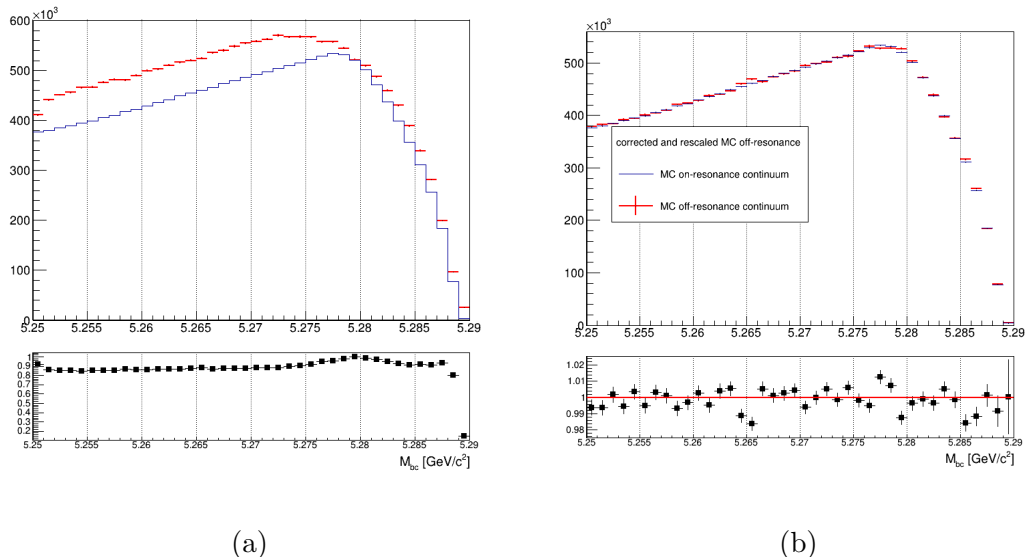


Figure (43) On the left: M_{bc} distributions of the MC off-resonance sample and the MC continuum sample with applied continuum suppression. On the right: M_{bc} distributions of the corrected scaled MC off-resonance and on-resonance MC continuum.

377 **4.4 B_{tag} fit**

378 An independent Monte Carlo stream was used to test the total fit model on tagged B meson
 379 candidates. As in the 2D fit, the parameter for the width, σ_{CB} , of the Crystal Ball is floated
 380 and the ratio between expected crossfeed background events and misreconstructed signal
 381 events is fixed from the MC. The Novosibirsk function describing the misreconstructed
 382 signal is also not fully constrained: the parameter describing the tail is free. To avoid
 383 introducing significant systematic uncertainties in the fit deriving from the M_{bc} endpoint
 384 region, where one has a smearing effect due to variations of the beam energy at the MeV
 385 level, the range for the fit is restricted to values between 5.250 and 5.287 GeV/c². Yields
 386 for the reconstructed and misreconstructed signal are obtained from the fit:

387

388

NrecSig	$4.2681 \cdot 10^6 \pm 5871$
NmisSig	$5.8787 \cdot 10^6 \pm 5128$

389 The Total Signal (the sum NrecSig+NmisSig) is 10146748 ± 4380 (to be compared with
 390 10158571 from the Monte Carlo). This reflects a $\sim 2.5\sigma$ discrepancy between the true MC
 391 value and the result from the fit. This can produce some systematic effect, but the relative
 392 error is at the $\sim \%$ level. This is still negligible compared to the systematic uncertainty
 393 corresponding to the the N_{tag} determination, and furthermore in the branching fraction
 394 calculation it is also negligible compared to the statistical uncertainty on the extracted
 395 yields from the two dimensional fit.

396 To check the stability of the fit model a toy MC study was performed with 3×10^3
 397 pseudo-datasets (as it was done for the two-dimensional fit model). No evidence for
 398 possible biases in the reconstructed signal yields was found (see Fig. 45).

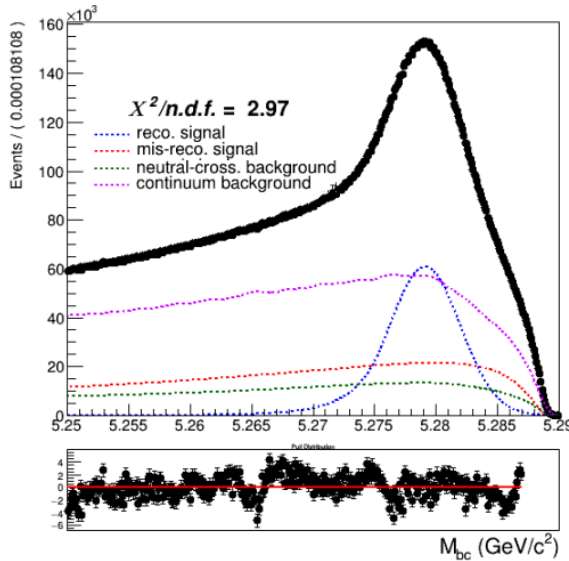


Figure (44) Total fit of tagged B mesons on Monte Carlo simulated data.

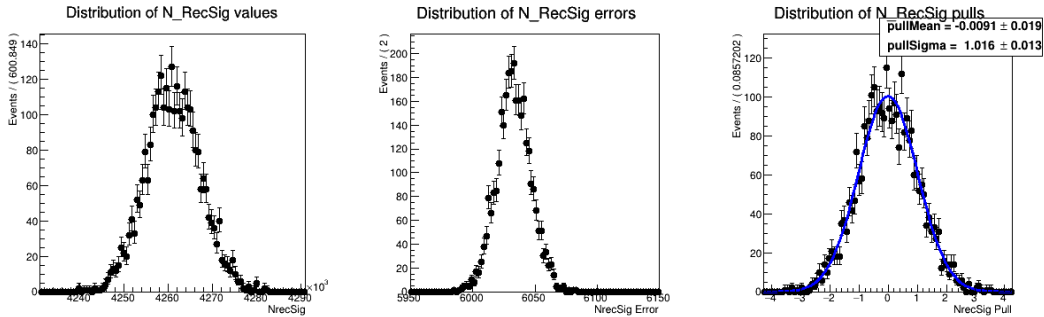


Figure (45) Plots showing distributions of the fitted signal yields, errors and the pull distribution of all pseudo-fits. (see Appendix .1 for the other free parameters' results)

399 4.5 Λ_c and FEI efficiency

400 The efficiency in reconstructing the Λ_c baryon after correctly tagging the charged B
 401 meson, can be estimated from Monte Carlo simulated data as the fraction of correctly
 402 reconstructed signal events that have a correctly reconstructed B_{tag} companion, i.e.:

$$\frac{N_{recSig}(B_{tag}, \Lambda_c)}{N_{recSig}(B_{tag}^{sig})} \quad (9)$$

403 where $N_{recSig}(B_{tag}, \Lambda_c)$ are the yields of reconstructed signal from the two dimensional
 404 fits (reported in Table 1) and $N_{recSig}(B_{tag}^{sig})$ are the yields of correctly reconstructed signal
 405 in a fit of B mesons tagged in events where one of the two mesons decayed hadronically
 406 and inclusively into a Λ_c baryon (see Fig 46). To minimize statistical uncertainties, in
 407 the efficiency calculation the results from all the two dimensional fits were used and six
 408 streams of B_{tag} candidates reconstructed in signal events were used for the M_{bc} shown
 409 below.

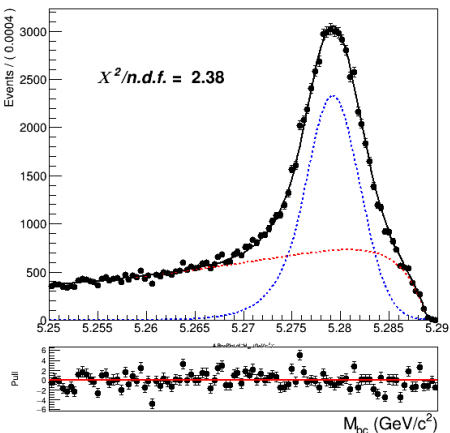


Figure (46) Fit of tagged B mesons in the "signal events" sample

410 From this and the results listed in sec. 4.2 the efficiency to reconstruct Λ_c is obtained :

411

$$412 \epsilon_{\Lambda_c} = \frac{N_{recSig}(B_{tag}, \Lambda_c)}{N_{recSig}(B_{tag})} = 44.83 \pm 0.32\%$$

413 The yields from the fit shown in (Fig. 46) can be used also to calculate the FEI tag-side
414 efficiency for signal events, i.e. the efficiency to tag the B meson accompanying a B_{sig}
415 decaying into a Λ_c on the signal side. Whereas results from the fit of charged B_{tag} shown
416 in Fig. 41 can be used to calculate the hadronic tag-side efficiency in the generic B^+B^-
417 events case.

418 The ratio between the two efficiencies is calculated: $\frac{\epsilon_{FEI,sig}^+}{\epsilon_{FEI}^+} = 0.908 \pm 0.017$
419

420 4.6 Studies of Systematic Effects

421 In Table 2 the systematic uncertainties of the various considered sources are summarized.
422 The full estimate of the systematic uncertainty is summed up in quadrature and applied
423 to the result in Section 4.17 Their individual calculation is outlined in the subsequent
424 subsections.

source	%
Continuum modeling	0.07
Crossfeed PDFs	0.07
Crossfeed fraction	0.06
2DFit crossfeed normalization	0.02
2DFit crossfeed peaking fraction	0.09*
$\epsilon_{FEI,sig}^+/\epsilon_{FEI}^+$	0.06
ϵ_{Λ_c}	0.02
Fit bias	0.06
PID	0.05
Tracking efficiency	0.01
Total	0.20

Table (2) Systematic uncertainties in the determination of the $B^+ \rightarrow \bar{\Lambda}_c^- X$ branching fraction in %.

425 * this represents the dominant uncertainty, but in Sec. 4.11 it will be explained how it
426 can be possibly reduced.

427 4.7 Continuum background modeling

428 Regarding this source of systematics, one has to take into account two different types.
429 First of all the statistical uncertainties, which are reflected in the uncertainties on the
430 PDF parameters. To estimate this type of uncertainty two-dimensional fits with varied
431 parameters' values by their uncertainties (a fit with +err and -err) were performed.
432 Whereas, the estimation of statistical uncertainty in the case of the B_{tag} should be
433 estimated in principle varying each bin content of its error. On first approximation this is
434 equivalent to vary the nominal number of events described with the histogram PDF by
435 Poissonian variation. Exemplary, fits used to estimate the impact of these uncertainties
436 are shown here in Figures 47 - 48. The yields obtained from those fits for benchmark
437 stream5 results are then compared with the ones already reported previously and a mean
438 deviation value is obtained for both the two-dimensional fit and the B_{tag} fit.

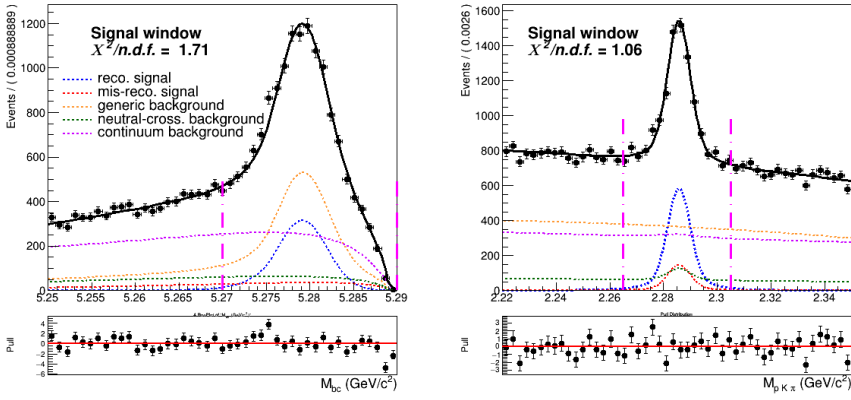


Figure (47) Signal window projections of a two dimensional fit on Monte Carlo simulated data where the shaping parameters were varied of their uncertainties.

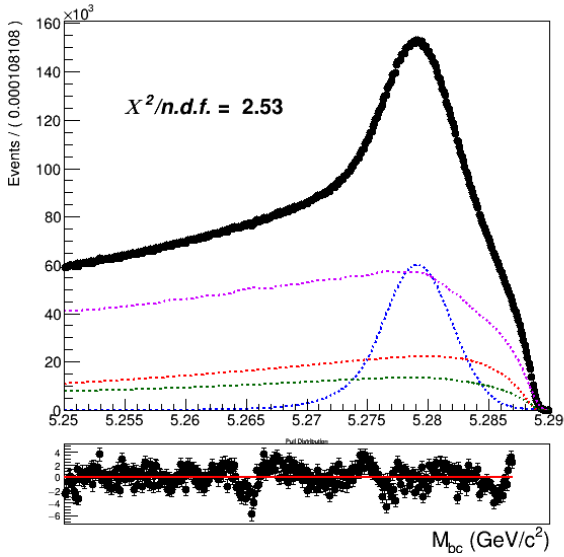


Figure (48) Fit of tagged B meson candidates on Monte Carlo simulated data where the amount of continuum was varied according to poissonian fluctuations.

Fit	$-\sigma$	$+\sigma$	$\pm\bar{\sigma}$
2D	87	53	70
B_{tag}	10218	10620	10419

Table (3) Offsets on the signal yields obtained in the two dimensional and B_{tag} fit and mean deviations reported in the last column.

⁴³⁹ The estimated systematic uncertainty on Br value from this source is 0.07%.

⁴⁴⁰ The other type of systematic uncertainty in modeling the continuum is originated by the

441 continuum suppression cut having a slightly different efficiency on data (as a consequence
 442 of the shift in off-resonance MC and data visible in the the *foxWolframR2* distribution
 443 in Fig. 29). As already discussed, it originates a possible discrepancy of about 2.25% in
 444 continuum background events in the two dimensional fit (and only 1.25% in the B_{tag} fit).
 445 The statistical uncertainty on this fraction of events can also be taken into account as
 446 systematics. Being the number of events in the off-resonance data sample without the
 447 continuum suppression applied is very small (less than 10^4 in the two dimensional fit and
 448 about 18500 in the B_{tag} fit), the uncertainty in the mentioned fraction of events is negligible
 449 compared to the statistical uncertainty on the on-resonance continuum background events
 450 in MC: it would account for 0.002% on the BR value. Therefore, this second source of
 451 uncertainty is not taken into account. There would be also a third of systematic uncertainty
 452 given by potential difference in the on-/off-resonance correction between data and MC,
 453 but there's no way one can estimate it properly.

454 **4.8 Crossfeed background modeling**

455 Since also the shapes of the PDFs describing the crossfeed background are fully fixed to the
 456 ones determined with the limited Monte Carlo statistics, also their statistical uncertainties
 457 need to be taken into account as possible source of systematics. The procedure to estimate
 458 this source of systematic uncertainty is the same described in the previous section regarding
 459 the continuum background. In the table below the signal yields' offsets are listed changing
 460 the parameters within their uncertainties, and the mean offsets value used to calculate the
 461 expected uncertainty on the BR value. The resulting absolute systematic uncertainty is
 462 about 0.07% on the BR value.

Fit	$-\sigma$	$+\sigma$	$\pm\bar{\sigma}$
2D	51	90	71
B_{tag}	5400	5700	5550

Table (4) Offsets on the signal yields obtained varying the parameters of crossfeed background PDFs within their uncertainties in the two dimensional and B_{tag} fit and mean deviations reported in the last column.

463 **4.9 Crossfeed ratio**

464 The crossfeed/misreconstructed signal "probability ratio" ($k = \frac{N_{crossfeed}/N_{B^0}}{N_{misRecSig}/N_{sig}}$) defined in
 465 Eq. (8) is kept fixed in the two-dimensional fit and the ratio bewteen crossfeed and
 466 misreconstructed events is also kept fixed in the B_{tag} fit to the values found in MC. This
 467 choice was made according to the fact that the two categories of events are similar: in both
 468 cases the B mesons were not correctly reconstructed, either because of missing or wrongly
 469 added partilces (misreconstructed signal events) or, in the case of crossfeed events because

470 the tagged B meson was not the required one (B^0 meson instead of a $B^{+/-}$ meson). The
 471 ratio between these two categories of events is therefore expected to be very similar in
 472 MC and data, though there's no guarantee that the efficiency to reconstruct them is the
 473 same in data in data and consequently the above mentioned ratios could be differ on data.
 474 Unfortunately there's no direct way to have an estimate of the possible discrepancy for
 475 them.

476 In [4] (and previously in [5]) it was found that there's a substantial difference in terms of
 477 tagging efficiency for FEI applied on Monte Carlo and on Belle data, being the discrepancy
 478 around $\sim 20\%$. We can assume that the efficiency for the two categories of events on data
 479 will both differ of that value and the ratio of the events being the same MC value, but in
 480 absence of any other method to estimate the uncertainty on it one can consider a maximal
 481 discrepancy of 20% between Monte Carlo and data to study the impact on the yields².

482 Therefore, for the two-dimensional fit the ratio k was artificially varied of $\pm 20\%$,
 483 whereas in the case of the B_{tag} fit the number of crossfeed events were varied artificially in
 484 order to have $\pm 20\%$ different ratio, keeping the previosuly determined Monte Carlo ratio
 485 fixed.

Fit	$-\sigma$	$+\sigma$	$\pm\bar{\sigma}$
2D	54	69	61
B_{tag}	2807	3940	3374

Table (5) Offsets on the signal yields obtained varying of $\pm 20\%$ the k ratio in the two dimensional and the ratio of crossfeed/misreconstructed events in the B_{tag} fit and mean deviations reported in the last column.

486 The estimated systematic uncertainty on Br value from this source is 0.06%.

487 4.10 Parametrization of crossfeed normalization in the 2D fit

488 In the previous section, regarding the two-dimensional fit, the uncertainties arising from
 489 the fixed "probability ratio" k were investigated. Besides those, one can consider also
 490 systematic uncertainties of statistical nature deriving from Eq. (8), were only the number
 491 of mis-/reconstructed signal events ($N_{recSig}/N_{misrecSig}$) are floated and fitted by the 2D fit.
 492 As already done in the case of continuum and crossfeed PDFs, this type of systematics is
 493 estimated repeating the 2D fit varying the parameters by their uncertainties. This source
 494 of systematics originates an uncertainty of 0.02% on the Br value.

²This method was also validated with the control decay sample and the originated uncertainty is well within the PDG reported ones.

495 4.11 Crossfeed peaking fraction in the 2D fit

496 When discussing the crossfed background modeling (see Fig. 17), it was said that among
 497 the crossfed background events there are also those that belong to $B^0 \rightarrow \Lambda_c$ decays, which
 498 peak in the Λ_c mass. The branching ratio of those decays is also still measured with poor
 499 accuracy (e.g. $\mathcal{B}(\bar{B}^0 \rightarrow \bar{\Lambda}_c^+ X) = (5.0^{+2.1})\%$), therefore the amount of crossfeed events
 500 peaking in $M(pK\pi)$ on data can differ significantly from MC. To estimate this source of
 501 systematics the amount of peaking events was varied in order to cover the uncertainties in
 502 the branching fraction mentioned above and repeating the two-dimensional fit.

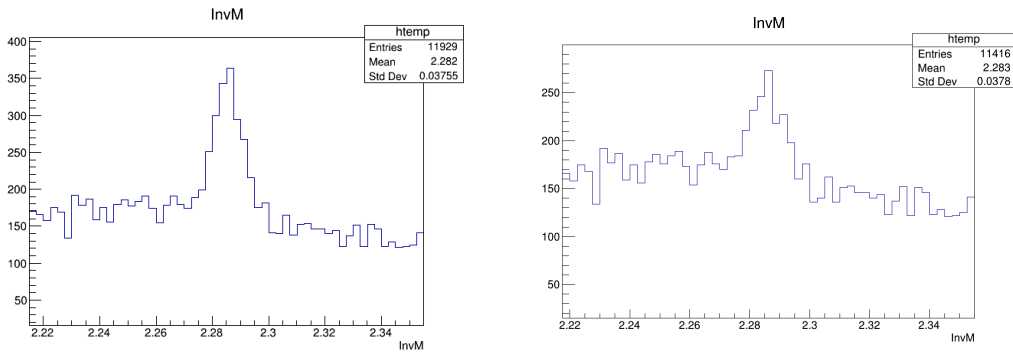


Figure (49) Λ_c invariant mass of crossfeed background with different amount of peaking events. On the left: Λ_c invariant mass corresponding to $\mathcal{B}(\bar{B}^0 \rightarrow \bar{\Lambda}_c^+ X) = 5.0 + 2.1\%$. On the right: Λ_c invariant mass corresponding to $\mathcal{B}(\bar{B}^0 \rightarrow \bar{\Lambda}_c^+ X) = (5.0 - 1.5)\%$

Fit	$-\sigma$	$+\sigma$	$\pm\bar{\sigma}$
2D	89	90	90

Table (6) Offsets on the signal yields obtained varying the amount of peaking crossfeed in the Λ_c invariant mass and mean deviation.

503 The uncertainty originated is estimated to be of 0.09% on the Br value. But once
 504 results from a new and more accurate measurement of $\mathcal{B}(\bar{B}^0 \rightarrow \bar{\Lambda}_c^+ X)$ (and the one
 505 corresponding to the flavor-anticorrelated decays) are available (once I obtained them)
 506 one can recompute this estimation with the updated uncertainties on the branching ratio
 507 of neutral decays, which should reduce the impact of this systematic uncertainty on the
 508 measurement.

509 4.12 Efficiencies

510 The ratio between the two FEI efficiencies is: $\frac{\epsilon_{FEI,sig}^+}{\epsilon_{FEI}^+} = 0.908 \pm 0.017$

511 The uncertainty on this value originates a systematic uncertainty of 0.06% on the Br

512 value. The Λ_c reconstruction efficiency is determined to be $\epsilon_{\Lambda_c} = 44.83 \pm 0.32\%$. The
 513 systematic uncertainty originated by its uncertainty is 0.02% on the Br value.

514 4.13 Fit biases

515 The small bias on the reconstructed signal seen in the two-dimensional fit model has to
 516 be corrected when fitting data, but the uncertainty on it has to be taken into account in
 517 the systematics. Also the discrepancy in the total signal fit result observed in the B_{tag}
 518 (Sec. 4.4) needs to be included in the systematic effects. Propagating the two sources of
 519 systematics in the branching fraction calculation results in an additional 0.06% uncertainty
 520 on the branching fraction value.

521 4.14 PID efficiency correction

522 The PID selection efficiency for the three charged particles in the signal decay needs to
 523 be corrected on MC due to various differences, when comparing to data. The Belle PID
 524 group has prepared a set of correction factors and tables of systematic uncertainties for
 525 PID efficiencies for all charged particles. The proton identification efficiency was studied
 526 in [6]. The inclusive Λ^0 decay $\Lambda^0 \rightarrow p\pi^-$ was used to examine the proton identification
 527 efficiency difference between data and MC in *Belle*. The datasets for the SVD1 and SVD2
 528 periods are treated separately, and the efficiency ratio dependence on proton charge,
 529 momentum and polar angle is considered. The study is done for the proton ID cut values
 530 0.6, 0.7, 0.8 and 0.9³. The binning on the momentum starts at 0.2 GeV. The proton ID
 531 efficiency is defined as

$$532 \\ 533 \epsilon_{PID} = \frac{\text{number of } p\text{ tracks identified as } p}{\text{number of } p\text{ tracks}} \\ 534$$

535 and the comparison between MC efficiency and data efficiency by a double ratio
 536 defined as

$$537 \\ 538 R_p = \epsilon^{data}/\epsilon^{MC} \\ 539$$

540 The average proton ID correction is estimated to be: $R_p = 0.969 \pm 0.003$.

541 The kaon identification efficiency was studied in detail in Belle Note 779 [7] (http://belle.kek.jp/secured/belle_note/gn779/bn779.ps.gz). The decay $D^{*+} \rightarrow D^0\pi^+$
 542 followed by $D^0 \rightarrow K^-\pi^+$, was used to examine it. As for the proton identification efficiency
 543 it considers the dependence on Kaon charge, momentum and polar angle and same ID cut
 544 values⁴.

³Here, proton ID cut value X means $\mathcal{L}_{p/K} > X$ and $\mathcal{L}_{p/\pi} > X$

⁴Here, Kaon ID cut value X means $\mathcal{L}_{K/\pi} > X$, so for values below X the tracks are identified as pions

546 For Kaons and Pions the average ID correction is estimated to be $R_K = 0.853 \pm 0.010$
547 and $R_\pi = 0.983 \pm 0.008$ respectivley.

548 The final PID efficiency systematic error is determined to be 0.01% on the branching
549 fraction value.

550 4.15 Tracking efficiency

551 The tracking efficiency correction for tracks with $p > 0.2$ GeV is studied in [8] . The track
552 finding efficiency is measured by comparing the number of partially and fully reconstructed
553 D^* decays. Based on this analysis, the measured difference in the tracking efficiency in
554 data and MC is $R = (-0.13 \pm 0.30 \pm 0.10)\%$ per track. Since the ratio is much smaller than
555 the statistical uncertainty, this ratio is not applied as a correction, instead, as done in [9],
556 a systematic uncertainty of 0.35% per track is applied. The total systematic uncertainty
557 is the sum over the three charged tracks used to reconstruct the Λ_c baryon: 1.05%. This
558 results in 0.01% uncertainty on the branching fraction value.

559 4.16 Sideband fit on data

560 As a preliminary check of the quality of the shapes modeling, a fit of the sideband
561 region $2.225 < M(pK\pi) < 2.245$ GeV/c² projection in M_{bc} was performed. The only
562 events present in this sideband region are: the generic, the crossfeed and the continuum
563 backgrounds. Therefore the only free parameters in the fit are:

- 564 • the width of the generic background Crystal Ball σ_{CB2}
- 565 • the normalization of the generic background
- 566 • the normalization of the crossfeed background

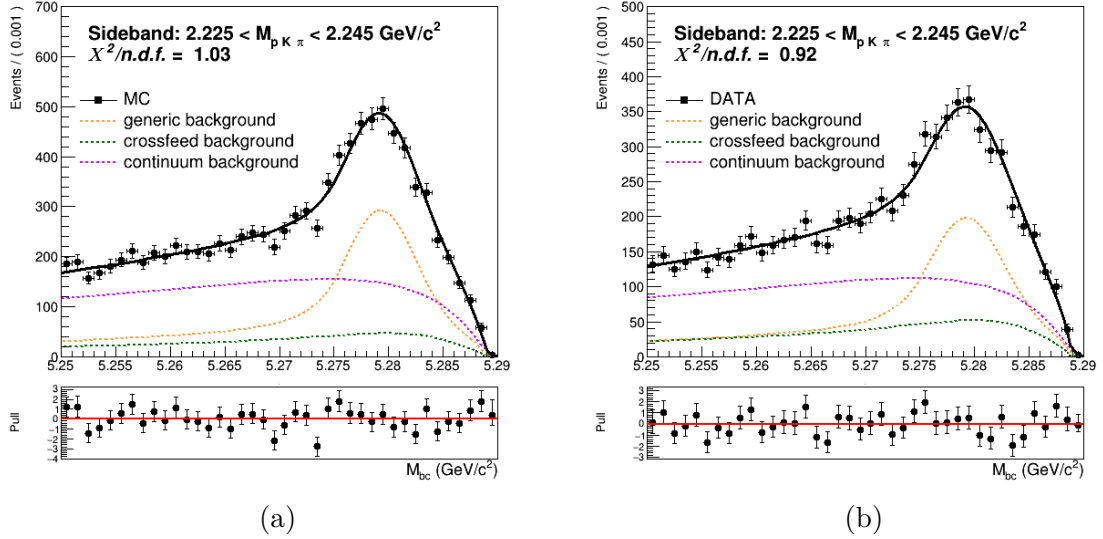


Figure (50) Fitted M_{bc} distributions corresponding to the projection in the sideband region of Λ_c invariant mass distribution in Monte Carlo and in data.

567 The fit shows a really good agreement with data points, from which one can assume that
 568 the shapes of the three main background contributions are describing at a good level the
 569 data. Moreover the fitted fractions of the background components present a quite good
 570 MC-data agreement:

	Background	MC truth	Fit on MC	Fit on Data
571	Crossfeed	10.66 %	12.22 ± 2.69 %	17.76 ± 3.21 %
572	Generic	38.49 %	37.11 ± 2.55 %	34.64 ± 3.04 %

574 4.17 Measured $B^+ \rightarrow \bar{\Lambda}_c^- X$ inclusive Branching Fraction

575 Now that all ingredients are available, it's possible by mean of the formula in Eq. 4 (at
 576 the beginning of this Chapter) , to calculate the branching ratio for the charged correlated
 577 decays into Λ_c baryons.

578 As the measurement is performed considering only the $\Lambda_c \rightarrow pK\pi$ decays, to evaluate the
 579 inclusive $B^+ \rightarrow \bar{\Lambda}_c^- X$ Branching Ratio on Monte Carlo simulated data one needs to take
 580 into account the value set for that particular final state: the total $Br(\Lambda_c^+ \rightarrow pK^-\pi^+) =$
 581 5.53% in Belle Generic MC (including resonant decays). Using the results from the two

dimensional fits, the B_{tag} fit (with/without background included) and with all the needed factors known, one can calculate $\mathcal{B}(B^+ \rightarrow \bar{\Lambda}_c^- X)$ on the six independent streams as displayed in Sec. 4.17. From the reported values one can notice first of all the effect of the bias encountered in Sec. 4.2, pushing the branching fraction to higher values (first column) compared to the expected ones and the branching ratio set in Belle MC. The discrepancy is of the order of 1σ statistical uncertainty.

	total fit	signal fit	BELLE MC VALUE
stream 0	(3.20 \pm 0.12)%	(2.96 \pm 0.07)%	(2.95 \pm 0.03)%
stream 1	(3.04 \pm 0.12)%	(2.99 \pm 0.07)%	(2.91 \pm 0.03)%
stream 2	(2.73 \pm 0.12)%	(2.99 \pm 0.07)%	(2.90 \pm 0.03)%
stream 3	(2.98 \pm 0.12)%	(2.90 \pm 0.07)%	(2.91 \pm 0.03)%
stream 4	(3.26 \pm 0.13)%	(3.07 \pm 0.07)%	(2.90 \pm 0.03)%
stream 5	(3.08 \pm 0.12)%	(2.85 \pm 0.07)%	(2.92 \pm 0.03)%
average	(3.05 \pm 0.05)%	(2.96 \pm 0.03)%	(2.93 \pm 0.01)%

Table (7) Measured branching fraction values obtained using the results listed in Table 1 for the six different streams (only statistical uncertainties are displayed) and its average.

Comparing the obtained values with the branching fraction measured by BaBar experiment (see results reported by *BaBar* [1]), the uncertainties appear substantially reduced (statistical uncertainties almost by factor four).

591

592 **5 $B^- \rightarrow D^0$ control decay**

593 To monitor the analysis steps, which are applied to both measured and simulated data, a
594 control decay of the form

595

596
$$B^+ \rightarrow D^0 X, D^0 \rightarrow K^+ \pi^-$$

597 is used. The statistics is much more abundant for this channel.

598 **5.1 Dataset used**

599 For this analysis the amount of data and Monte Carlo simulated data used was restricted
600 to the SVD2 period: experiments ranging from 31 to 65. This choice was made to save
601 processing time, anyway most of the $B\bar{B}$ meson pairs were produced in this range of
602 experiments (620×10^6 out of almost 800×10^6).

603 **5.2 Event selection and reconstruction**

604 The approach used for the inclusive decays reconstruction is the same as for the $B \rightarrow \Lambda_c$
605 analysis. The same FEI training was used, though excluding the signal decay $D^0 \rightarrow K^+ \pi^-$
606 from the decay chains used by the FEI to reconstruct the B_{tag} . Same preliminary selection
607 criteria were applied to the tag-side B meson candidates as well.
608 In the *rest of event* (ROE) of the reconstructed B_{tag} meson, to select $D^0 \rightarrow K^+ \pi^-$ signal
609 candidates, the following event selection criteria are applied:

- 610 • $dr < 2$ cm and $|dz| < 4$ cm
611 • $\frac{\mathcal{L}_K}{\mathcal{L}_K + \mathcal{L}_\pi} > 0.6$

612 For the D^0 candidates a vertex fit is performed with `TreeFitter`, requiring it to converge.
613 If there are more than one D^0 combination, then the best candidate based on the χ^2
614 probability is chosen. The D^0 signal region is defined to be $|M_{D^0} - m_{D^0}| < 30$ MeV/ c^2
615 ($\sim 3\sigma$), where m_{D^0} is the nominal mass of D^0 .

616

617 **5.3 Signal selection optimization**

618 Following the same procedure as for the $B \rightarrow \Lambda_c$ analysis, the optimized selection cuts
619 obtained for the event based ratio of the 2-nd to the 0-th order Fox-Wolfram moments,
620 the B_{tag} signal probability and the momentum of the D^0 candidates in the center of mass
621 system are⁵:

- 622 • $foxWolframR2 < 0.3$

⁵illustrative plots can be found in Appendix .2

- 623 • SignalProbability > 0.004

- 624 • $p_{CMS}^{D^0} > 1 \text{ GeV}/c^2$

625 Figure 51 shows the distributions of M_{bc} and invariant mass in the signal region⁶ for the
626 $B^- \rightarrow D^0 X$ reconstructed events after the selection cuts were applied.

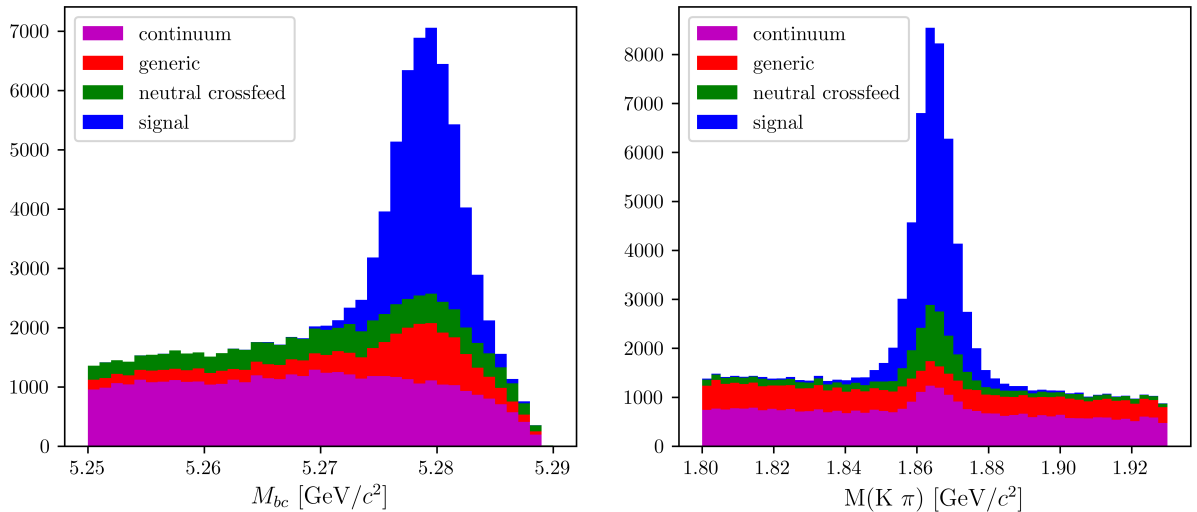


Figure (51) Distribution of M_{bc} (left) and invariant mass of charged correlated D^0 candidates (right), in the signal region after the above mentioned selection cuts.

627 5.4 Probability Density Functions (PDFs) for two dimensional 628 fit

629 As already said the main goal of the control sample analysis is to ensure that the method
630 used to extract the signal yields discriminating the correctly reconstructed from the
631 misreconstructed signal events by fitting is valid. The reconstructed events in M_{bc} are
632 fitted with a Crystal Ball, the misreconstructed signal with a Novosibirsk function. As in
633 the $B \rightarrow \Lambda_c$ analysis both components have a correspondent peak in the D^0 mass which is
634 fitted with a sum of three gaussians with a common mean. The fitted distribution of M_{bc}
635 and $M(\pi K)$ are shown in Fig. 52 with signal MC sample.

⁶signal region: $M_{bc} > 5.27 \text{ GeV}/c^2$ and $|M_{D^0} - m_{D^0}| < 30 \text{ MeV}/c^2$

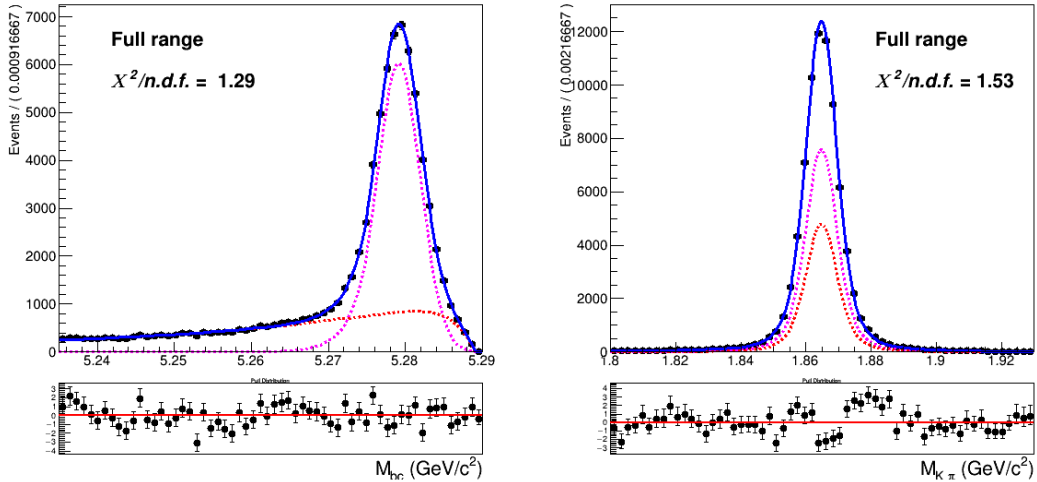


Figure (52) Two dimensional fit of total signal events in M_{bc} and $M(pK\pi)$ (in magenta reconstructed signal PDF, misreconstructed signal PDF in red)

As already seen in the $B \rightarrow \Lambda_c$ analysis besides the misreconstructed signal the other background components are:

- **generic** (charged B) background
- **crossfeed** (neutral B) background
- **continuum** background

Generic background

The generic background deriving from other B^+B^- events presents a similar shape in M_{bc} : it is fitted again with a sum of Crystal Ball and Novosibirsk function. Instead the distribution in the D^0 mass is fitted with a sum of first order Polynomial function and a small gaussian peak, which is due to the small amount of flavor anti-correlated $B^+ \rightarrow D^0$ reconstructed events (see Fig. 53). The total two-dimensional PDF is a product of the one-dimensional PDFs in M_{bc} and D^0 mass:

$$P_{B,D^0}^{GenBkg}(M_{bc}, M(K\pi)) = [\Gamma_{CB}(M_{bc}) + \Gamma_{Nov}(M_{bc})] \times [\rho_{pol1}(M(K\pi)) + \rho_G(M(K\pi))] \quad (10)$$

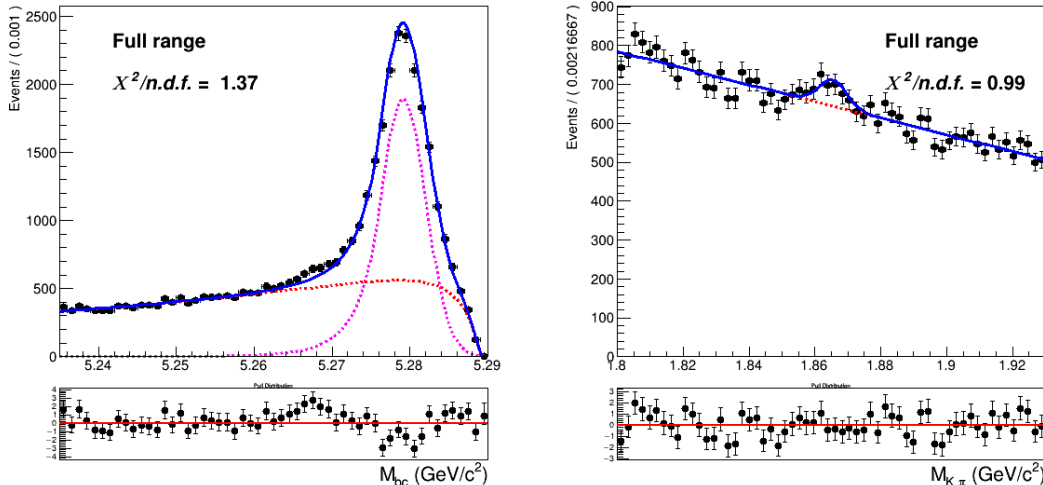


Figure (53) Two dimensional fit of generic ($B^+ B^-$) background events in M_{bc} and $M(K\pi)$.

648 **Crossfeed background** The crossfeed background deriving from $B^0 \bar{B}^0$ events is shown
 649 in Fig. 54. The M_{bc} distribution is fitted with a sum of Novosibirsk and Argus functions.
 650 The distribution in the D^0 mass is fitted with a first order Chebyshev polynomial and the
 651 D^0 mass peak is fitted with the same sum of three gaussians used to describe the signal
 652 peak (same parametrization used already in $B \rightarrow \Lambda_c$ analysis).

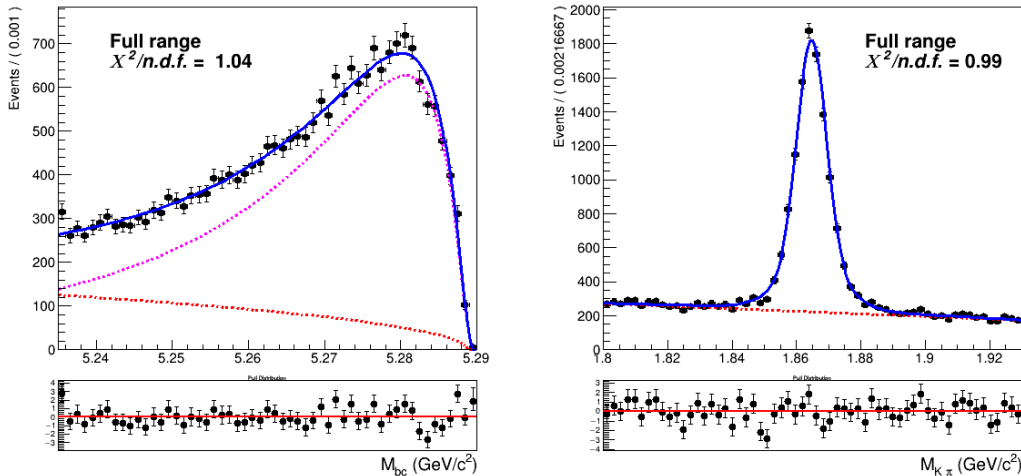


Figure (54) Two dimensional fit of crossfeed ($B^0 \bar{B}^0$) events in M_{bc} and $M(K\pi)$.

653 Continuum background

654 The procedure adopted to model the continuum background is the same used for the
 655 $B \rightarrow \Lambda_c$ decays, but in this case the available statistics is enough to perform the scaling
 656 with all the selection cuts also in the case of the two-dimensional fit (not removing the
 657 continuum suppression).

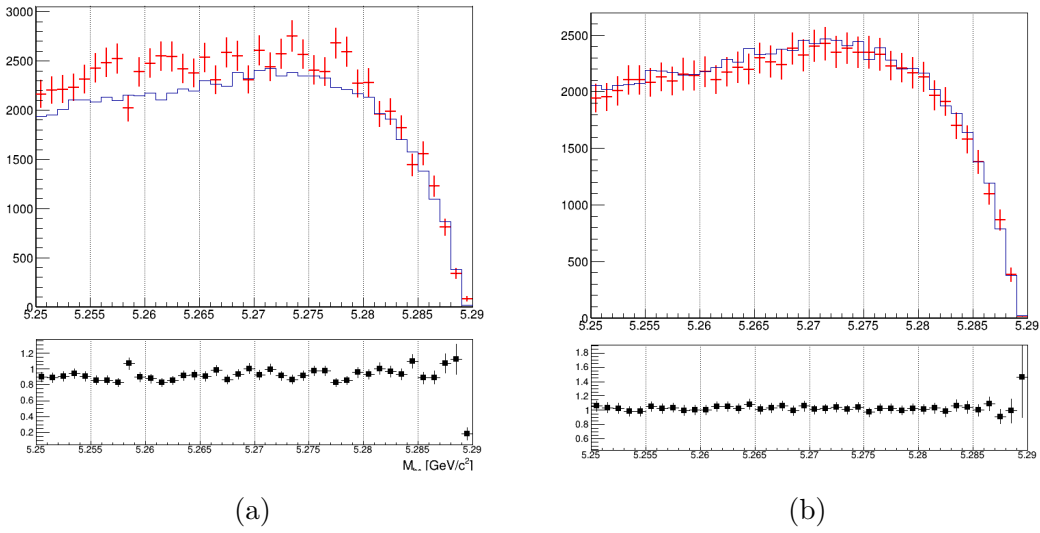


Figure (55) In Fig. 55a M_{bc} distributions of the MC (scaled) off-resonance sample (in red) and on-resonance (in blue). In Fig. 55b M_{bc} distributions of the corrected scaled off-resonance and on-resonance MC continuum.

For each bin a correction factor is calculated, in order to have a reasonable match with the expected continuum background. Fig. 55b shows the applied correction on an independent MC sample. As in the case of $B \rightarrow \Lambda_c$ analysis, then the resulting M_{bc} distribution is fitted with a Novosibirsk function , whereas the D^0 mass distribution is fitted with a sum of first order Chebyshev polynomial and the sum of three gaussians used to describe the signal peak (as shown in Fig. 56). The fraction of events in the peak is the same in on- and off-resonance MC. This method is applied also to scale the off-resonance data.

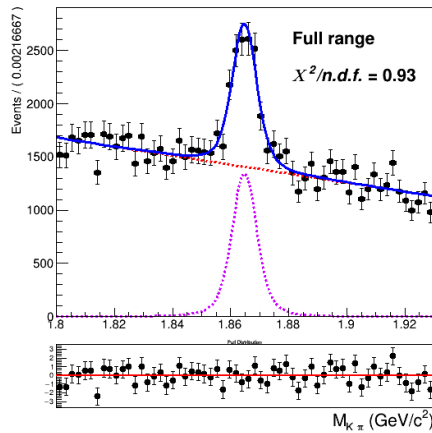


Figure (56) D^0 mass fit of scaled off-resonance Monte Carlo

665 **5.5 2D Fit on Monte Carlo simulated data**

666 As in the $B \rightarrow \Lambda_c$ study, five streams of Monte Carlo simulated data have been used to
 667 get values for the shaping parameters for the individual components described in the
 668 previous section and the fit model is tested on an independent stream.

669 For the six fits, the same conditions were applied to the widths:

- 670 • σ_{G1} : the width of the wider of the three Gaussian functions in $\rho_G(M(K\pi))$
- 671 • σ_{CB} parameter for the Crystal Ball describing the signal
- 672 • the σ_{CB} parameter for the Crystal Ball describing the generic background is expressed
 673 as function of the signal σ_{CB} with a ratio fixed from the MC.

674 For the fits on Monte Carlo simulated data the crossfeed normalization is expressed as
 675 ratio of its contribution and the misreconstructed signal as found in MC and kept fixed (to
 676 see how the parametrized form impacts a fit on data is then performed). Exemplary, the
 677 distributions of stream 0 overlaid by the fitted PDF are depicted in Fig. 57 (see Appendix
 678 .2 for the projections of signal regions and sidebands).

679 In Table 8 the yields for reconstructed and misreconstructed signal are listed for each
 680 stream.

681

stream	0	1	2	3	4	5
NrecSig	56986 ± 400	57766 ± 437	55607 ± 426	57068 ± 372	58385 ± 369	57501 ± 437
NmisSig	31453 ± 321	30513 ± 350	32580 ± 350	33340 ± 399	29966 ± 390	32012 ± 355

Table (8) reconstructed and misreconstructed signal yields obtained fitting 6 independent streams

682 To be sure that the PDFs enables us to extract the signal yield in an unbiased way, the
 683 sum of reconstructed and misreconstructed signal yields, i.e. total signal, from the fits are
 684 compared to the true values of each stream (Table 9). There are quite some differences
 685 between the fitted signal yield and the true values in individual streams. However, all
 686 these deviations are within statistical expectations.

687

streams	fit	MC truth	fit - MC truth
stream 0	88439 ± 340	88144	+ 295 (+0.33%)
stream 1	88279 ± 361	88551	- 272 (- 0.31%)
stream 2	88187 ± 360	88487	-300 (- 0.34%)
stream 3	90408 ± 372	90149	+ 259 (+ 0.29%)
stream 4	88351 ± 383	87981	+ 370 (+ 0.42%)
stream 5	89513 ± 366	89710	-197 (- 0.22%)
sum	533177	533022	+155 (+0.03%)

Table (9) Comparison of fitted and truth-matched total signal events in each stream.

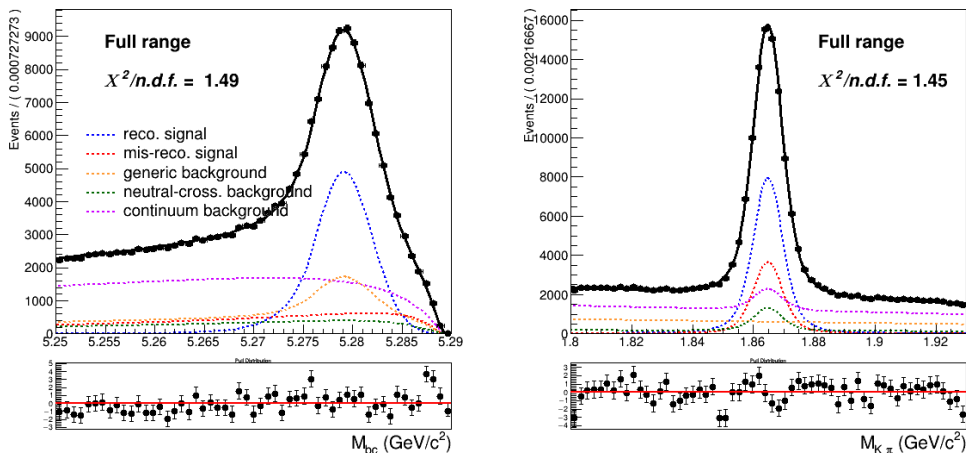


Figure (57) Two dimensional fit on stream 0 Monte Carlo simulated data.

5.6 2D Fit on data

After obtaining the model for the continuum background scaling and correcting the M_{bc} distribution of the off-resonance data, the model tested on Monte Carlo simulated data is applied on data with same free parameters and yields. Fig. 58 shows the projections of the two dimensional fit (see Appendix .2 for the projections of signal regions and sidebands). Yields for the reconstructed and misreconstructed signal and for generic background are obtained from the fit:

NrecSig	35629 ± 368
NmisSig	24425 ± 311
Generic	24596 ± 407

The total normalization from the fit is 174230 ± 407 (to be compared with the total data events: 173964).

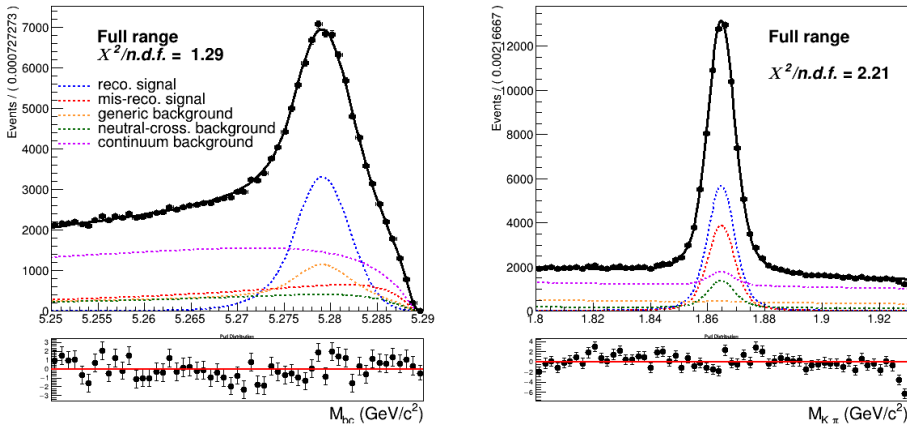


Figure (58) Two dimensional fit on Data (same conditions applied as in Fig. 57)

ratio	MC	DATA
NmisSig/NrecSig	0.56 ± 0.01	0.68 ± 0.01
NmisSig/Generic	0.90 ± 0.02	0.99 ± 0.02
Generic/NrecSig	0.62 ± 0.01	0.69 ± 0.02

Table (10) Comparison of ratios of yields from the two dimensional fits on Monte Carlo simulated data and on Data.

700

701 Since in the case of the two dimensional fit for the measurement of $B^- \rightarrow \Lambda_c^+ X$ decays
 702 the crossfeed normalization was parametrized in the form described by Eq. (8), the
 703 2D fit shown above is repeated with the parametrized normalization for the crossfeed
 704 background. The signal reconstruction efficiency that enters the formula to estimate
 705 the true number of signal events ($N_{sig} = N_{recSig}/\epsilon$) is now the signal reconstruction
 706 efficiency on data: ϵ_{data} . It can be estimated scaling the one found on Monte Carlo by
 707 a correction factor that takes into account the different FEI efficiency on data and the
 708 signal-side reconstruction corrected for the different PID efficiency (see Sec. 5.10-Sec. 5.11),
 709 $\epsilon_{data} = \epsilon_{MC} \cdot c_{FEI} \cdot c_{D^0} = (0.216 \pm 0.016)\%$.

710

711 where $c_{FEI} = 0.810^{+0.013}_{-0.012} \pm 0.054$ is the correction factor for the FEI efficiency determined
 712 in [5]

713 whereas the factor c_{D^0} is the PID correction reported in Sec. 5.10.

714 Fig. 59 shows this second fit.

ratio	MC	DATA
NmisSig/NrecSig	0.56 ± 0.01	0.66 ± 0.01
NmisSig/Generic	0.90 ± 0.02	0.93 ± 0.02
Generic/NrecSig	0.62 ± 0.01	0.71 ± 0.02

Table (11) Comparison of ratios of yields from the two dimensional fits on Monte Carlo simulated data and on Data (from the fit shown in Fig. 59).

715 In the following table yields for the reconstructed and misreconstructed signal and for
 716 generic background obtained from this second fit are reported:

NrecSig	36553 ± 360
NmisSig	24115 ± 283
Generic	25900 ± 409

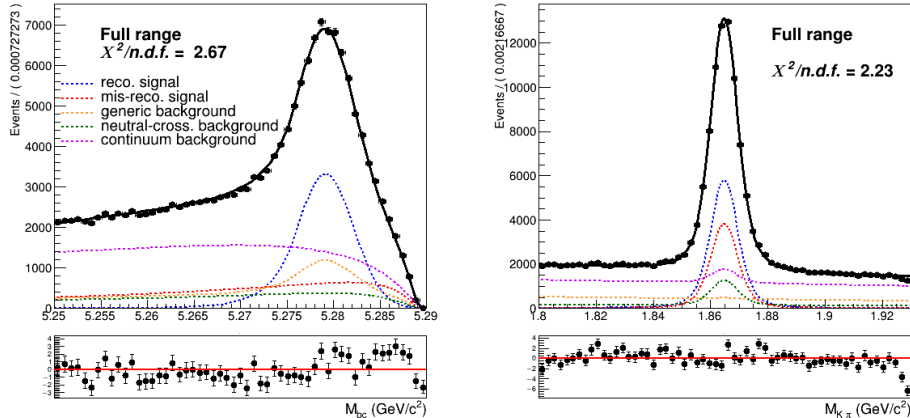


Figure (59) Two dimensional fit on Data with parametrized normalization of crossfeed background

719 5.7 Probability Density Functions (PDFs) for the B_{tag}

720 Like for the signal model in the 2D fit the M_{bc} distribution of the tagged charged B
 721 mesons is fitted with a Crystal Ball as for the reconstructed signal component, whereas
 722 the misreconstructed signal component is fitted with a Novosibirsk function (Fig. 60a).

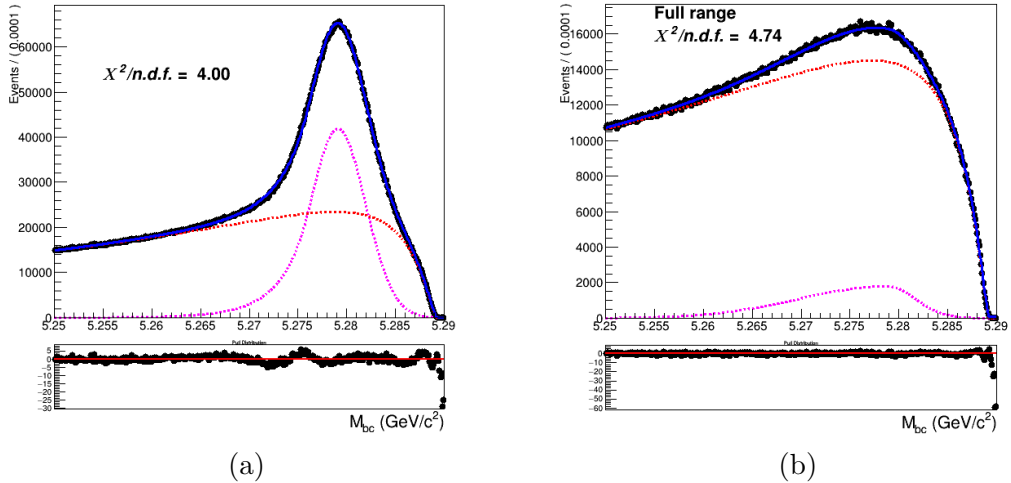


Figure (60) On the left: fitted distribution of tagged charged B mesons, reconstructed signal events (magenta) are described by a Crystal Ball whereas the misreconstructed signal events (red) are described by a Novosibirsk function. On the right: Crossfeed distribution fitted with a sum of Novosibirsk (red) and asymmetric Gaussian PDF (magenta)

723 The crossfeed background is fitted instead with a sum of a Novosibirsk and an asymmetric
 724 Gaussian PDF (Fig. 60b).

725

726 Regarding the continuum background component, same procedure used for the 2D fit was
 727 applied to the M_{bc} distribution of the continuum background in this case (see Fig. ?? for
 728 the result).

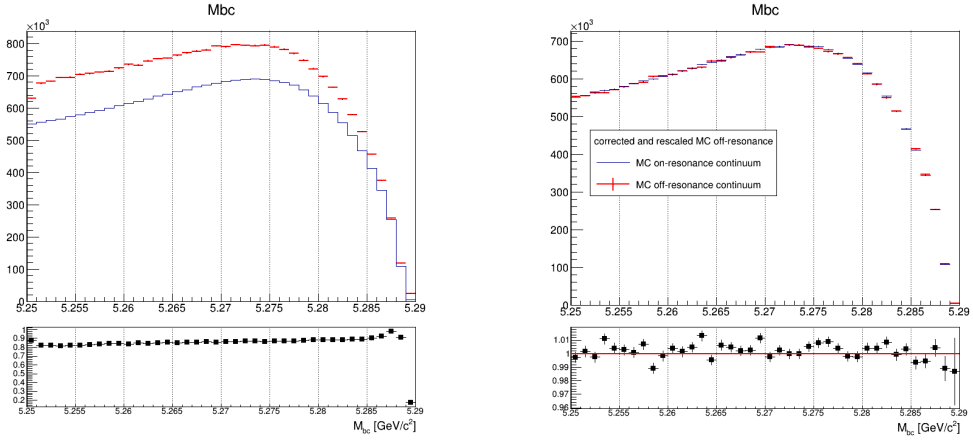


Figure (61) On the left: M_{bc} distributions of the MC off-resonance sample and the MC continuum sample. On the right: M_{bc} distributions of the corrected scaled MC off-resonance and on-resonance MC continuum.

729 5.8 B_{tag} Fit on Monte Carlo simulated data

730 An independent Monte Carlo stream was used to test the total fit model on tagged B
 731 mesons candidates. The usual condition is applied to the crossfeed background events:
 732 the ratio between its contribution and misreconstructed signal events is fixed from the
 733 other Monte Carlo stream.
 734 In this fit the shaping parameters that are not kept fixed are the Crystal Ball width (σ_{CB})
 735 and the width of the Novosibirsk function describing the misreconstructed signal events.
 736 As in the case of B_{tag} fit in Sec. 4.4 the range for the fit is restricted to values between
 737 5.250 and 5.287 GeV/c^2 .

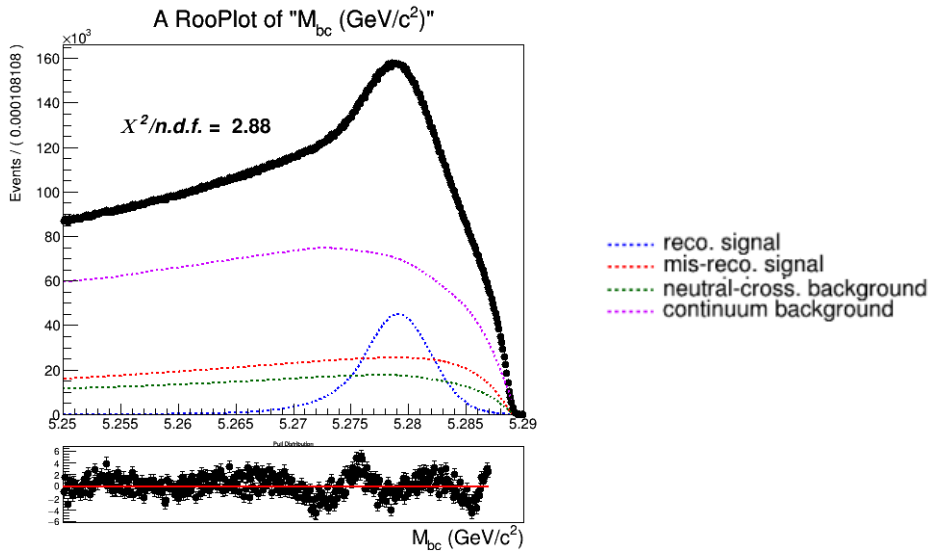


Figure (62) Total fit of tagged B mesons

Yields for the reconstructed and misreconstructed signal are obtained from the fit:

NrecSig	$3.25110 \cdot 10^6 \pm 6759$
NmisSig	$7.41107 \cdot 10^6 \pm 5341$

One can then compare the sum NrecSig+NmisSig (the so called total signal) with the true value known from the Monte Carlo and the same for the total number of events in this particular stream:

	fit	MC value
Total Signal	$10.662 \cdot 10^6 \pm 5249$	$10.671 \cdot 10^6$
Total events	$38.601 \cdot 10^6 \pm 6886$	$38.610 \cdot 10^6$

The discrepancy in the total signal events from the fit and the MC here is about 1.7σ , but the relative error is an order of magnitude smaller than the one found in B_{tag} fit in 4.4 (below the %level), therefore it's negligible.

748 **5.9 B_{tag} Fit on data**

749 The fit model tested on Monte Carlo simulated data is then applied with the same method
 750 on data Fig. 63.

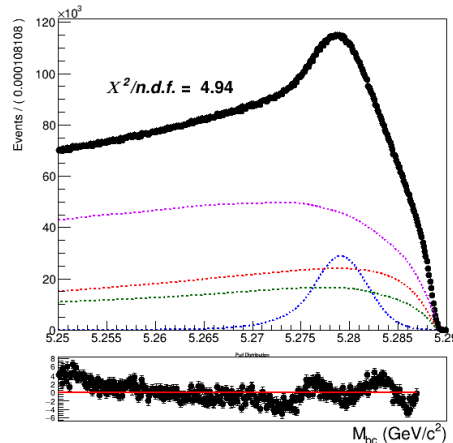


Figure (63) Total fit of tagged B^+ mesons candidates on data

751 Yields for the reconstructed and misreconstructed signal are obtained from the fit:

NrecSig	$2.011 \cdot 10^6 \pm 5858$
NmisSig	$6.975 \cdot 10^6 \pm 4667$
Total Signal	$8.982 \cdot 10^6 \pm 4587$

ratio	MC	DATA
NmisSig/NrecSig	2.28 ± 0.01	3.47 ± 0.01

Table (12) Comparison of ratios of yields from the tagged B mesons fits on Monte Carlo simulated data and on Data.

753 5.10 PID efficiency correction

754 The PID selection is applied only to Kaons: $\frac{\mathcal{L}_K}{\mathcal{L}_K + \mathcal{L}_\pi} > 0.6$

755 Using the values provided in the global tag **BellePID** (as done in the $B \rightarrow \Lambda_c$ study),
 756 the average Kaon ID correction for this analysis is estimated to be $R = 0.976 \pm 0.008$.

757 5.11 D^0 and FEI efficiency

758 The efficiency in reconstructing the D^0 after correctly tagging the charged B meson, can
 759 be estimated from the 2D fit on Monte Carlo simulated data, using the reconstructed
 760 signal yield and from a sample of B_{tag} candidates reconstructed in signal events in the
 761 Monte Carlo: where from B^+B^- at least a D^0 decaying into πK is produced.

762 For the latter a fit is performed to extract the yield of correctly tagged B mesons (Fig.
 763 64)

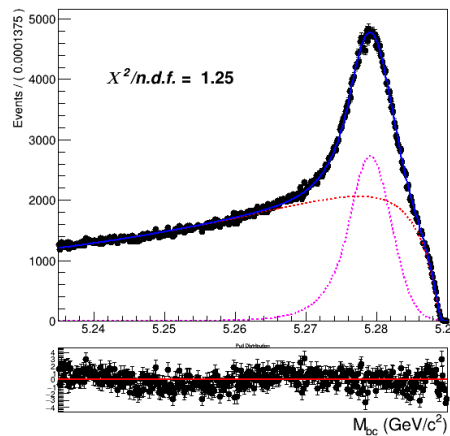


Figure (64) Fit of tagged B mesons in the "signal events" sample

764 Yields for the reconstructed and misreconstructed signal :

NrecSig	$1.46779 \cdot 10^{-5} \pm 767$
NmisSig	$6.16717 \cdot 10^{-5} \pm 1028$

766 From this and the results listed in Sec. 5.5 the efficiency to reconstruct D^0 is obtained :

767

$$768 \epsilon_{D^0} = \frac{N_{recSig}(2D)}{N_{recSig}((B_{tag}^{sig})} = 39.1 \pm 0.4\%^7 \quad (\text{KID efficiency corrected value for data: } 38.2 \%)$$

769

770 The results from the fit shown in (Fig. 64) can be used also to calculate the FEI tag-side
 771 efficiency for signal events, i.e. the efficiency to tag the B meson accompanying a B_{sig}
 772 decaying into a D^0 on the signal side. Whereas results from the fit of charged B_{tag} shown

⁷the error reflects the limited Monte Carlo statistics

773 in Fig. 60a can be used to calculate the hadronic tag-side efficiency in the generic B^+B^-
 774 events case.

775 The ratio of the two efficiencies is found to be: $\frac{\epsilon_{FEI,sig}^+}{\epsilon_{FEI}^+} = 1.50 \pm 0.01$
 776

777 5.12 Studies of Systematic Effects

778 The systematic uncertainties are studied the same way as in the case of the $B^+ \rightarrow \bar{\Lambda}_c^- X$
 779 branching fraction. The values are reported in the next section. The dominant systematic
 780 uncertainty is the one originated by the continuum background modeling and its incidence in
 781 terms of relative error on the branching fraction value is same as for the $B^+ \rightarrow \bar{\Lambda}_c^- X$ study.
 782 For this control sample study the uncertainty that would be caused by the uncertainty of
 783 the crossfeed peaking events is not estimated, since the uncertainty on $\mathcal{B}(B^0 \rightarrow \bar{D}^0 + X)$
 784 is only of few percent and the possible effect can be considered negligible compared to the
 785 other systematic uncertainties.

786 5.13 Measured $B^+ \rightarrow \bar{D}^0 X$ inclusive Branching Fraction

787 The inclusive branching fraction of $B^+ \rightarrow \bar{D}^0 X$ can be determined by:

$$Br(B^+ \rightarrow \bar{D}^0) = \frac{r}{Br(D^0 \rightarrow K^+\pi^-)\epsilon_{D^0}} \cdot \frac{\epsilon_{FEI}^+}{\epsilon_{FEI,sig}^+} \quad (11)$$

788 Where

- 789 • $r = \frac{N_{tag,D^0}}{N_{tag}}$ is the ratio of reconstructed signal yield in the two dimensional fit and in
 790 the M_{bc} fit of the tagged B mesons.
- 791 • ϵ_{D^0} is the D^0 reconstruction efficiency calculated as fraction of reconstructed signal
 792 events with correct tag of which then also a correctly reconstructed D^0 is recon-
 793 structed in the signal side.
- 794 • $\frac{\epsilon_{FEI}^+}{\epsilon_{FEI,sig}^+}$ is the ratio of the FEI efficiencies: the hadronic tag-side efficiency for generic
 795 B^+B^- events (ϵ_{FEI}^+) and signal-side dependent one ($\epsilon_{FEI,sig}^+$) where one of the two B
 796 mesons decays inclusively into the signal channel ($D^0 \rightarrow K^+\pi^-$)
- 797 • $Br(D^0 \rightarrow K^+\pi^-) = 3.8\%$ in Belle DECAY.DEC table, $Br(D^0 \rightarrow K^+\pi^-) = 3.95\%$
 798 in PDG.

799 In Monte Carlo: $Br(B^+ \rightarrow \bar{D}^0) = 79.4 \pm 0.6^{(stat.)}\%$ (true MC value: 79.1%)
 800

801 As for the Data, the value obtained using a fixed ratio of crossfeed events with respect to
 802 misreconstructed signal events is: $Br(B^+ \rightarrow \bar{D}^0) = 78.3 \pm 0.8^{(stat.)}\%$

804 While, introducing the parametrization of the crossfeed normalization in the two dimen-
 805 sional fit gives a larger value: $Br(B^+ \rightarrow \bar{D}^0) = 80.3 \pm 0.8^{(stat.)}\%$
 806 Nevertheless, the latter is in agreement with the value reported by the PDG: $(79 \pm 4)\%$
 807 One can conclude that the obtained results have proven the validity of the method chosen
 808 for the measurements.
 809 The systematic uncertainties are dominating as one can see from the Table below, listing
 810 the contribution of the various sources of systematics in terms of Branching Fraction in
 811 percentage.
 812

continuum modelling	1.8 %
Crossfeed PFDs	0.4 %
Crossfeed fraction	0.8 %
2DFit crossfeed normalization	0.4 %
FEI efficiency	0.5 %
ϵ_{D^0}	0.8 %
PID	0.6 %
Tracking efficiency	0.8 %
Total	2.5 %

Table (13) Sources of systematic uncertainties and their contributions.

813 **6 $B^- \rightarrow \bar{\Lambda}_c^-$ decays**

814 Applying the same procedure already illustrated in Sec. 4, the optimized selection cuts for
 815 the charged flavor-anticorrelated decays are:

- 816 • $\text{foxWolframR2} < 0.3$
 817 • $\text{SignalProbability} > 0.1$
 818 • $p_{CM\text{S}}^{\Lambda_c} < 1.5 \text{ GeV}/c$

819 **6.1 Probability Density Functions (PDFs) for the two dimensional fit**
 820

821 The PDFs used to describe the signal distributions are the same already used in Sec. 4.1
 822 (only the shaping parameters differ) and an example of the 2D fit is shown in Fig. 65.
 823 Also the generic background deriving from other B^+B^- events presents similar shapes of
 824 the distributions as shown already in Sec. 4.1, therefore the probability density functions
 825 used are the same (fit is shown in Fig. 66).

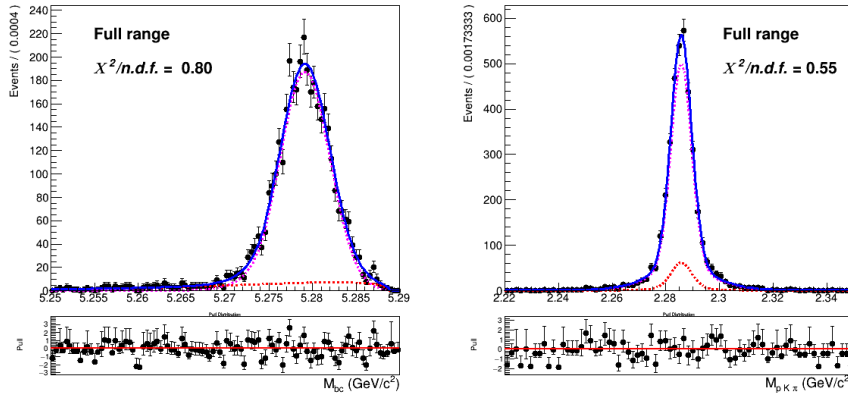


Figure (65) Two dimensional fit of total signal events in M_{bc} and $M(pK\pi)$.

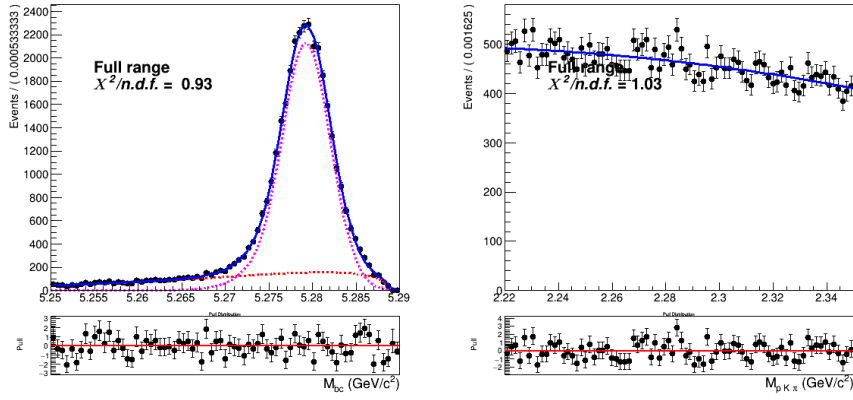


Figure (66) Two dimensional fit of generic (B^+B^-) events in M_{bc} and $M(pK\pi)$.

826 The same can be said about the misreconstructed B^0 events (Fig. 67)

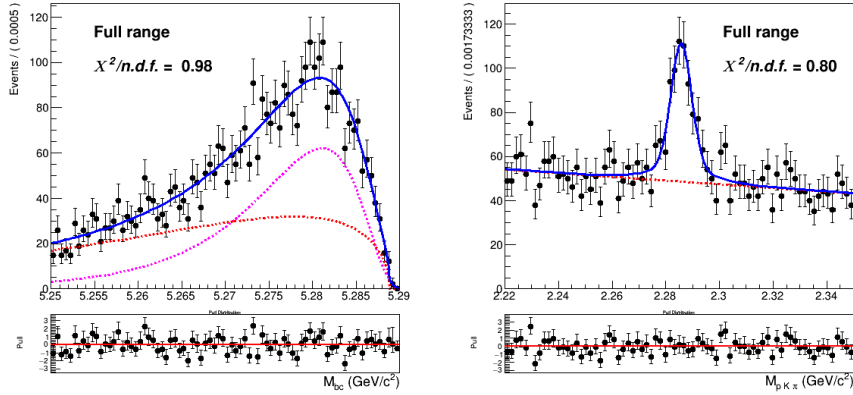


Figure (67) Two dimensional fit of crossfeed ($B^0\bar{B}^0$) events in M_{bc} and $M(pK\pi)$.

827 To check that the shapes determined using 5 streams of Monte Carlo are describing with
 828 reasonable accuracy the 2D distribution, the projections of the fit of the two-dimensional
 829 distributions in the signal and sideband regions are plotted (Fig. 69 - Fig. 71). One can see
 830 the same tendencies of undershooting/overshooting the Λ_c invariant mass peak, as in the
 831 case of charged correlated decays (Figures 18 - 19). But when examining the independent
 832 Monte Carlo stream distribution overlaid by the determined PDF in the very same regions
 833 (see Figures 72 - 74) those effects are so much diminished, according to the statistics, that
 834 the effects are within statistical fluctuations and therefore negligible, contrary to the case
 835 of charged flavor-correlated decays.

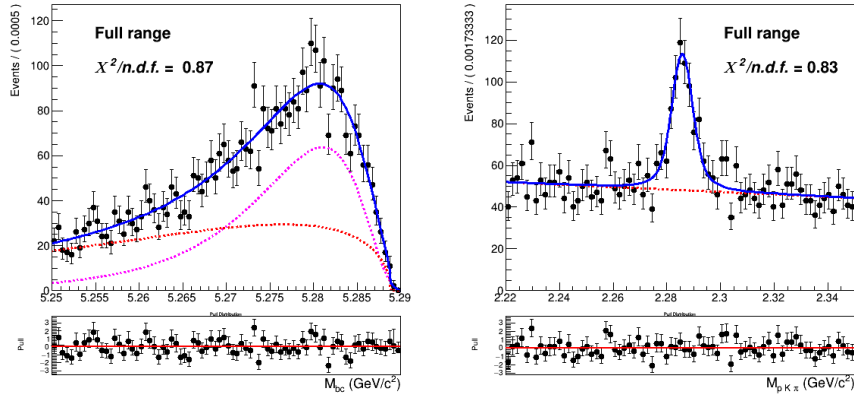


Figure (68) Two dimensional fit of crossfeed ($B^0 \bar{B}^0$) events in M_{bc} and $M(pK\pi)$.

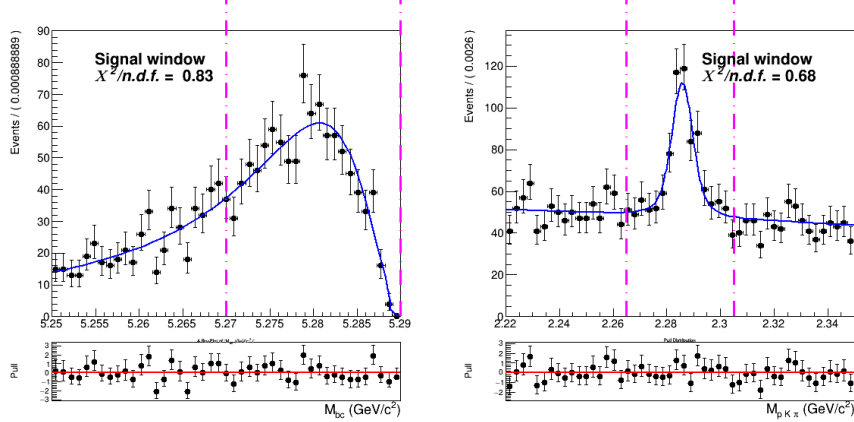


Figure (69) Signal region projections in M_{bc} and $M(pK\pi)$ of the fit of crossfeed events.

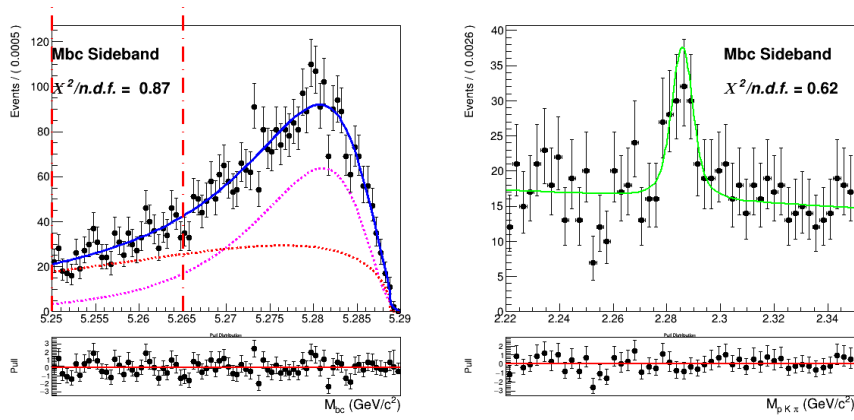


Figure (70) M_{bc} sideband region projection of the fit of crossfeed events in $M(pK\pi)$.

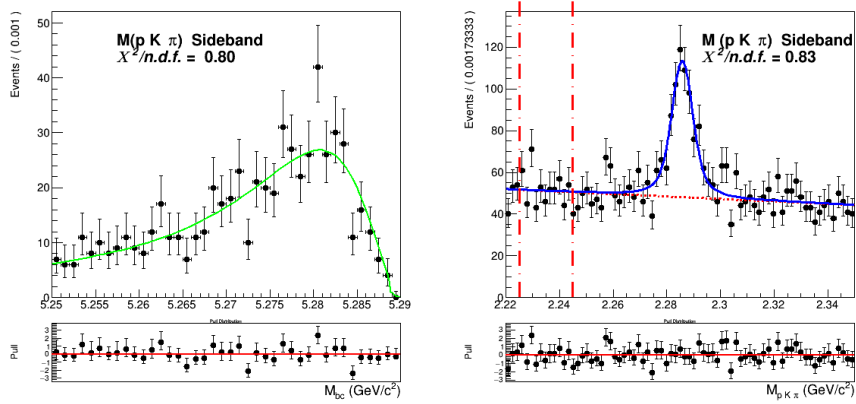


Figure (71) $M(pK\pi)$ sideband region projection of the fit of crossfeed events in M_{bc} .

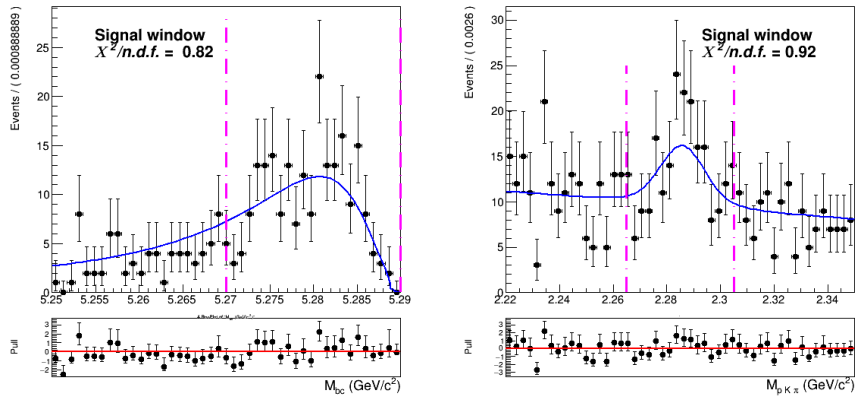


Figure (72) Signal region projections in M_{bc} and $M(pK\pi)$ of the fit of crossfeed events.

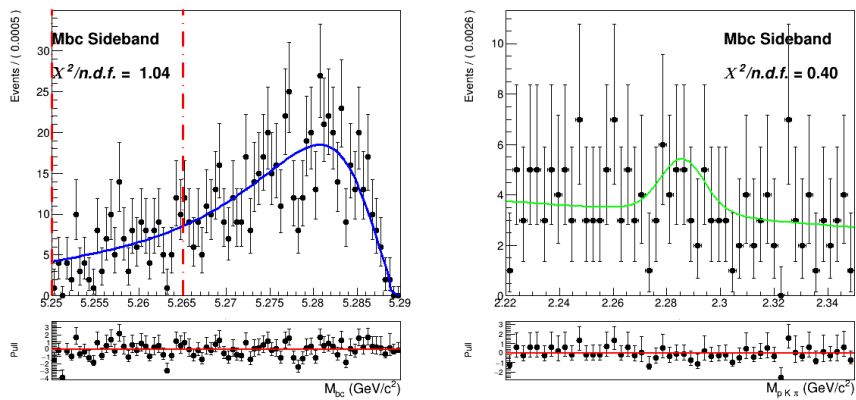


Figure (73) Two dimensional fit of crossfeed ($B^0\bar{B}^0$) events in M_{bc} and $M(pK\pi)$.

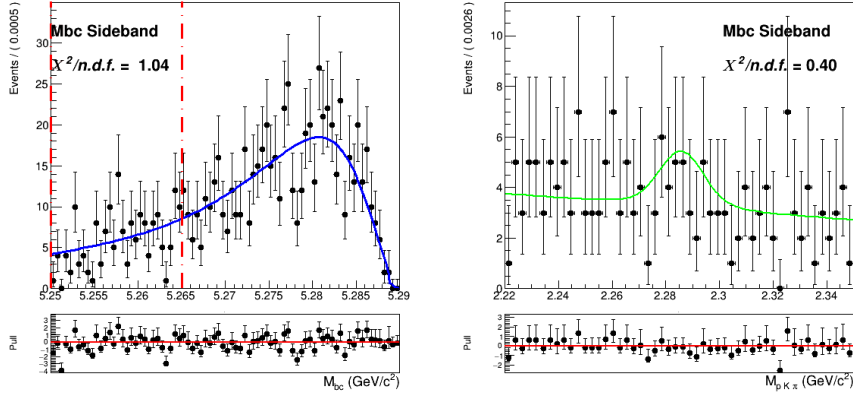


Figure (74) Two dimensional fit of crossfeed ($B^0 \bar{B}^0$) events in M_{bc} and $M(pK\pi)$.

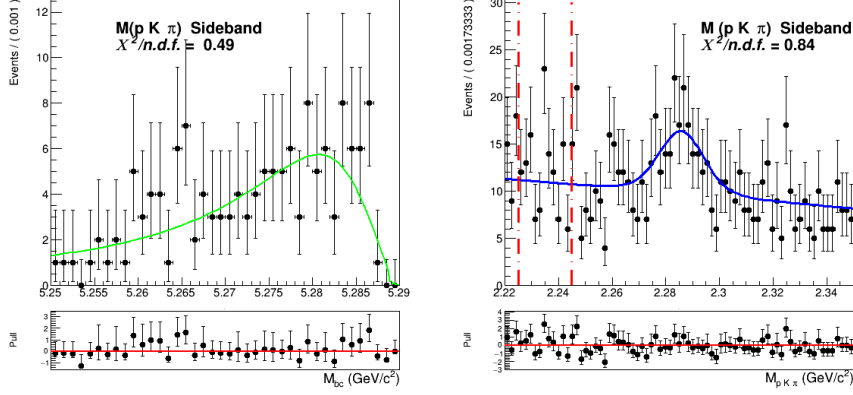


Figure (75) Two dimensional fit of crossfeed ($B^0 \bar{B}^0$) events in M_{bc} and $M(pK\pi)$.

836 The procedure adopted to model the continuum background is the same used for the
 837 charged correlated $B \rightarrow \Lambda_c$ decays. To obtain the shape that can describe the continuum
 838 background M_{bc} distribution, the continuum suppression is not applied on the off-resonance
 839 continuum sample in order to acquire more statistics. It is then scaled and corrected for
 840 the *SignalProbability* correlated effects. The scaling and bin-correction procedure was
 841 carried out on a sample of five streams of on- and off-resonance MC. From a ratio plot,
 842 like the one in Fig. 76a, showing the continuum on-resonance distribution in M_{bc} and the
 843 scaled continuum on-resonance distribution without the continuum suppression applied,
 844 the bin-correction is obtained to correct the off-resonance data in the scaling procedure.

845 The validity of this procedure is first tested on the sixth independent MC sample: Fig.
 846 76b shows the scaled and bin-corrected off-resonance continuum histogram compared with
 847 the continuum on-resonance distribution of the independent stream. Compared to the
 848 charged correlated decays one can notice larger statistical fluctuations but the overall
 849 result looks still fairly reasonable. In order to obtain the PDF describing the distribution
 850 the histogram is fitted (see Fig. 77a), i.e. with a Novosibirsk function.
 851 Since in the Λ_c invariant mass one doesn't expect correlation effects, one can fit directly the
 852 properly scaled distribution with a first order polynomial (see Fig. 77b) It is possible then
 853 to check the validity of the whole procedure on the on-resonance Monte Carlo independent
 854 stream (Fig. 78)

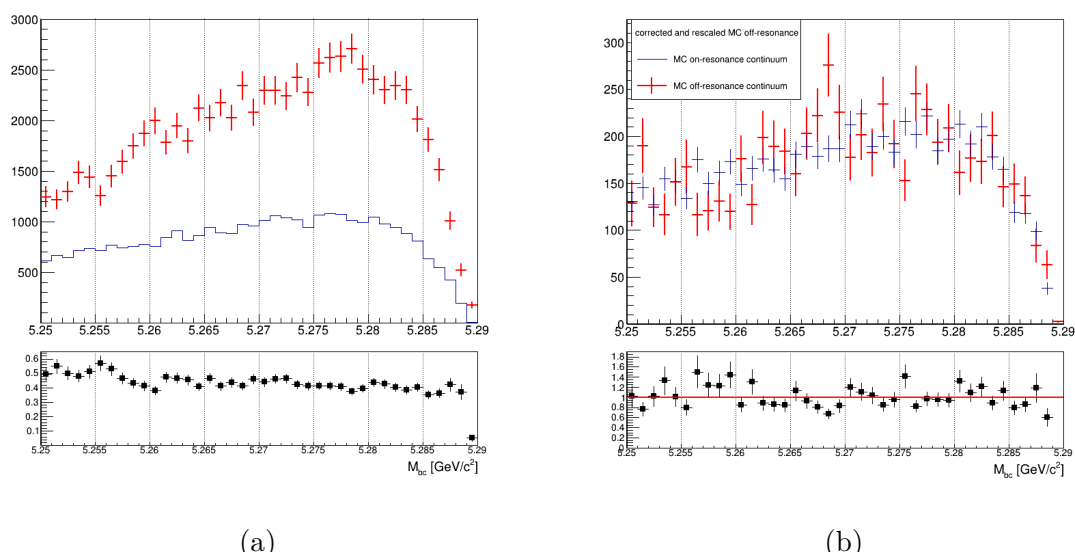


Figure (76) On the left: M_{bc} distributions of the MC off-resonance sample without continuum suppression and the MC continuum sample with applied continuum suppression (5 streams). On the right: M_{bc} distributions of the corrected scaled MC off-resonance and on-resonance MC continuum (independent stream).

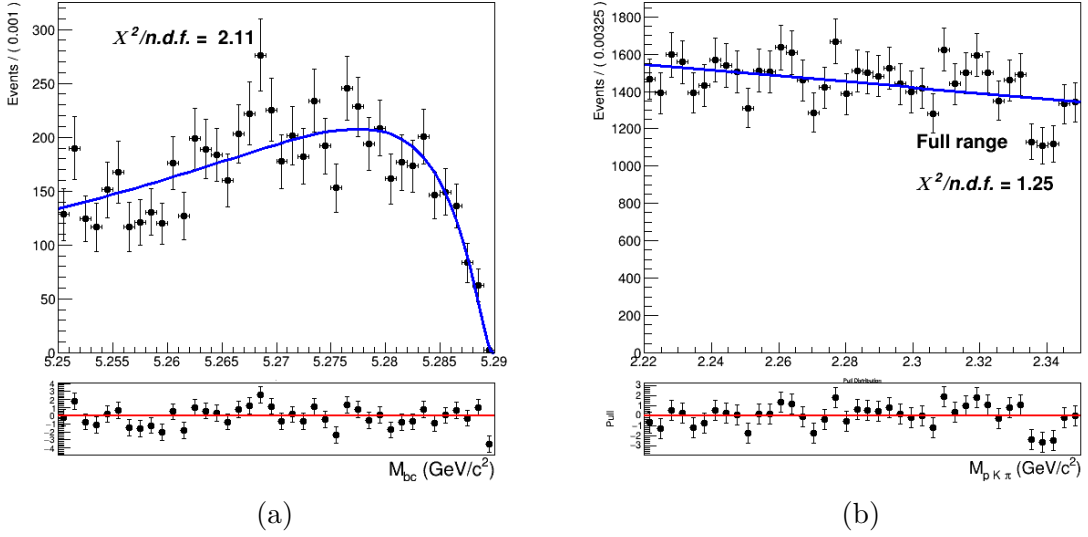


Figure (77) On the left: fit of the M_{bc} distribution MC (scaled and corrected) off-resonance continuum (one stream). On the right: fit of the Λ_c invariant mass distribution of five stream scaled off-resonance continuum.

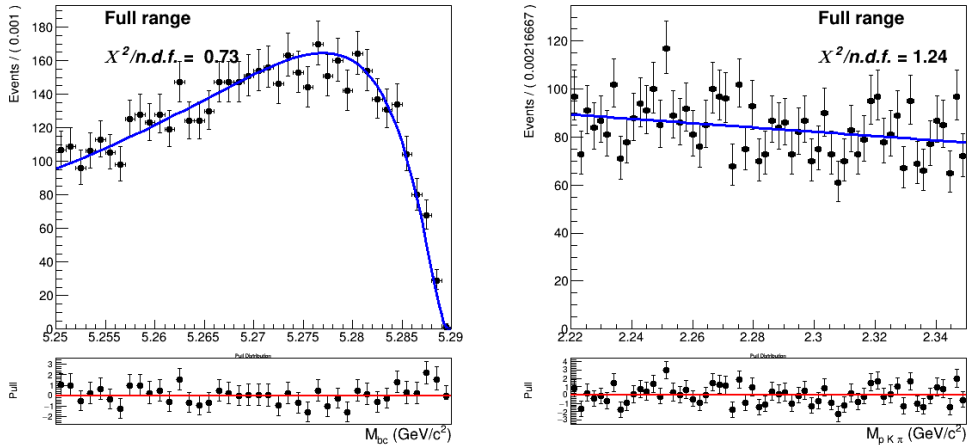


Figure (78) Continuum M_{bc} and $M(pK\pi)$ distributions overlaid by the PDFs obtained in fits shown in Figures 77a - 77b

6.2 Two dimensional fit

After obtaining the PDFs describing the various signal/background components using five streams statistics, the fit model is tested with six fits on the six independent Monte Carlo streams. The conditions for these six two dimensional fits are again the same used for the charged correlated decays (see Sec. 4.2). Exemplary, the distributions of stream 0 overlaid

860 by the fitted PDF are depicted in Fig. 79 (see Appendix .3 for the projections in signal
861 and sideband regions). In Table 1 the signal yields of the fits (**Reconstructed Signal**)
862 to the two dimensional distributions for the six streams of $B^- \rightarrow \bar{\Lambda}_c^-$ flavor-anticorrelated
863 decays are listed and compared to the expected yields of reconstructed signal, and fitted
864 and truth-matched total signal events are also compared, together with their deviations.

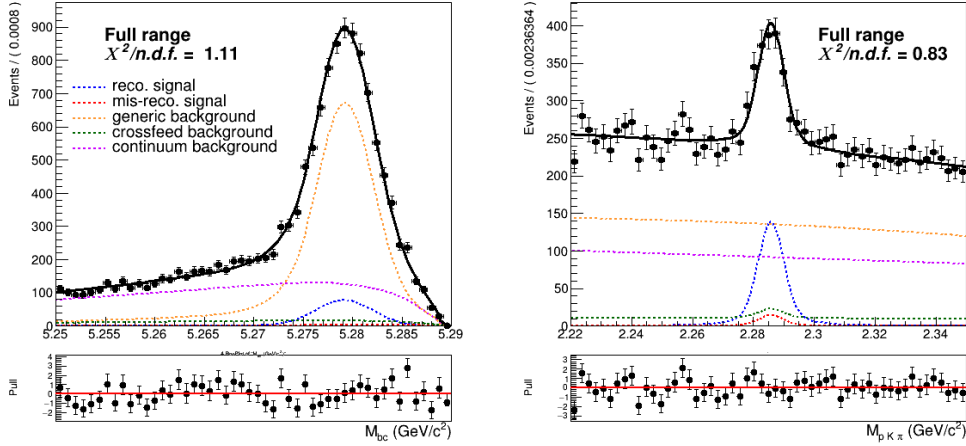


Figure (79) Two dimensional fit on stream 0 Monte Carlo simulated data.

	Reconstructed Signal		Total Signal			fit - MC truth
	fit	expected	fit	MC truth	fit - MC truth	
stream 0	730 ± 60	660 ± 21	805 ± 65	765	40	5.2 %
stream 1	732 ± 60	698 ± 29	794 ± 63	785	9	1.1%
stream 2	759 ± 65	718 ± 29	800 ± 67	797	3	0.4%
stream 3	725 ± 58	702 ± 29	769 ± 60	802	-33	-4.1%
stream 4	829 ± 67	710 ± 29	944 ± 76	804	140	17.4%
stream 5	650 ± 61	675 ± 29	703 ± 62	760	-57	-8.1%
sum	4425	4163	4815	4718	102	+ 2.2%

Table (14) Comparison of fitted and expected signal yields, fitted and truth-matched total signal for six streams of Belle generic MC when fitting the two dimensional distributions of M_{bc} and $M(pK\pi)$.

865 Except for stream 4 all the fits show values of reconstructed signal within the 1σ uncer-
866 tainties in agreement with the expected ones, but as already encountered in Sec. 4.2 a
867 tendency of overestimation can be seen also in these fits, confirmed by the fit shown in Fig
868 81. Again this small, but not negligible, bias has to be taken into account while fitting the
869 data.

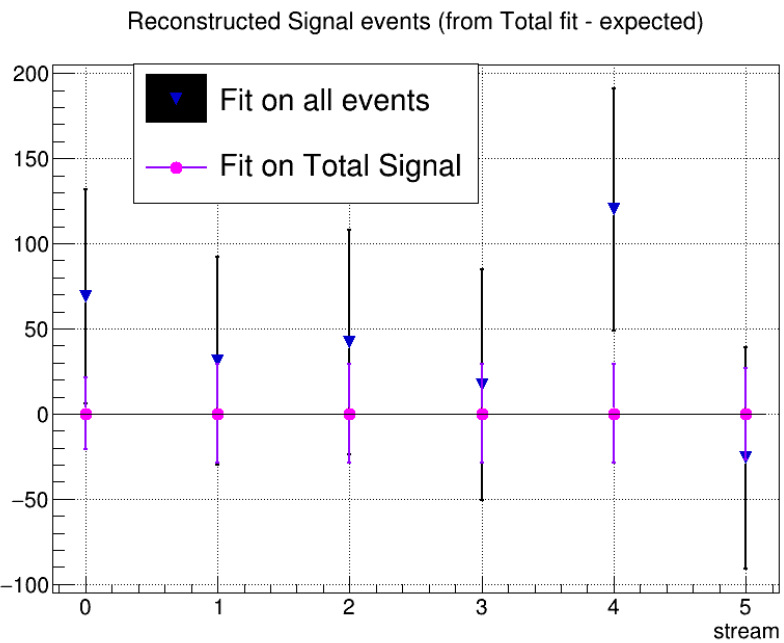


Figure (80) Differences between results from the fits and "expected" values for signal yields as reported in the first columns on Table 14 .

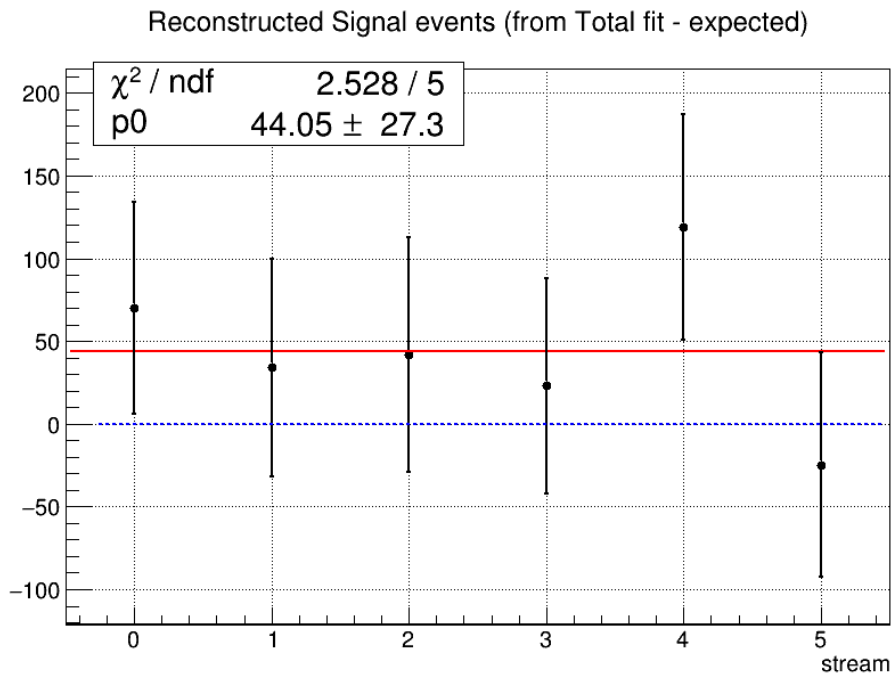


Figure (81)

⁸⁷⁰ Also the behaviour for different signal-to-background ratio was investigated using the six

871 independent streams of continuum and all the ten independent streams of $B\bar{B}$ events
 872 for the generic and crossfeed backgrounds and for the signal events. The amount of
 873 total signal is varied between 50% and 275% of the nominal (MC) values, in order to
 874 cover the values spanned by the uncertainties on the measurement performed by *BaBar*
 875 ($\mathcal{B}(B^+ \rightarrow \bar{\Lambda}_c^+ X) = 2.1^{+0.9}_{-0.6}$) and even the values covered by twice larger uncertainties as
 876 one can see in Fig. 83. The values seem to distribute according to a linear dependence,
 877 therefore also for this decay channel one doesn't expect any systematics due to different
 878 signal-to-background ratio.

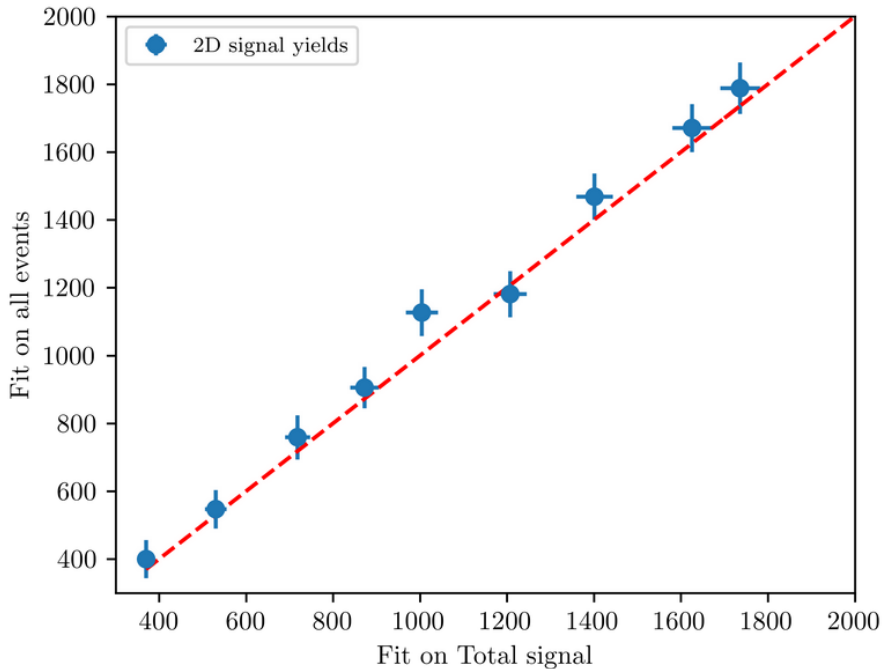


Figure (82) Linearity test: on the x-axis the obtained reconstructed signal yields from fits on different amounts of total signal; on y-axis the yields of reconstructed signal obtained fitting all events (as in Fig. 34). The dashed red line represents the 1:1 linear dependence.

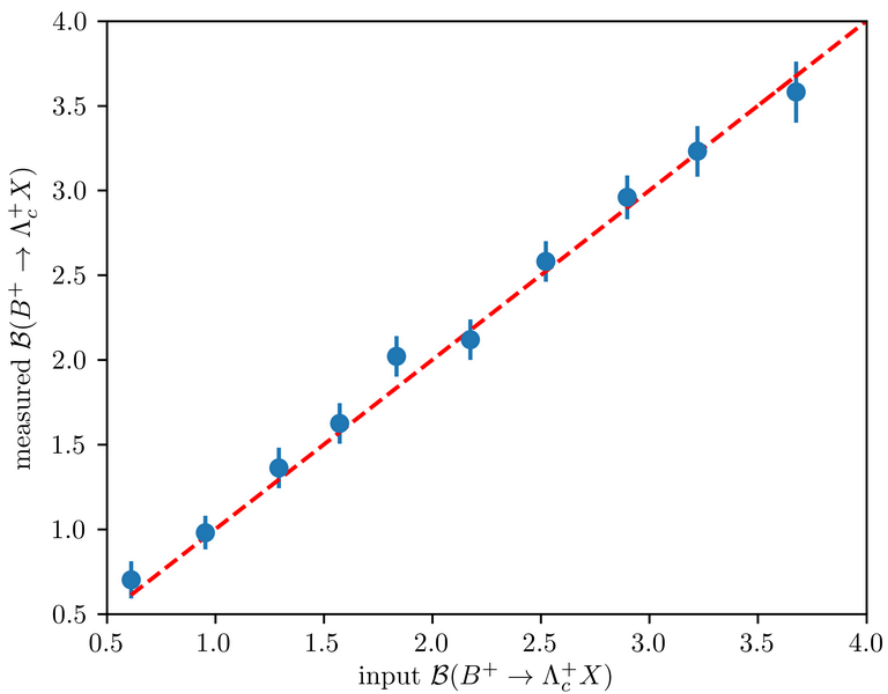


Figure (83) Linearity test: on the x-axis the input branching ratio value corresponding to the signal yields displayed on the x-axis in Fig. 82; on y-axis the measured branching fraction values corresponding to the signal yields of reconstructed signal displayed on the y-axis in Fig. 82.

⁸⁷⁹ Toy MC pseudo-experiments were performed as well (see Appendix).

880 6.3 Probability Density Functions (PDFs) for the B_{tag}

881 The M_{bc} distribution of the tagged B mesons is fitted with a Crystal Ball as for the
 882 "peaking" component and the "flat" component is fitted with a Argus function (Fig. 84a).
 883 The crossfeed background, consisting of neutral B mesons tagged as charged B , is fitted
 884 instead with a sum of a Novosibirsk and an asymmetric Gaussian PDF (Fig. 84b).

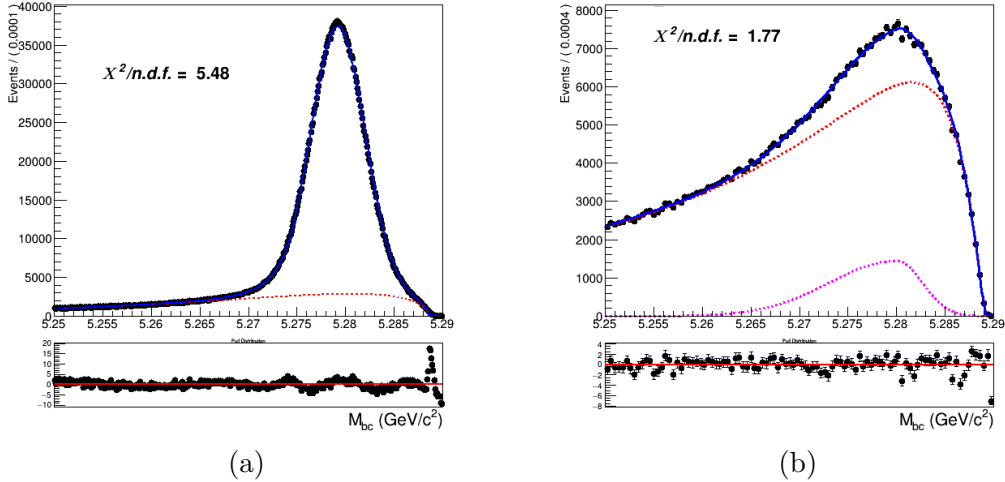


Figure (84) On the left: fitted distribution of tagged charged B mesons, reconstructed signal events (magenta) are described by a Crystal Ball whereas the misreconstructed signal events (red) are described by an Argus function. On the right: Crossfeed distribution fitted with a sum of Novosibirsk (red) and asymmetric Gaussian PDF (magenta)

885 As for the continuum background, same procedure as the one in the case of charged
 886 flavor-correlated decays is adopted:

- 887 • first the off-resonance sample is scaled accordingly with all the included cuts.
- 888 • the ratio between the scaled off-resonance and the on-resonance in MC is calculated
 889 in each bin (see Fig. 85a)
- 890 • the bin-correction is applied on an independent stream and the scaled and bin-
 891 corrected M_{bc} distribution is compared with the on-resonance distribution as shown
 892 in Fig. 85b

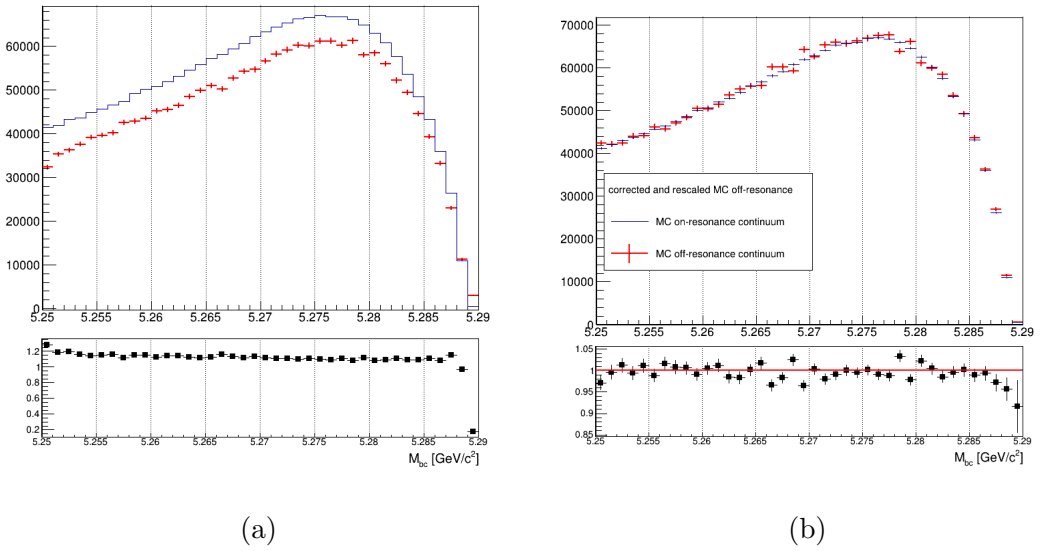


Figure (85) On the left: M_{bc} distributions of the MC off-resonance sample and the MC continuum sample with applied continuum suppression. On the right: M_{bc} distributions of the corrected scaled MC off-resonance and on-resonance MC continuum.

893 **6.4 B_{tag} fit**

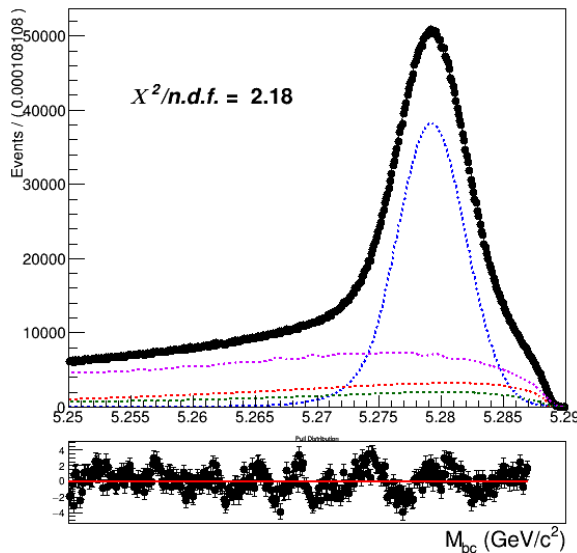


Figure (86) Total fit of tagged B mesons on Monte Carlo simulated data.

894 An independent Monte Carlo stream was used to test the total fit model on tagged B
 895 meson candidates. As in the 2D fit, the parameter for the width, σ_{CB} , of the Crystal Ball is
 896 floated and the ratio between expected crossfeed background events and misreconstructed
 897 signal events is fixed from the MC. The Argus function describing the misreconstructed
 898 signal is also not fully constrained: the parameter describing the tail is free. As in the
 899 previous B_{tag} fits, the range for the fit is restricted to values between 5.250 and 5.287
 900 GeV/c^2 . Yields for the reconstructed and misreconstructed signal are obtained from the
 901 fit:

902

NrecSig	$2.5099 \cdot 10^6 \pm 4408$
NmisSig	$7.82307 \cdot 10^5 \pm 2936$

903 The Total Signal (the sum NrecSig+NmisSig) is 3292168 ± 2423 (to be compared with
 904 3299629 from the Monte Carlo), which means a $\sim 3\sigma$ underestimation. As in the case of
 905 charged flavor-correlated decays, this can produce some systematic effect which needs to
 906 be taken into account. In fact, a slight underestimation of the Total Signal is found also
 907 in the result of the toy Monte Carlo study⁸: Fig. 87 shows the results for the Total Signal
 908 events and one can notice a mean value for the pulls consistently below zero.
 909

⁸as usual performed with 3×10^3 pseudo-datasets

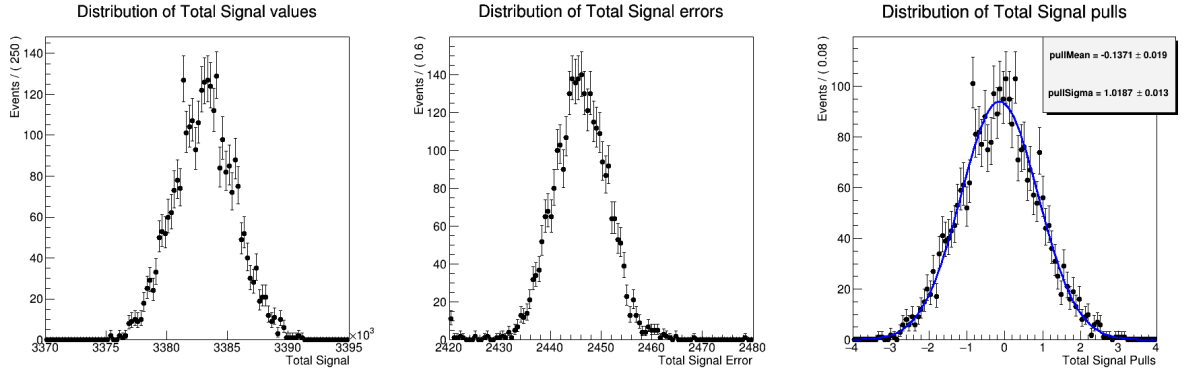


Figure (87) Toy MC fits of pseudo-data showing the Total Signal yield (left), Total Signal yield errors (center) and the pull distribution of the Total Signal (right).

910 6.5 Λ_c and FEI efficiency

911 The efficiency in reconstructing the Λ_c baryon after correctly tagging the charged B meson,
 912 is as usual estimated as the ratio:

$$\frac{N_{recSig}(B_{tag}, \Lambda_c)}{N_{recSig}(B_{tag}^{sig})} \quad (12)$$

913 where $N_{recSig}(B_{tag}, \Lambda_c)$ are the yields of reconstructed signal from the two dimensional fits
 914 (reported in Table 14) and $N_{recSig}(B_{tag}^{sig})$ are the yields of correctly reconstructed signal in
 915 a fit of B mesons tagged in events where one of the two mesons decayed hadronically and
 916 inclusively into a Λ_c baryon (see Fig 46). This ratio was calculated upon six streams of
 917 Monte Carlo simulated data.

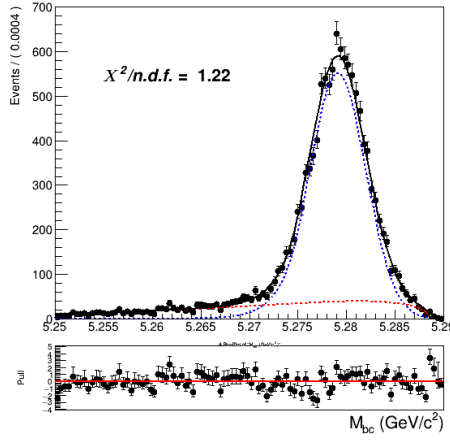


Figure (88) Fit of tagged B mesons in the "signal events" sample

918 From this and the results listed in Sec. 6.2 the efficiency to reconstruct Λ_c is obtained :

919

$$920 \quad \epsilon_{\Lambda_c} = \frac{N_{recSig}(B_{tag}, \Lambda_c)}{N_{recSig}(B_{tag})} = 40.95 \pm 1.77\%$$

921 The yields from the fit shown in Fig. 88) are then used to calculate the FEI tag-side
 922 efficiency for signal events. The yields from the fit of charged B_{tag} shown in Fig. 84a can
 923 be used to calculate the hadronic tag-side efficiency in the generic B^+B^- events case.

924 The ratio between the two efficiencies is calculated: $\frac{\epsilon_{FEI,sig}^+}{\epsilon_{FEI}^+} = 0.973 \pm 0.009$

925

926 6.6 Studies of Systematic Effects

927 The systematic uncertainties are estimated the same way as in the case of charged flavor-
 928 correlated decays (see Sec. 4.7 and the following Sections). In Table 15 the systematic
 929 uncertainties of the various considered sources are summarized. Their individual calculation
 930 is outlined in the subsequent subsections (the uncertainties on the PID efficiency corrections
 931 are the same already discussed in Sec. 4.14)

source	%
Continuum modeling	0.04
Crossfeed PDFs	0.01
Crossfeed fraction	0.01
2DFit crossfeed normalization	0.01
2DFit crossfeed peaking fraction	0.08*
$\epsilon_{FEI,sig}^+/\epsilon_{FEI}^+$	0.01
ϵ_{Λ_c}	0.05
Fit bias	0.05
PID	0.02
Tracking efficiency	0.01
Total	0.12

Table (15) Systematic uncertainties in the determination of the $B^- \rightarrow \bar{\Lambda}_c^- X$ branching fractions in %.

932 * as in the case of charged flavor-correlated decays this uncertainty can be possibly
 933 reduced with a new measurement of $B^0 \rightarrow \Lambda_c$ decays.

934 6.7 Continuum background modeling

935 Exemplary, fits used to estimate the impact of these uncertainties deriving from statistical
 936 uncertainties are shown here in Figures 89 - 90. Mean deviation values are then obtained
 937 for both the two-dimensional fit and the B_{tag} fit.

938

Fit	$-\sigma$	$+\sigma$	$\pm\bar{\sigma}$
2D	21	22	22
B_{tag}	5800	5800	5800

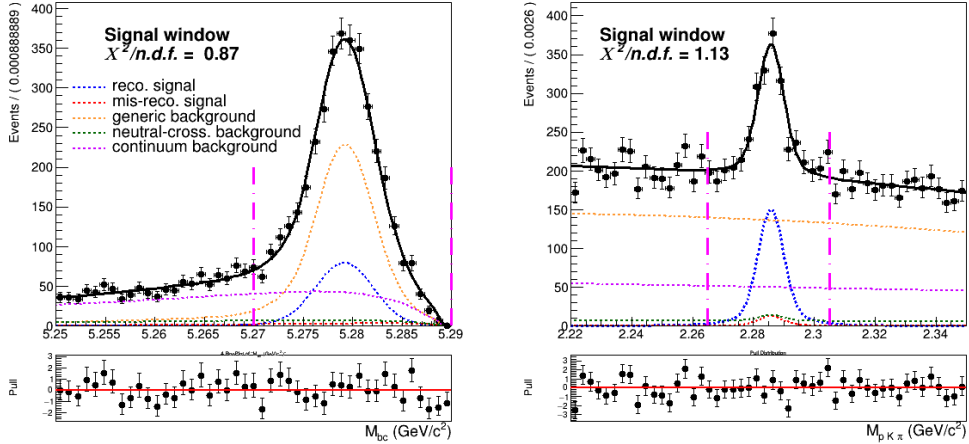


Figure (89) Signal window projections of a two dimensional fit on Monte Carlo simulated data where the shaping parameters were varied of their uncertainties.

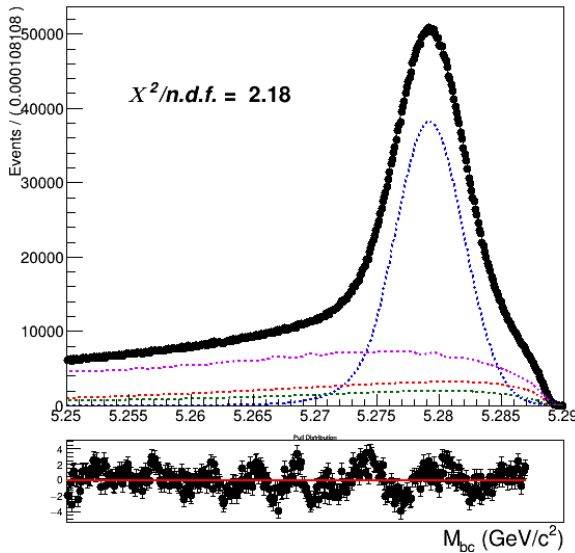


Figure (90) Fit of tagged B meson candidates on Monte Carlo simulated data where the shaping parameters were varied of their uncertainties.

939 The estimated systematic uncertainty on Br value from this source is 0.04%.

940 The continuum suppression cut is found to reject about 68% of the continuum back-
941 ground in data, whereas it rejects 64% of the continuum background in MC (66.5% in

942 on-resonance MC). This means that in data one can expect about 1.4% less continuum
 943 background events. The statistical uncertainty on this fraction of events can be also be
 944 taken into account as systematics. But again, as already seen in the case of charged flavor-
 945 correlated decays, the statistical uncertainty on the on-resonance continuum background
 946 events in MC originates a much larger systematic uncertainty: the relative systematic
 947 uncertainty deriving from the different impact on data of the continuum suppression would
 948 account for just 0.004% on the BR value (one order of magnitude smaller than systematics
 949 deriving from the statistical uncertainties). This second source is again consequently
 950 neglected.

951 6.8 Crossfeed background modeling

952 This source of systematic uncertainty is again estimated performing the fits varying the
 953 parameters of the Crossfeed PDFs by their uncertainties (see the table below for the
 954 deviations in terms of signal yields). The resulting absolute systematic uncertainty is
 955 about 0.006% on the BR value, which is rounded up to 0.01%.

Fit	$-\sigma$	$+\sigma$	$\pm\bar{\sigma}$
2D	3	3	3
B_{tag}	1500	1100	1300

Table (16) Offsets on the signal yields obtained varying the parameters of crossfeed background PDFs within their uncertainties in the two dimensional and B_{tag} fit and mean deviations reported in the last column.

956 6.9 Crossfeed ratio

957 As already done for the charged flavor-correlated decays, the systematic uncertainty
 958 on the crossfeed/misreconstructed signal "probability ratio" for the 2D fit and cross-
 959 feed/misreconstructed ratio is studied considering a maximal discrepancy up to 20%
 960 between Monte Carlo and data (the procedure adopted is the same as illustrated in
 961 Sec. 4.9).

Fit	$-\sigma$	$+\sigma$	$\pm\bar{\sigma}$
2D	4	8	6
B_{tag}	5800	800	3300

Table (17) Offsets on the signal yields obtained varying of $\pm 20\%$ the k ratio in the two dimensional and B_{tag} fit and mean deviations reported in the last column.

962 The estimated systematic uncertainty on Br value from this source is 0.01%.

963 **6.10 Parametrization of crossfeed normalization in the 2D fit**

964 The statistical uncertainties on the parameters used in the parametrization of crossfeed
965 normalization in the 2D fit are estimated to originate a systematic uncertainty of 0.01%
966 on the Br value.

967 **6.11 Crossfeed peaking fraction in the 2D fit**

968 As already done for the charged correlated decays, to estimate this systematic uncertainty
969 the amount of crossfeed events peaking in $M(pK\pi)$ was varied in order to cover the
970 uncertainties on the branching fraction for neutral decays and the two-dimensional fit
971 repeated with those values. The difference in signal yields obtained is reported in the
972 following table.

Fit	$-\sigma$	$+\sigma$	$\pm\bar{\sigma}$
2D	15	18	16

Table (18) Offsets on the signal yields obtained varying the amount of peaking crossfeed in the Λ_c invariant mass and mean deviation.

973 The uncertainty originated is estimated to be of 0.08% on the Br value.

974 **6.12 Efficiencies**

975 The ratio between the two FEI efficiencies is: $\frac{\epsilon_{FEI,sig}^+}{\epsilon_{FEI}^+} = 0.973 \pm 0.009$

976 The uncertainty on this value originates a systematic uncertainty of 0.01% on the Br
977 value. The Λ_c reconstruction efficiency is determined to be $\epsilon_{\Lambda_c} = 40.95 \pm 1.77\%$. When
978 propagating its uncertainty, a systematic error of 0.07% on the Br value is calculated.

979 **6.13 Fit biases**

980 The small bias on the reconstructed signal seen in the two-dimensional fit model produces
981 a not negligible systematic uncertainty on the branching fraction. The discrepancy in the
982 amount of the total signal estimated by the B_{tag} fit needs to be included as well in the
983 systematic effects. Propagating the two sources of systematics in the branching fraction
984 calculation results in an additional 0.05% uncertainty on the branching fraction value.

985 **6.14 Tracking efficiency**

986 As for the charged correlated decays, a systematic uncertainty of 0.35% per track is applied
987 and the total systematic uncertainty is the sum over the three charged tracks used to
988 reconstruct the Λ_c baryon: 1.05%. This results in 0.01% uncertainty on the branching
989 fraction value.

990 **6.15 Measured $B^+ \rightarrow \Lambda_c^+$ inclusive Branching Fraction**

991 Using the results from the two dimensional fit reported in Table 14 with all the needed
 992 factors known, it's possible to examine the agreement between the branching ratio
 993 value used in MC generation and the measured ones. As in the charged flavor-correlated
 994 decays the average of measured values are about 1σ statistical uncertainty away from
 995 the average value of the branching ratio set in MC (actually already the average value
 996 obtained with the total signal fits shows this tendency).

	total fit	signal fit	BELLE MC VALUE
stream 0	(1.32 ± 0.11)%	(1.19 ± 0.04)%	(1.233 ± 0.007)%
stream 1	(1.32 ± 0.11)%	(1.26 ± 0.05)%	(1.218 ± 0.007)%
stream 2	(1.37 ± 0.12)%	(1.29 ± 0.05)%	(1.218 ± 0.007)%
stream 3	(1.31 ± 0.11)%	(1.26 ± 0.05)%	(1.215 ± 0.007)%
stream 4	(1.50 ± 0.12)%	(1.26 ± 0.05)%	(1.218 ± 0.007)%
stream 5	(1.12 ± 0.12)%	(1.22 ± 0.05)%	(1.217 ± 0.007)%
average	(1.32 ± 0.05)%	(1.25 ± 0.02)%	(1.220 ± 0.003)%

Table (19) Measured branching fraction values obtained using the results listed in Table 14 for the six different streams (only statistical uncertainties are displayed) and its average.

997 As in the charged flavor-correlated decays the precision obtained on Monte Carlo simulated
 998 data is improved by factors compared to the branching fraction measured by BaBar
 999 experiment (see [1]).

¹⁰⁰⁰ Appendices

1001 .1 $B^- \rightarrow \Lambda_c^+$ decays: additional plots

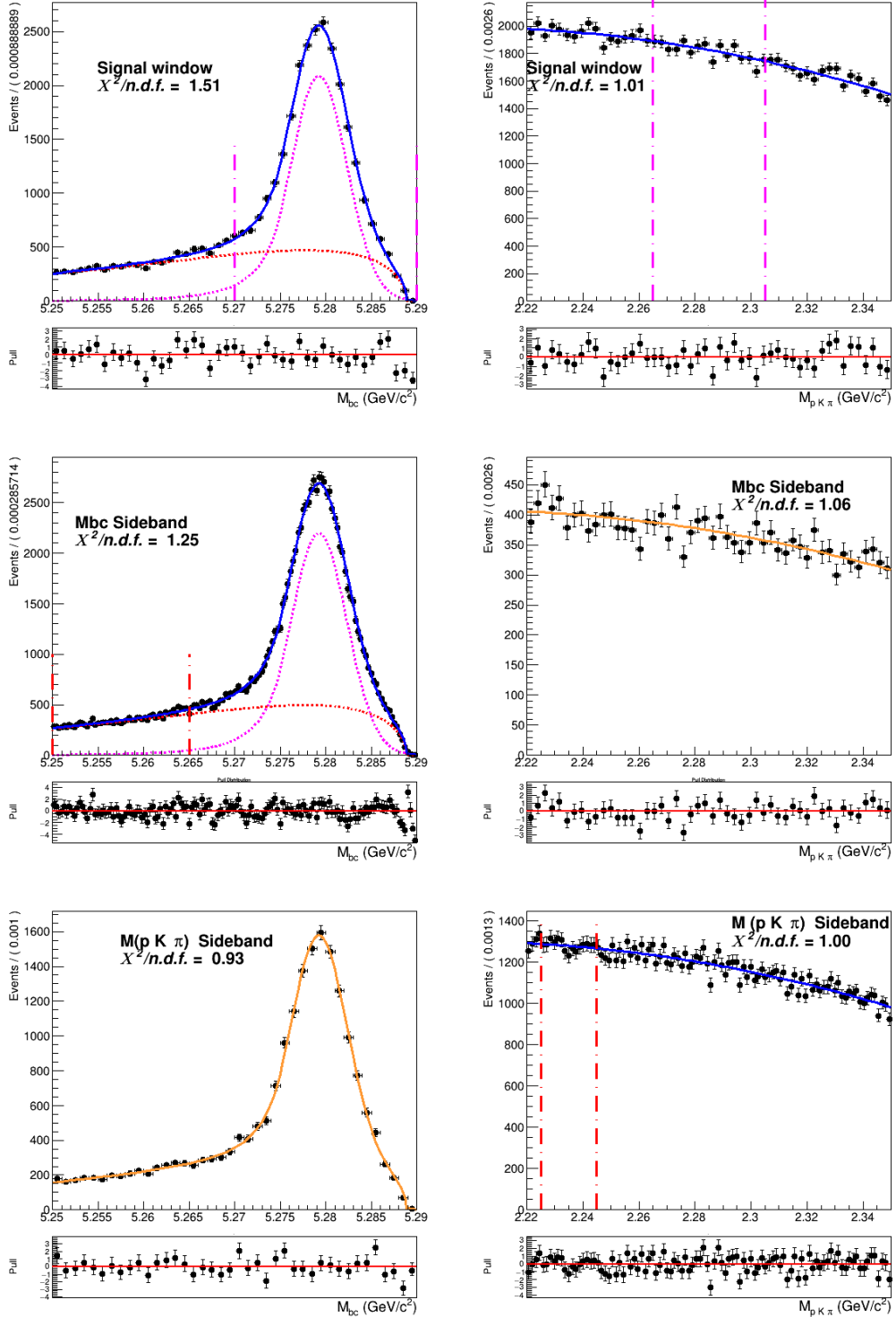


Figure (91) Signal region and sidebands of the two dimensional fit of generic background shown in Fig. 13

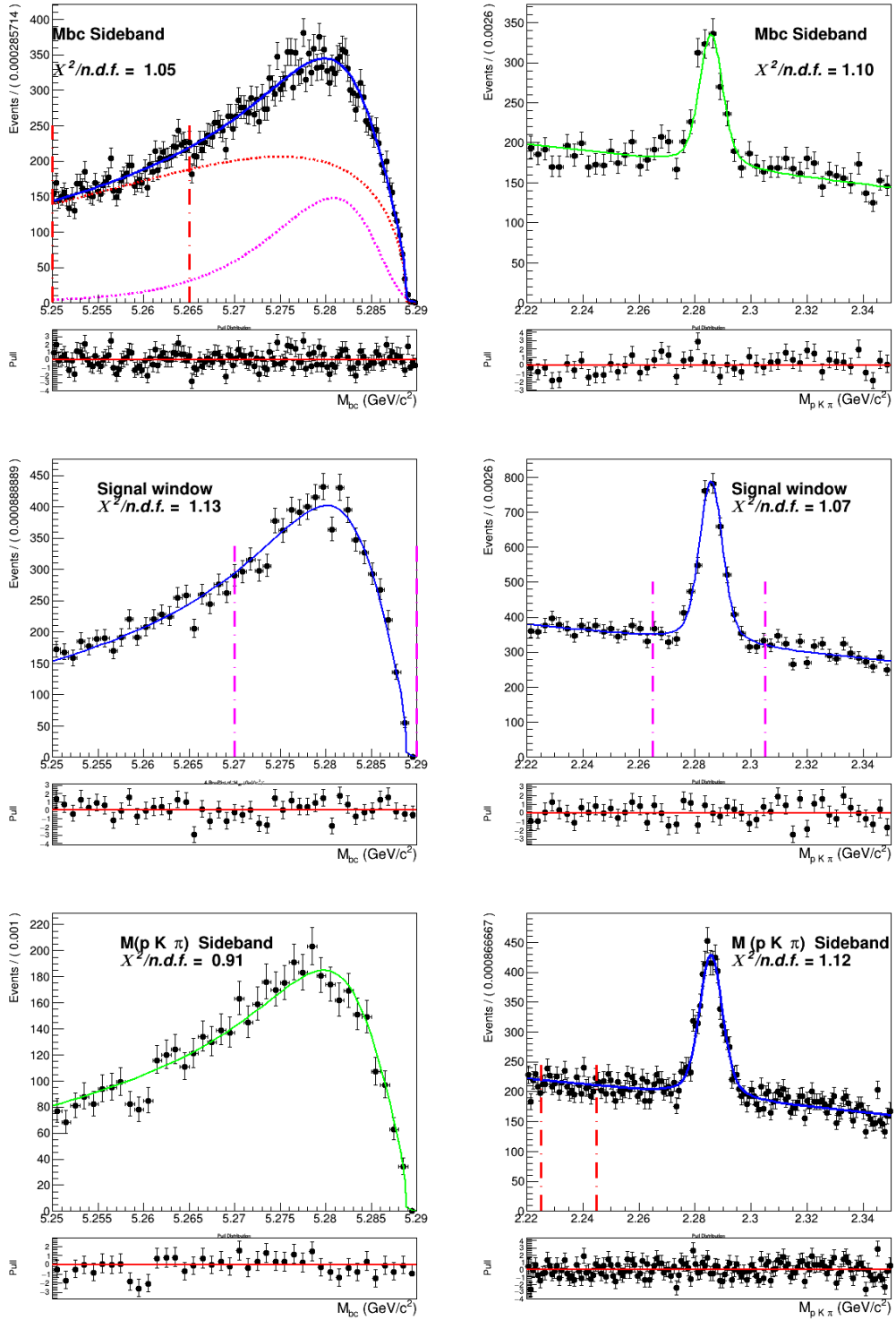


Figure (92) Signal region and sidebands of the two dimensional fit of crossfeed background after parametrization

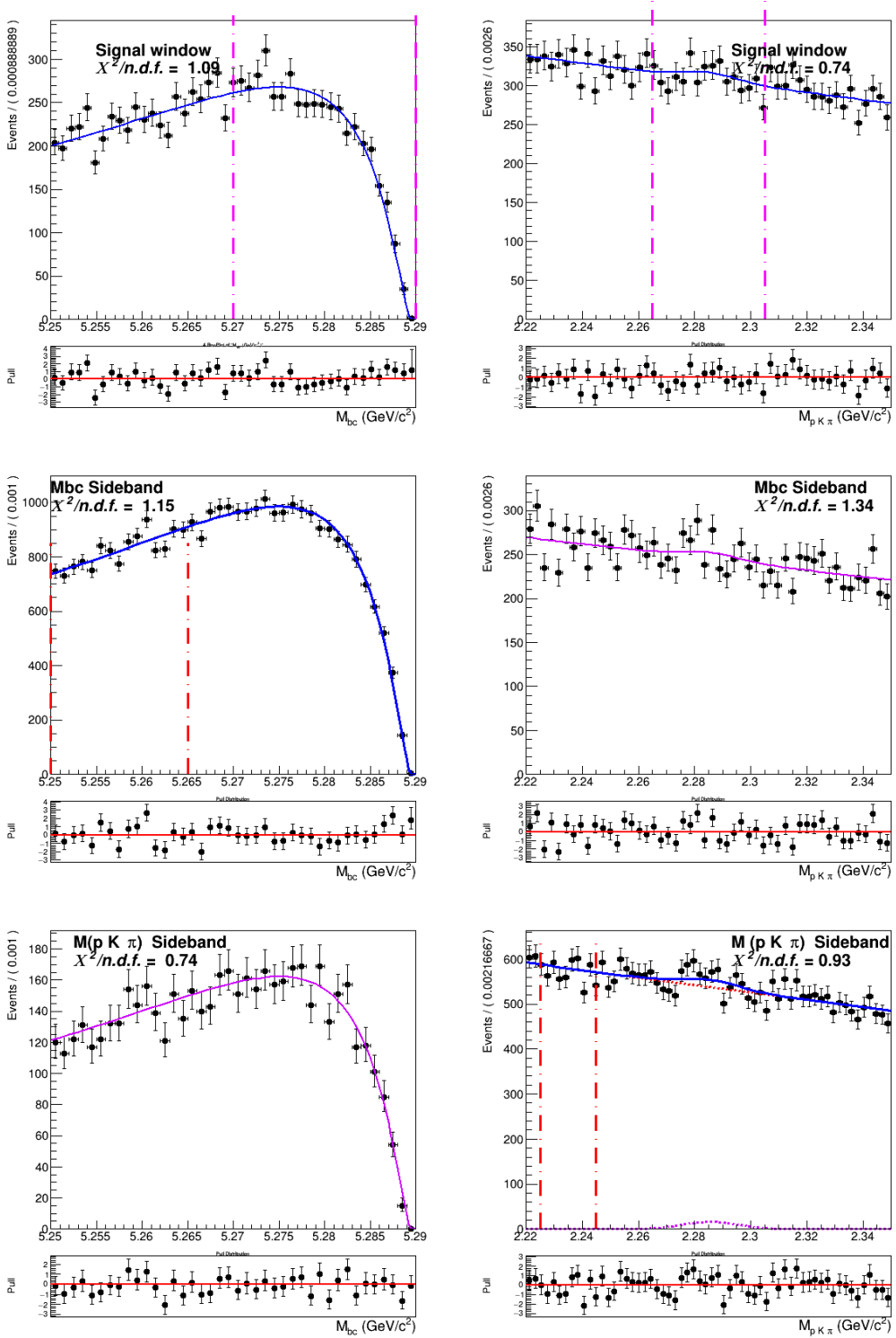


Figure (93) Signal region and sidebands of the two dimensional fit of continuum background shown in Fig. 33

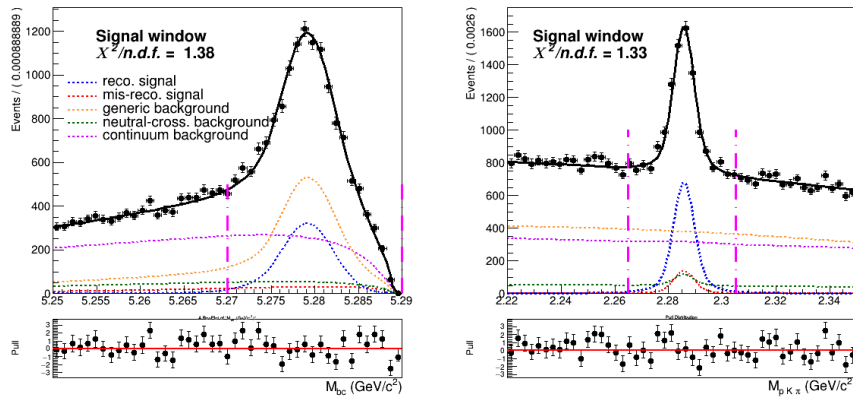


Figure (94) Signal region ($2.22 < M(pK\pi) < 2.35 \text{ GeV}/c^2$ and $5.27 < M_{bc} < 5.29 \text{ GeV}/c^2$) projections pf the dimensional fit on stream 0 Monte Carlo simulated data.

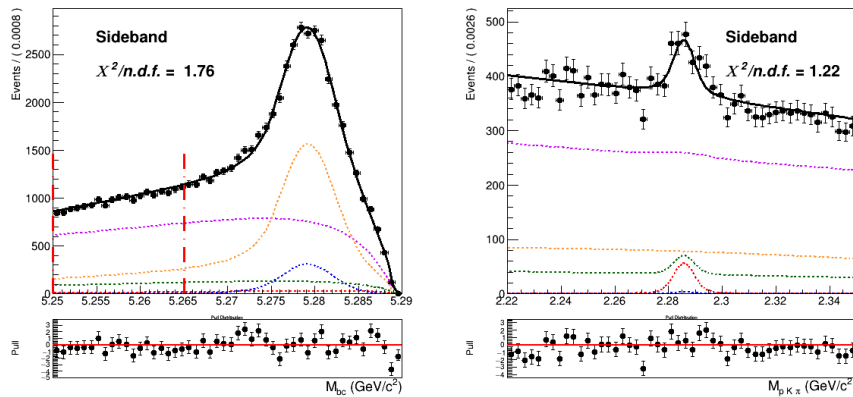


Figure (95) Sideband region of $5.25 < M_{bc} < 5.265 \text{ GeV}/c^2$ projection of the two dimensional fit on stream 0 Monte Carlo simulated data.

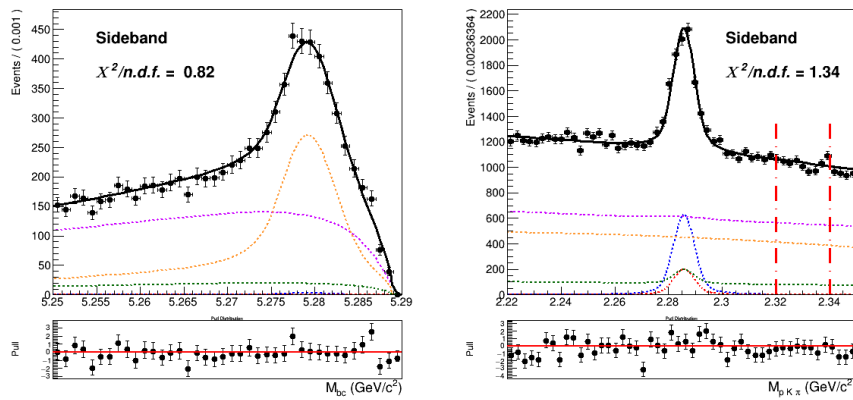


Figure (96) Sideband region of $2.22 < M(pK\pi) < 2.35 \text{ GeV}/c^2$ projection of the two dimensional fit on stream 0 Monte Carlo simulated data.

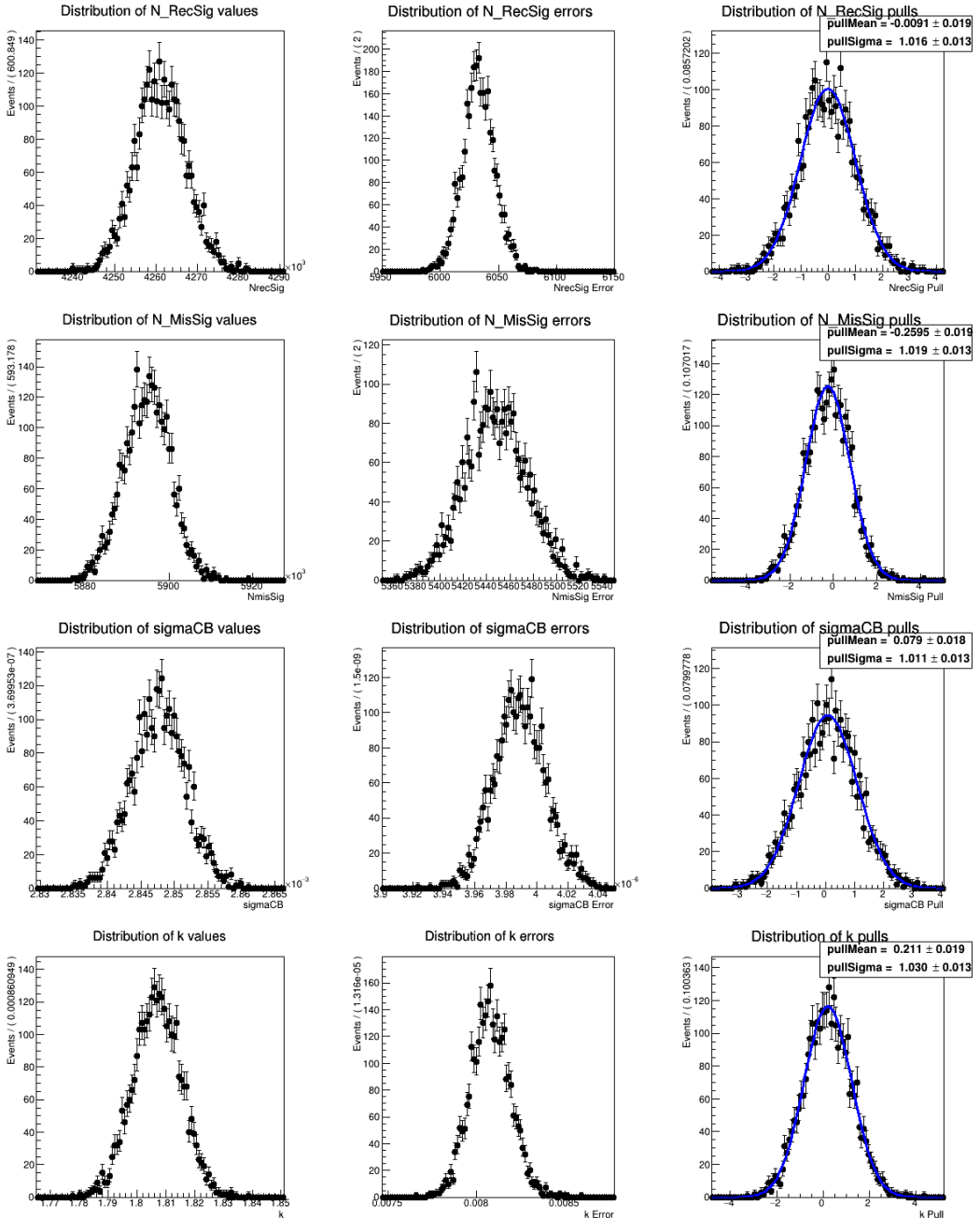


Figure (97) Toy MC study for the B_{tag} fit model described in Sec. 4.4

.2 $B^- \rightarrow D^0$ decays: additional plots

Figures 98-99 show the FOM values at various cuts on *foxWolframR2* and *SignalProbability* variables respectively. After the cuts on the first two variables were optimized, the cut on D_{CMS}^0 is chosen considering the momenta distributions plotted on 100: $p_{CMS}^{D^0} > 1$ GeV/c² removes a good portion of background events while retaining most of the signal events.

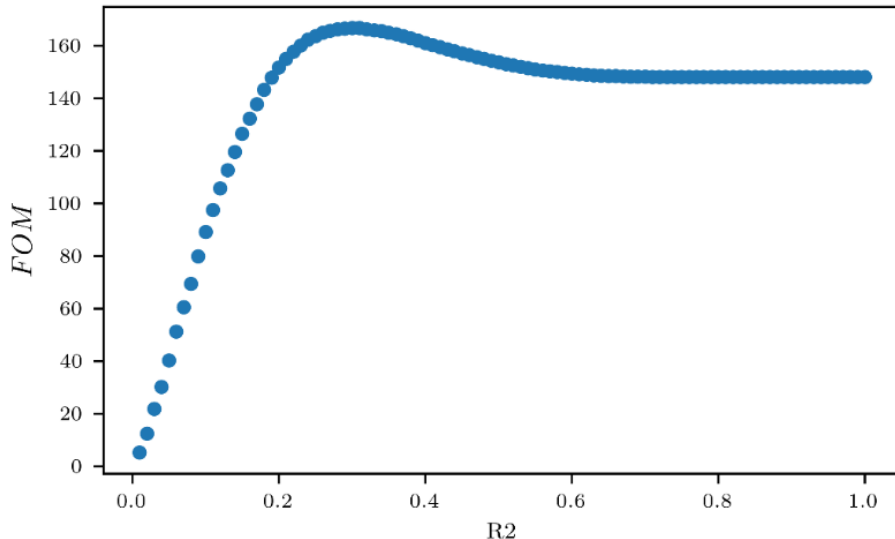


Figure (98) Figure of Merit values calculated at several cuts on the *foxWolframR2* variable.

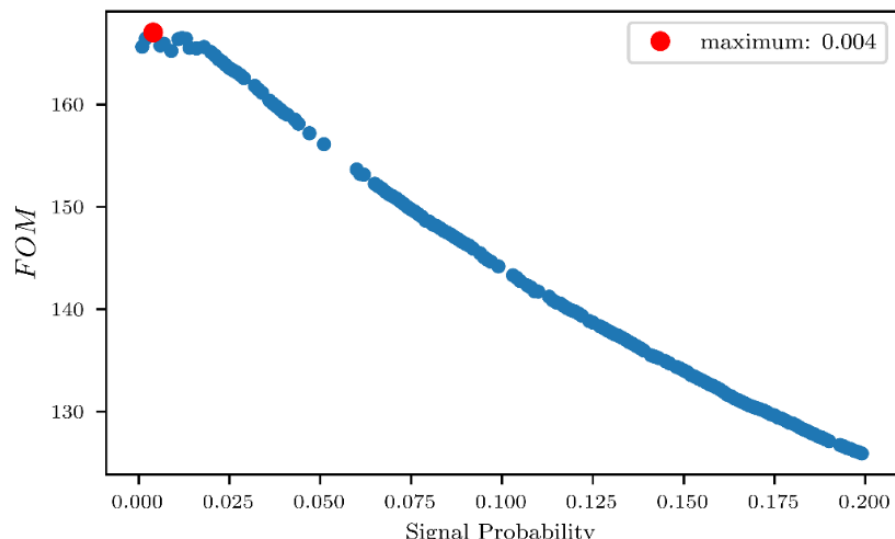


Figure (99) Figure of Merit values calculated at several cuts on the *SignalProbability* variable.

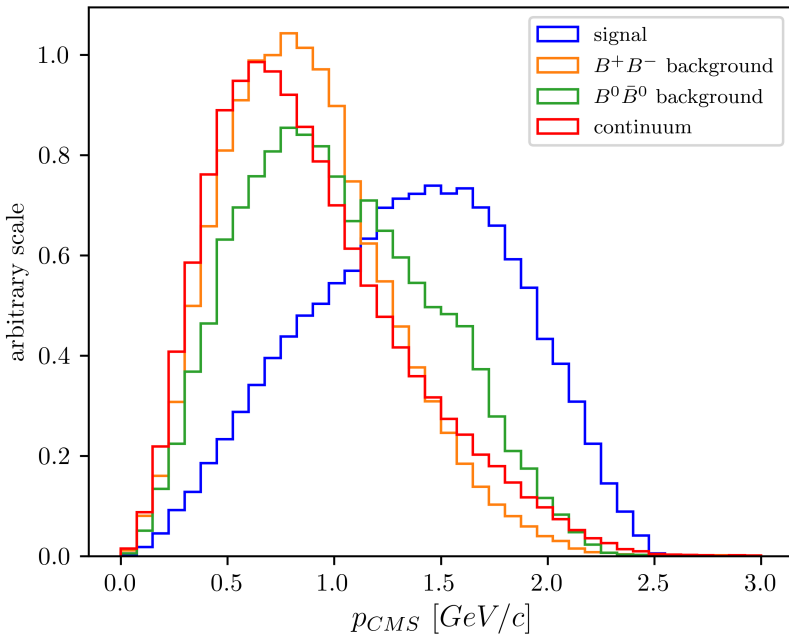


Figure (100) Distribution of D^0 candidates momenta in the center of mass system after the cuts on *foxWolframR2* and *SignalProbability* variables were applied.

1008 Figures 101-103 show the projections of signal regions and sidebands in M_{bc} and in the
 1009 D^0 invariant mass of the two dimensional fit on stream 0.

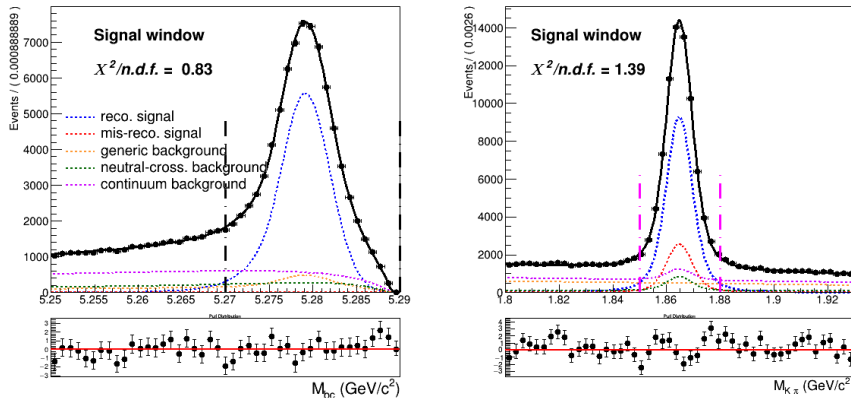


Figure (101) Signal region ($1.85 < M(\pi K) < 1.88 \text{ GeV}/c^2$ and $5.27 < M_{bc} < 5.29 \text{ GeV}/c^2$) projections of the two dimensional fit on stream0 (Fig. 57).

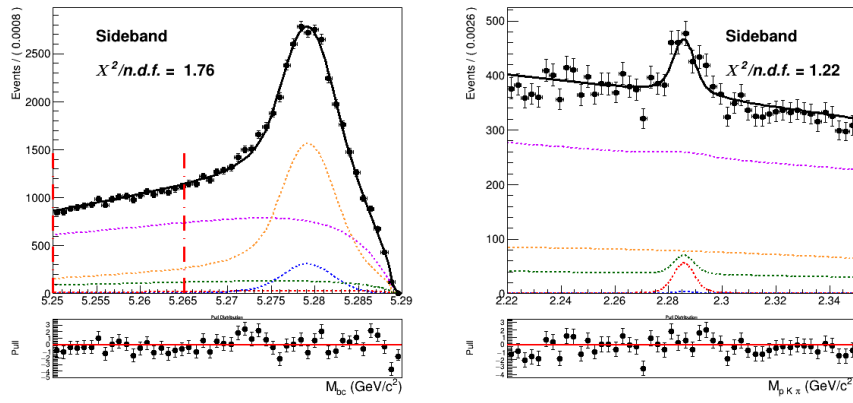


Figure (102) Sideband region of $5.25 < M_{bc} < 5.265 \text{ GeV}/c^2$ projection in $M(\pi K)$ of the two dimensional fit on stream 0.

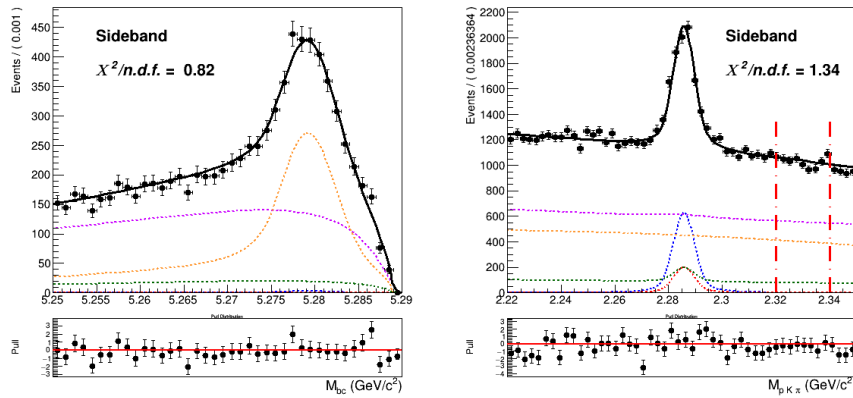


Figure (103) Sideband region of $1.8 < M(\pi K) < 1.84 \text{ GeV}/c^2$ projection in M_{bc} of the two dimensional fit on stream 0.

1010 Figs. 104 to 106 show the projections in M_{bc} and in the D^0 invariant mass of the two
 1011 dimensional fit on data.

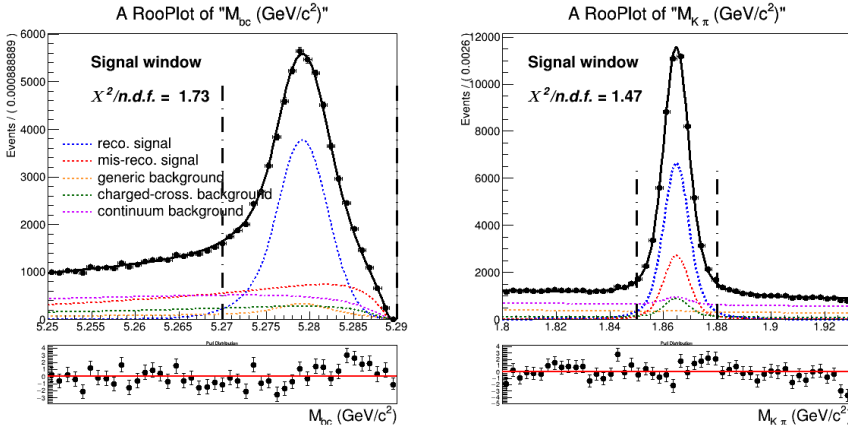


Figure (104) Signal region ($1.85 < M(\pi K) < 1.88 \text{ GeV}/c^2$ and $5.27 < M_{bc} < 5.29 \text{ GeV}/c^2$) projections of the two dimensional fit on data described in Sec. 5.6

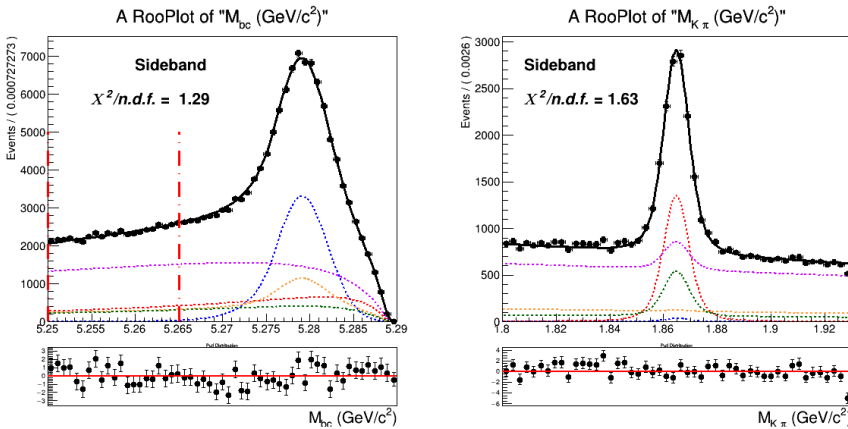


Figure (105) Sideband region of $5.25 < M_{bc} < 5.265 \text{ GeV}/c^2$ projection in $M(\pi K)$ of the two dimensional fit on data

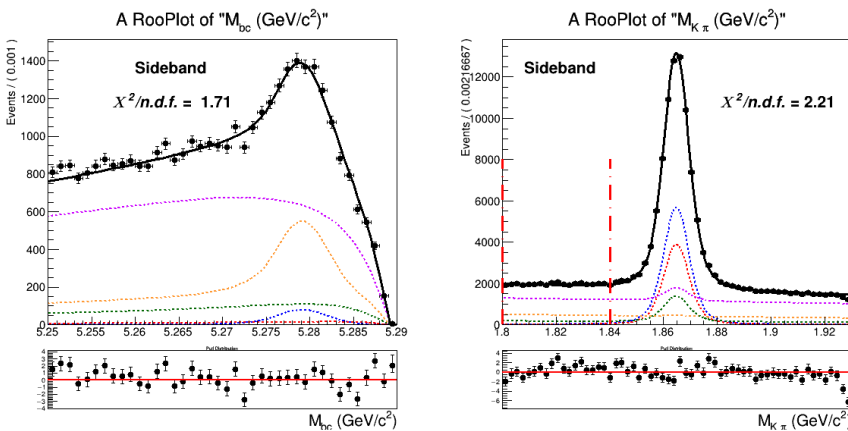


Figure (106) Sideband region of $1.8 < M(\pi K) < 1.84 \text{ GeV}/c^2$ projection in M_{bc} of the two dimensional fit on data.

1012 .3 $B^- \rightarrow \bar{\Lambda}_c^-$ decays: additional plots

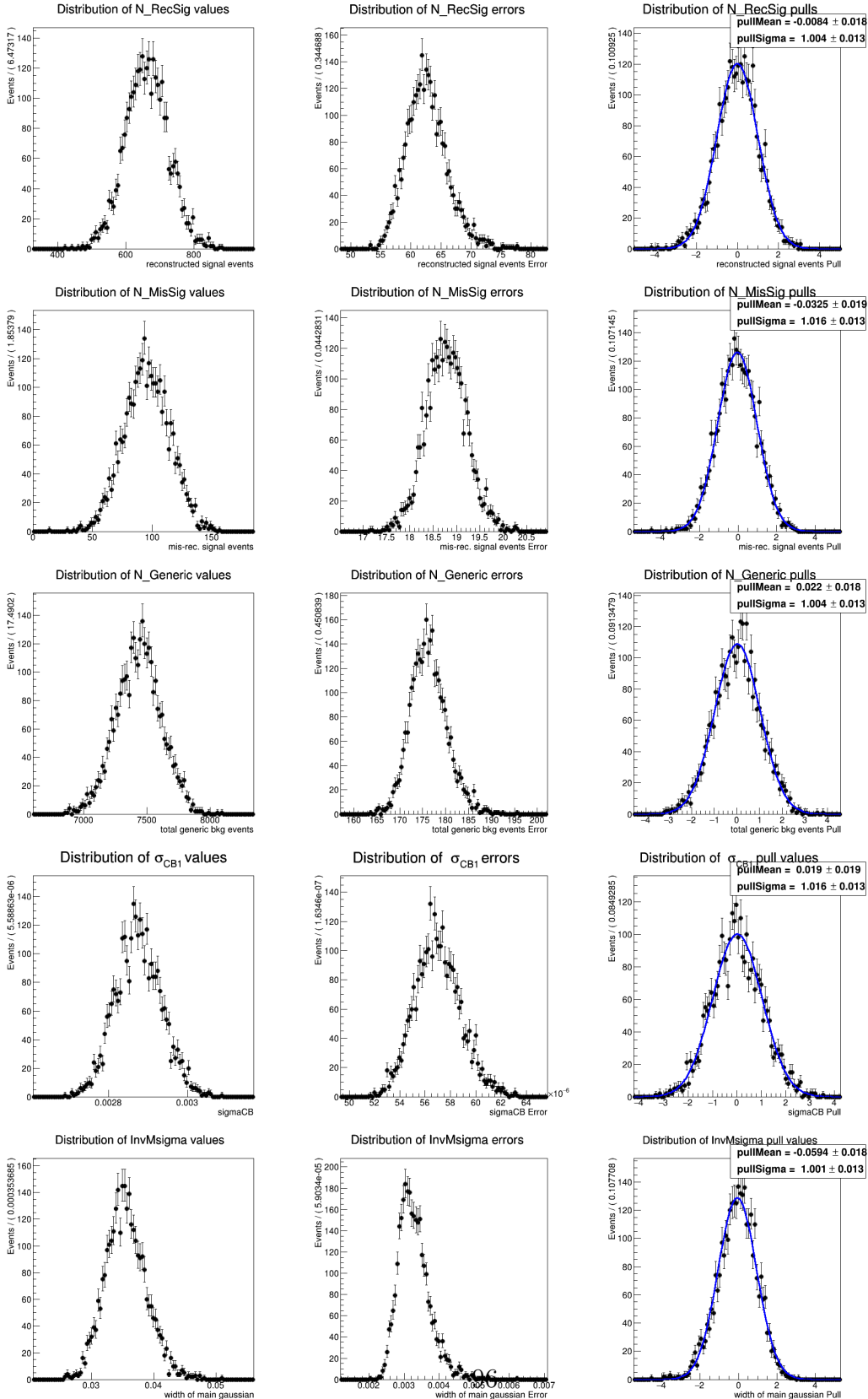


Figure (107) Toy MC study for the two dimensional fit model described in Sec. 6.2

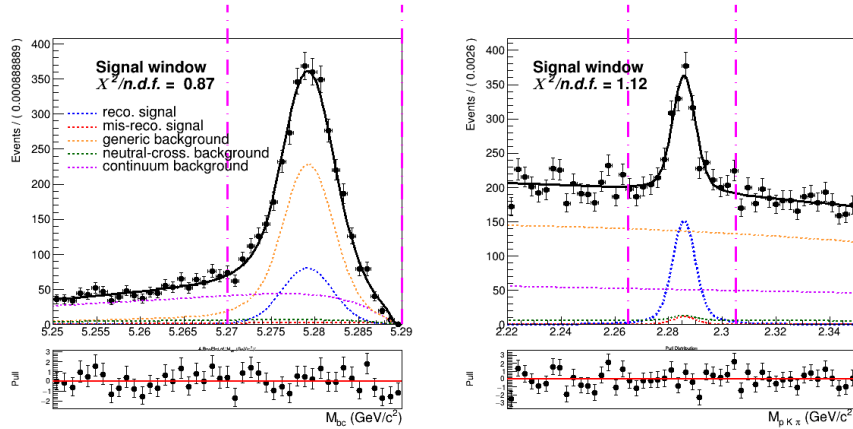


Figure (108) Signal region ($2.22 < M(pK\pi) < 2.35$ GeV/c² and $5.27 < M_{bc} < 5.29$ GeV/c²) projections of the dimensional fit on stream 0 Monte Carlo simulated data.

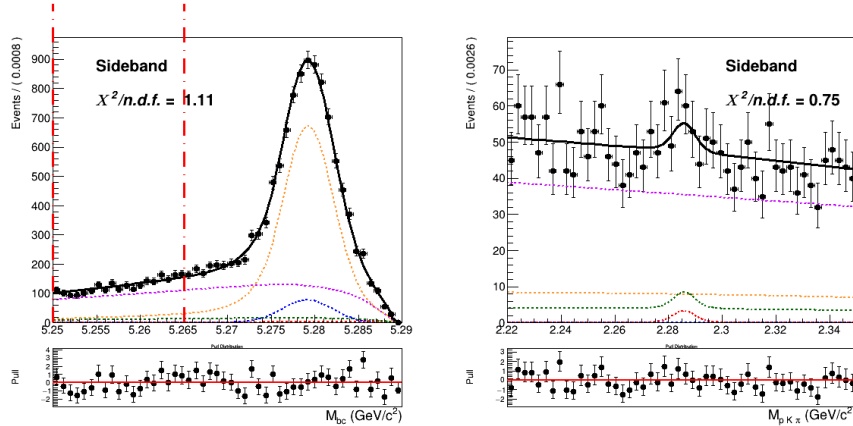


Figure (109) Sideband region of $5.25 < M_{bc} < 5.265$ GeV/c² projection of the two dimensional fit on stream 0 Monte Carlo simulated data.

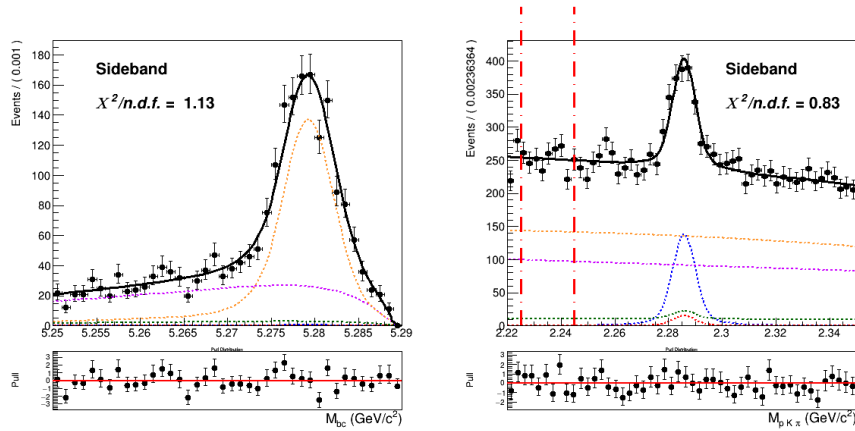


Figure (110) Sideband region of $2.22 < M(pK\pi) < 2.35 \text{ GeV}/c^2$ projection of the two dimensional fit on stream 0 Monte Carlo simulated data.

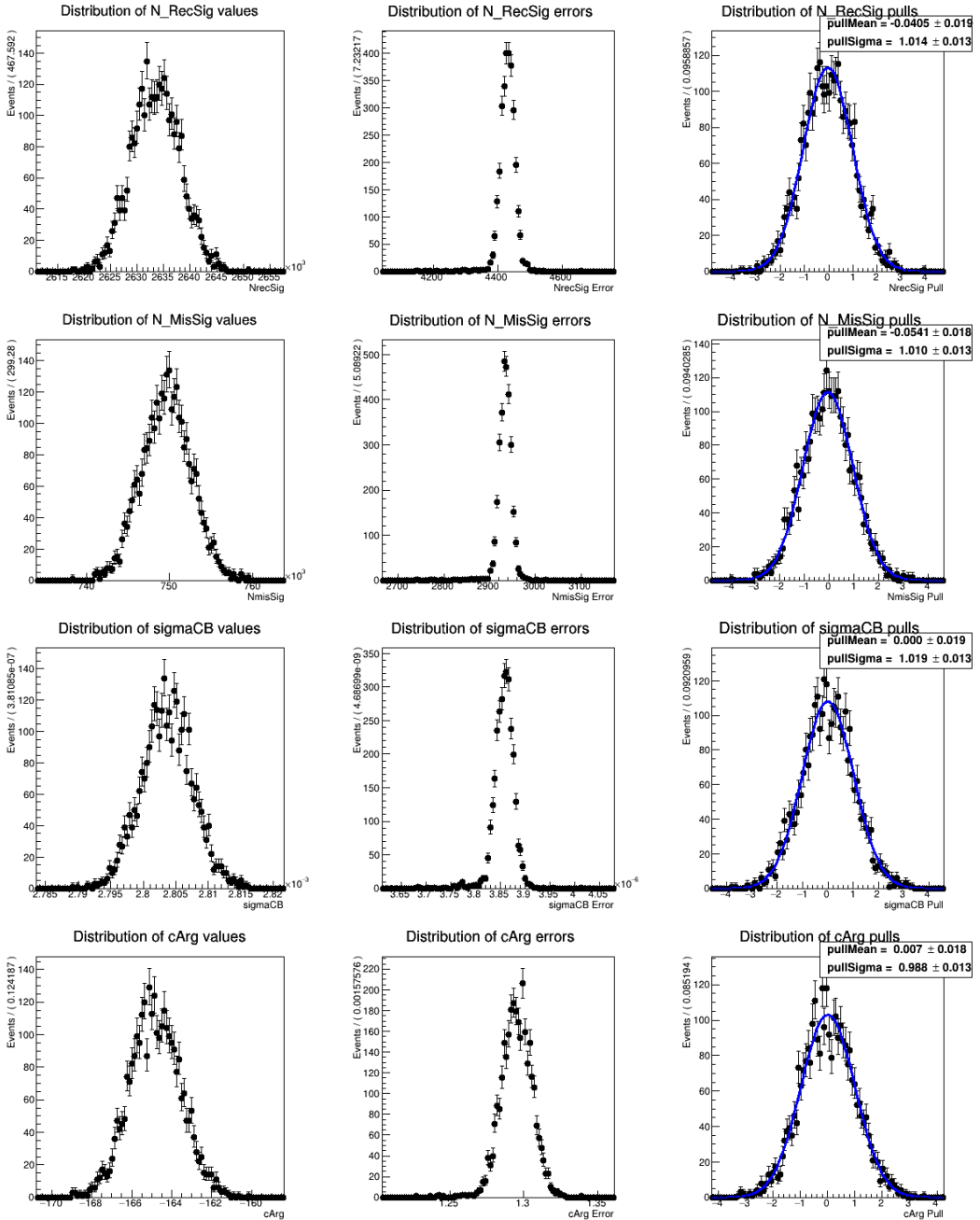


Figure (111) Toy MC study for the B_{tag} fit model described in Sec. 6.4

- 1013 **References**
- 1014 [1] B. Aubert et al., BaBar, *Study of inclusive B^- and \bar{B}^0 decays to flavor-tagged D , D_s*
1015 *and Λ_c^+* , Phys. Rev. D **75** (2007) 072002, [arXiv:hep-ex/0606026](https://arxiv.org/abs/hep-ex/0606026).
- 1016 [2] I. Grach, I. Narodetskii, S. Simula, and K. Ter-Martirosyan, *Exclusive and inclusive*
1017 *weak decays of the B -meson*, Nuclear Physics B **502** (1997) no. 1-2, 227–248.
- 1018 [3] Y. Hsiao, S.-Y. Tsai, C.-C. Lih, and E. Rodrigues, *Testing the W -exchange mechanism*
1019 *with two-body baryonic B decays*, Journal of High Energy Physics **2020** (apr, 2020) .
1020 [https://doi.org/10.1007/JHEP04\(2020\)035](https://doi.org/10.1007/JHEP04(2020)035).
- 1021 [4] M. Gelb, *Search for the Rare Decay $B^+ \rightarrow \ell^+ \nu_\ell \gamma$ with the Full Event Interpretation at*
1022 *the Belle Experiment*. PhD thesis, Karlsruhe Institute of Technology (KIT), 2018.
- 1023 [5] J. Schwab, *Calibration of the Full Event Interpretation for the Belle and the Belle II*
1024 *Experiment*, Master's thesis, Karlsruhe Institute of Technology (KIT), 2017.
- 1025 [6] K.-J. Tien and M.-Z. Wang, *Proton identification efficiency study*, BELLE NOTE 1279.
- 1026 [7] S. Nishida, *Study of Kaon and Pion Identification Using Inclusive D^* Sample*, BELLE
1027 NOTE 779.
- 1028 [8] B. Bhuyan, *High P_T Tracking Efficiency Using Partially Reconstructed D^* Decays*,
1029 BELLE NOTE 1165.
1030 https://belle.kek.jp/secured/belle_note/gn1165/BN1165_v1.pdf.
- 1031 [9] C. H. e. a. B. Fulsom, *Search for $B^0 \rightarrow \Lambda^0 \Psi_{DM}$ decays*, BELLE NOTE 1584.
1032 https://belle.kek.jp/secured/belle_note/gn1584/BN1584_v1.pdf.